INVESTIGATIONS ON STABILITY AND CONTROL FOR UNDERACTUATED SYSTEMS

A Thesis Submitted in Partial Fulfilment of the Requirements for the Award of the Degree of

DOCTOR OF PHILOSOPHY

By

NEELAM VERMA

(Enrolment No. 2K18/PhD/EE/10)

Under the Supervision of

PROF. SUDARSHAN K. VALLURU



DEPARTMENT OF ELECTRICAL ENGINEERING
DELHI TECHNOLOGICAL UNIVERSITY
(Formerly Delhi College of Engineering)
Shahabad Daulatpur, Main Bawana Road, Delhi-110042, India

`May 2026

©DELHI TECHNOLOGICAL UNIVERSITY, DELHI-2026

ALL RIGHTS RESERVED



DELHI TECHNOLOGICAL UNIVERSITY
(Formerly Delhi College of Engineering)
Shahbad Daulatpur, Main Bawana Road, Delhi-42

Candidate's Declaration

I hereby certify that the work which is being presented in the thesis entitled "**Investigations on Stability and Control for Underactuated Systems"** in partial fulfilment of the requirements for the award of the Degree of Doctor of Philosophy and submitted in the Department of Electrical Engineering at the Delhi Technological University is an authentic record of my own work under the supervision of Prof. Sudarshan K. Valluru, Department of Electrical Engineering. The matter presented in this thesis has not been submitted by me for the award of any other degree of this or any other Institute.

NEELAM VERMA
(2K18/PhD/EE/10)

This is to certify that the student has incorporated the corrections suggested by the examiners into the thesis, and that the candidate's statement is correct to the best of our knowledge.

(Prof. Sudarshan K. Valluru)
Signature of Supervisor

Signature of External Examiner



DELHI TECHNOLOGICAL UNIVERSITY
(Formerly Delhi College of Engineering)
Shahbad Daulatpur, Main Bawana Road, Delhi-42

Certificate

I hereby certify that Neelam Verma (2K18/PHD/EE/10) has carried out their work presented in this thesis titled **"Investigations on Stability and Control for Underactuated Systems"** for the award of the degree of **Doctor of Philosophy** from the Department of Electrical Engineering, Delhi Technological University, Delhi, under my supervision. constitutes an original contribution to existing knowledge. The thesis embodies the results of original work, and studies are carried out by the student herself. The content of the thesis does not form the basis for the award of any other degree to the candidate or to anybody else from this or any other University/Institute.

(Prof. Sudarshan K. Valluru)
Supervisor

The PhD viva voce of **Ms. Neelam Verma**, research scholar, has been held on…….

Date:

Acknowledgements

It has been both fascinating and extremely rewarding to write this thesis. I am grateful to God for giving me an opportunity to learn and acquire knowledge. First, I would like to express my sincere gratitude to my esteemed supervisor, Prof. Sudarshan K. Valluru for his constant guidance and encouragement throughout the research work. I am truly blessed to have him as my mentor. I want to extend my special thanks to him for dedicating his valuable time whenever I needed to discuss the research work. Working under his guidance has been a transformative experience, and I sincerely appreciate his support. I would also like to thank the reviewers of our papers for their valuable suggestions and comments which motivated me to improve my research work. I would truly be grateful for my student research committee members, Dr. S. Subramanyam IIT Kanpur, Prof. D.R. Bhaskar, Prof. M. Singh for continuous support and suggestions throughout this research work. I would also like to thank Prof. Rachna Garg, Head of the Department, and Chairman, DRC Electrical Engineering Department, Delhi Technological University, New Delhi for being a visionary and supporting the concept of the research work. I would like to use this opportunity to express my gratitude to all the university staff members who contributed to the cause. I extend my heartfelt thanks to my parents, in-laws, husband, lovely daughters and friends whose encouragement has been a pillar of strength throughout my research journey.

Date:

Neelam Verma

Abstract

The Cart–Inverted Pendulum (CIP) system is a classical benchmark for analysing underactuated, nonlinear, and inherently unstable systems, and it widely represents real-world applications such as robotics, aerospace systems, and self-balancing platforms. This thesis presents a systematic progression of control strategies for the stabilization and performance enhancement of the CIP system, from conventional approaches to intelligent and hybrid control architectures. It also explores metaheuristic approaches and their hybrid combinations to tune controller parameters and improve system performance. Unlike conventional approaches that primarily focus on pendulum angle, this work considered the simultaneous regulation both cart position and pendulum dynamics.

Initially, the impact of CIP system parameters, cart mass, pendulum mass, and pendulum length, on its performance are investigated using a Proportional–Integral–Derivative (PID) controller. The analysis demonstrates that even small variations in these parameter values can significantly affect the transient response and system stability, thereby highlighting the limitations of conventional PID control in handling parametric uncertainties.

To overcome these limitations, a Fractional-Order PID (FOPID) controller is introduced, offering enhanced flexibility through additional tuning parameters. The controllers are optimized using metaheuristic algorithms, namely Particle Swarm Optimization (PSO), the Water Cycle Algorithm (WCA), and the Grasshopper Optimization Algorithm (GOA). A comparative analysis among these optimization algorithms, the GOA-tuned FOPID controller achieves superior performance, with reduced overshoot, faster settling time, and improved stability in both cart position and pendulum angle control.

Building upon this, a novel hybrid control architecture is proposed by integrating a cascaded (FOPI–FOPD) controller with a Backstepping Linear Quadratic Gaussian Controller (BLQGC). Further, a hybrid GOA–Firefly (GOA-FA) optimization framework is employed for optimal parameter tuning. The proposed system

demonstrates significant improvements in transient and frequency domain characteristics, including reduced rise and settling times, minimized steady-state error, and enhanced stability margins. The implemented control model has shown great robustness against external disturbances and parametric variations.

Finally, to address system nonlinearity and uncertainty more effectively, an intelligent control framework based on an Adaptive Neuro- Fuzzy controller is developed. The controller parameters are tuned using a hybrid Ant Colony Optimization–Particle Swarm Optimization (PSO–ACO) algorithm. The proposed AI-based model, incorporating multiple hidden layers and fuzzy rules, exhibits superior learning capability and adaptability, achieving minimal rise and settling times and low error indices such as Integral Squared Error, Steady State Error, and Mean Squared Error.

Overall, this thesis demonstrates a structured evolution from classical PID control to advanced fractional-order, hybrid, and intelligent control strategies. The proposed methodologies significantly enhance the stability, robustness, and dynamic performance of the CIP system, thereby enabling the development of efficient control solutions for complex underactuated systems. From the investigations, it is inferred that the advanced hybrid intelligent controllers work well in stabilizing CIP system under different parametric variations and enhances the dynamic responses.

Contents

Acknowledgement v

Abstract vi

Contents vi - xi

List of Figures xii

List of Tables xiv

List of Abbreviations xvi

List of Symbols xvii

Chapter 1 Introduction and Motivation 1 - 18

1.1 Background 1

1.2 Underactuated System 1

1.3 Literature Review 3

1.3.1 Review of PID Controller 4

1.3.2 Review of FOPID Controller 5

1.3.3 Review of Cascaded FOPID Controller 6

1.3.4 Review of Neuro-Fuzzy Controller 8

1.3.5 Review of Metaheuristic Optimization Techniques 10

1.4 Research Gaps 13

1.5 Research Objectives 13

1.6 Research Contributions 14

1.7 Organization of Thesis 14

1.8 Concluding Remarks 18

Chapter 2 Modelling and Dynamics of the Cart–Inverted Pendulum System 19 – 27

2.1 Introduction 19

2.2 Internal Dynamics of CIP System 20

2.3 Transfer Function Representation of CIP Dynamics 22

2.4 State Space Representation of CIP Dynamics 24

2.5 Concluding Remarks 27

Chapter 3 PID-based Control and Parametric Sensitivity Analysis of Cart–Inverted Pendulum 28 – 45

3.1 Introduction 28

3.2 Implemented Control Model 29

3.3 Results and Discussion 30

3.3.1 Transient Response of PID Controller CIP System 31

3.3.2 Parametric Variation Sensitivity Analysis 32

3.4 Concluding Remarks 44

Chapter 4 Metaheuristic Optimization of FOPID Controller for Cart–Inverted Pendulum 46– 64

4.1 Introduction 46

4.2 FOPID Controller Design 47

4.3 Metaheuristic Optimization Technique Used for FOPID Tuning 49

4.3.1 Grass-Hopper Optimization Technique 50

4.3.2 Particle Swam Optimization 53

4.3.3 Water Cycle Algorithm 54

4.4 Design of Implemented FOPID Controller for CIP Model 57

4.5 Results and Discussion 59

4.5.1 Transient Analysis of GOA-FOPID for CIP System 59

4.5.2 Comparative Analysis of FOPID Tuned with GOA, PSO and WCA 61

4.6 Concluding Remarks 64

Chapter 5 Hybrid Cascaded FOPI–FOPD–BLQGC Controller for Robust Stabilization of Cart–Inverted Pendulum 65 – 86

5.1 Introduction 65

5.2 Cascade FOPI-FOPD Controller Design 67

5.3 Backstepping Linear Quadratic Gaussian Controller (BLQGC) 67

5.4 Hybrid Meta-Heuristic (GOA-FA) Algorithm 71
5.4.1 Phase 1: Grass-Hopper Optimization Algorithm (GOA) 71
5.4.2 Phase 2: Firefly Algorithm (FA) 72
5.4.3 Hybrid GOA-FA Algorithm 73
5.5 Proposed Cascaded FOPI-FOPD-BLQGC Controller 74
5.6 Results and Discussion 75
5.6.1 Transient Performance Analysis 76
5.6.2 Closed-Loop Stability Analysis under Impulsive Disturbances 78
5.6.3 Robustness Analysis under Parametric Uncertainties 79
5.6.4 Frequency Domain Analysis 84
5.7 Concluding Remarks 85

Chapter 6 Hybrid Metaheuristic-Optimized Adaptive Neuro-Fuzzy Controller for Cart–Inverted Pendulum System 87 – 102
6.1 Introduction 87
6.2 Overview of Artificial Intelligence-based Controllers 88
6.3 Hybrid Neuro-Fuzzy Controller Design 89
6.4 Hybrid PSO-ACO Algorithm 93
6.5 Results and Discussion 98
6.5.1 Training Performance of Neural Network 98
6.5.2 Transient System Response 99
6.5.3 Comparative Performance Analysis 100
6.6 Concluding Remarks 102

Chapter 7 Conclusions and Future Scope of Work 103 – 106
7.1 Introduction 103
7.2 Main Conclusions 103
7.3 Future Scope of Work 105

References **107 – 121**

List of Publications 122

Brief Biodata 123

List of Figures

Figure No.	*Titles*	*Page No.*
2.1	Cart Inverted Pendulum Control System	20
2.2	Free Body Diagram of Cart-Inverted Pendulum System	23
3.1	Implemented Dual Loop PID Controllers for CIP System	29
3.2	Transient Response of PID-Tuned CIP System	31
3.3	Transient Response of PID-Tuned CIP System with $m = 0.15kg$	32
3.4	Transient Response of PID-Tuned CIP System with $m = 0.205kg$	33
3.5	Transient Response of PID-Tuned CIP System with $m = 0.215kg$	33
3.6	Transient Response of PID-Tuned CIP System with $m = 0.22kg$	34
3.7	Transient Response of PID-Tuned CIP System with $m = 0.225kg$	34
3.8	Transient Response of PID-Tuned CIP System with $l = 0.27m$	37
3.9	Transient Response of PID-Tuned CIP System with $l = 0.28m$	37
3.10	Transient Response of PID-Tuned CIP System with $l = 0.29m$	37
3.11	Transient Response of PID-Tuned CIP System with $l = 0.32m$	38
3.12	Transient Response of PID-Tuned CIP System with $l = 0.34m$	38
3.13	Transient Response of PID-Tuned CIP System with $M = 2.42kg$	41
3.14	Transient Response of PID-Tuned CIP System with $M = 2.45kg$	41
3.15	Transient Response of PID-Tuned CIP System with $M = 2.25kg$	42
3.16	Transient Response of PID-Tuned CIP System with $M = 2.22kg$	42
4.1	Architecture of FOPID Controller	48
4.2	λ–μ Plane with FOPID Region and PID Family	49
4.3	GOA Algorithm Flow Diagram	52
4.4	Flowchart of PSO Algorithm	54
4.5	Flowchart of WCA Algorithm	56
4.6	Control Structure of the CIP System using an Optimized FOPID Controller	57

Figure No.	*Titles*	*Page No.*
4.7	Implemented FOPID-controlled CIP system	58
4.8	Cart Position Response for the GOA-tuned FOPID Controller	60
4.9	Pendulum angle response for the GOA-tuned FOPID controller	60
4.10	Cart position control with GOA-FOPID, PSO-FOPID and WCA-FOPID	61
4.11	Pendulum angle control with GOA-FOPID, PSO-FOPID, and WCA-FOPID	62
4.12	Comparative Convergence Curve	63
5.1	Cascaded FOPI-FOPD controller	67
5.2	BLQGC Controller Design for Cart Inverted Pendulum	68
5.3	GOA-FA Algorithm Flowchart	73
5.4	Proposed Cascaded FOPI-FOPD-BLQGC Controlled CIP model	74
5.5	Proposed (FOPI-FOPD-BLQGC) Controller Response Tuned with GOA-FA Algorithm	77
5.6	Stability Response of Proposed Controller with Application of 1(N) Impulse Force	79
5.7	Comparative responses with $M = 2.1kg, m = 0.1kg$ and $l = 0.1m$	80
5.8	Comparative responses with $M = 2.2kg$, $m = 0.2kg$ and $l = 0.2m$	82
5.9	Comparative responses with $M = 2.3kg$, $m = 0.3kg$ and $l = 0.3m$	83
5.10	Comparative Bode plot of the Cascaded FOPI-FOPD-BLQGC, FOPD, FOPI and BLQGC Controllers	85
6.1	Architecture of Neuro-Fuzzy Controller	90
6.2	Flow Chart of Neuro-Fuzzy Controller Implementation	92
6.3	Flowchart of Hybrid PSO-ACO Algorithm	94
6.4	Output and the Target of the fitness function	98
6.5	Training and validation results	99
6.6	Transient Response of the Neuro-Fuzzy Controller	99
6.7	Controller Effort Signal	100
6.8	Transient Response with PID Controller	100
6.9	Comparative analysis [155]	101

List of Tables

Table No.	*Titles*	*Page No.*
3.1	PID Controller's Gain Parameters	30
3.2	Transient Parameters of PID-Tuned CIP System	31
3.3	Cart Position Response Comparison of Five Values Pendulum Mass	35
3.4	Pendulum Angle Response Comparison of Five Values Pendulum Mass	35
3.5	Control Signal Response Comparison of Five Values Pendulum Mass	35
3.6	Cart Position Response Comparison of Five Values Pendulum length	39
3.7	Pendulum Angle Response Comparison of Five Values Pendulum length	39
3.8	Control Signal Response Comparison of Five Values Pendulum length	40
3.9	Cart Position Response Comparison of Four Values Pendulum Mass	43
3.10	Pendulum Angle Response Comparison of Four Values Pendulum Mass	43
3.11	Control Signal Response Comparison of Four Values Pendulum Mass	43
4.1	Tunned FOPID Controller Parameters and ITAE	59
4.2	Comparative Analysis of Pendulum Angle	62
4.3	Comparative Analysis of Cart Position	62
5.1	Proposed BLQGC Controller Parameter Values	70
5.2	Proposed Controller Gain Value of BLQGC Controller	70
5.3	Optimized Cascaded FOPI-FOPD Controller Parameters	75
5.4	Comparative Transient Analysis	78
5.5	Comparative Transient Parameters for Case 1	81

Table No.	*Titles*	*Page No.*
5.6	Comparative Transient Parameters for Case 2	83
5.7	Comparative Transient Parameters for Case 3	84
5.8	Frequency Domain (Bode Plot) Parameters	85
6.1	PID Controller's Gain Parameters	100
6.2	Comparative Performance Analysis with PID Controller	101
6.3	Comparative Analysis with Reference [156]	102

List of Abbreviations

ACO	Ant Colony Optimization
ANFIS	Adaptive Neural Fussy Interface System
ANN	Artificial Neural Network
BLQGC	Backstepping Linear Quadratic Gaussian Controller
Cascaded FOPI-FOPD	Cascaded Fractional Order Proportional Integral-Fractional Order Proportional Derivative
CIP	Cart Inverted Pendulum
DOF	Degree of Freedom
FFA	Firefly Algorithm
FIS	Fussy Interface System
FOPD	Fractional Order Proportional-Derivative
FOPI	Fractional Order Proportional-Integral
FOPID	Fractional Order Proportional-Integral-Derivative
GOA	Grasshopper Optimization Algorithm
ISE	Integral Squared Error
ITAE	Integral Time Absolute Error
LQGC	Linear Quadratic Gaussian Controller
LQR	Linear Quadratic Regulator
MSE	Mean Squared Error
PD	Proportional-Derivative
PI	Proportional-Integral
PID	Proportional-Integral-Derivative
PSO	Particle Swarm Optimization
WCA	Water Cycle Algorithm

List of Symbols

$x(t)$	Cart Position
$\theta(t)$	Pendulum Angle
$\dot{x}(t)$	Cart's Translational Velocity
$\dot{\theta}(t)$	Pendulum's Angular Velocity
$e(t)$	Error
$u(t)$	Controller Force
M	Cart Mass
m	Pendulum Mass
l	Pendulum length
F	External Force
k_p	Proportional Gain
k_i	Integral Gain
k_d	Derivative Gain
t_r	Rise Time
t_p	Peak Time
M_p	Maximum Overshoot
e_{ss}	Steady State Error
t_s	Settling Time
$J(t)$	Cost Function
μ	Fractional Derivative Order
λ	Fractional Integral Order
K_c	LQR Gain
K_b	Backstepping Control Gain

Chapter 1

Introduction and Motivation

1.1 Background

In recent years, significant attention has been devoted to the analysis and control of underactuated mechanical systems, owing to their wide applicability across modern engineering domains. To control and stabilize the nonlinear, under-actuated systems remain one of the most researched problems in modern control engineering. The Cart–Inverted Pendulum (CIP) system remains a benchmark platform for validating advanced control strategies. It is an inherently unstable equilibrium, with strong nonlinear coupling between translational and rotational dynamics and sensitivity to parametric variations. These characteristics make the CIP system a benchmark for testing and validating the robustness, adaptability, and optimality of advanced controllers and optimizing algorithms.

1.2 Underactuated System

An underactuated systems have degrees of freedom (DOF) more than the externally available control inputs. In simple terms, this means that not all parts or motions of the system can be controlled directly using independent actuators. As a result, some states of the system must be controlled indirectly through the natural interactions and couplings among system variables. This inherent limitation makes the analysis and control of such systems more complex and challenging compared to fully actuated systems [1]. Due to this complexity, underactuated systems are often used as benchmark problems in control engineering to test the effectiveness of advanced and intelligent control strategies.

Common examples of underactuated systems include the cart inverted pendulum, mobile robots, quadrotors, underwater vehicles, and Translational Oscillator with

Rotational Actuator (TORA) systems [2]. These systems are widely studied because they represent real-world engineering problems where achieving stability and control is difficult due to limited actuation [3]. Electromechanical systems are broadly categorized based on the relationship between the number of actuators and system DOF:

(a) Fully Actuated Systems: Number of control inputs equals DOF. Each state can be independently controlled, resulting in a relatively simpler control design.

(b) Overactuated Systems: Number of control inputs exceeds DOF, providing redundancy and flexibility in control allocation.

(c) Underactuated Systems: The DOF to be controller is more than the number of external control inputs available. Only a subset of system dynamics is directly controlled, while the remaining internal dynamics must be indirectly stabilized, posing significant control challenges [4].

Underactuated systems are classified into Class I, Class II, and Class III based on whether certain coordinates are directly actuated. This classification helps researchers and engineers choose suitable control techniques for different system configurations [5]. The general nonlinear dynamic model of a two-DOF underactuated system is expressed as given in equation (1.1)

$$\boldsymbol{M}(\boldsymbol{q})\ddot{\boldsymbol{q}} + \boldsymbol{C}(\boldsymbol{q}, \dot{\boldsymbol{q}})\dot{\boldsymbol{q}} + \boldsymbol{G}(\boldsymbol{q}) = \boldsymbol{\tau} \tag{1.1}$$

Where the generalized coordinated are given as $\boldsymbol{q} = [\boldsymbol{q_1}, \boldsymbol{q_2}]^{\boldsymbol{T}}$, and matrix of inertia is $\boldsymbol{M}(\boldsymbol{q})$, $\boldsymbol{C}(\boldsymbol{q}, \dot{\boldsymbol{q}})$ represents centrifugal effects, $\boldsymbol{G}(\boldsymbol{q})$ is the gravitational vector, and $\boldsymbol{\tau}$ is the control input vector. This formulation highlights the coupled nonlinear dynamics and the challenge of controlling unactuated states.

Underactuated systems offer several advantages, such as reduced weight, lower energy consumption, and greater cost-effectiveness, due to fewer actuators. However, these benefits come at the cost of increased control complexity, strong nonlinear interactions, and challenges in maintaining stability and robustness. Despite these challenges, underactuated systems are still used in wide fields of engineering such as robotics, aerospace, transportation, and automation. They are also recognized as important

benchmark systems for evaluating modern control techniques and developing efficient and reliable control solutions [1], [4], [5].

1.3 Literature Review

The standard inverted pendulum, such as a cart and a pole system, has been broadly employed in control labs to validate the efficacy of the control systems in correspondence with the control of various actual systems. A cart-inverted pendulum is a distinctive benchmark, particularly in underactuated schemes, as it exhibits intrinsic unbalanced nonlinear behavior with minimal phase complications [6]. The cart-inverted pendulum system poses numerous challenges in designing the controller, which gives optimal performance with robustness against disturbances. The main reason for CIP system being considered as one of the most researched control problems across the fields is that its dynamics have resemblance to various real time engineering systems. For example, rocket guidance system, gantry crane system, missile launching mechanism, bipedal walking, wheel-balancing motion systems, a robot system, etc. [7]. Underactuated schemes associated with the groups of schemes, which are least on the passive joint. They cannot have regulated all degrees of movement for some reason. The unavailability of direct actuation of each DOF externally increases the demand for advanced controller strategies [8]. Consequently, the challenges of real-time tracking, upright position regulation and the stability of the cart inverted pendulum become among the most important dynamic control issues. It also requires fast, accurate performance [9-12]. To address the diverse challenges of stabilizing the inverted pendulum, numerous methods have been employed in literature. These techniques range from conventional and well stabilized PID, Energy based control techniques, Linear Quadratic Regulator (LQR), and advanced methods as Fractional PID, Cascaded FOPID, Fuzzy logic controller, Neural-Network inspired controllers and their hybrid methods, etc. [13-14].

Nonlinear, unbalanced inverted pendulum systems face near-real-time challenges in industrial applications. Their behaviour changes with varying operating conditions and is affected by external disturbances and physical parameter limits [15]. These systems are divided into three groups. First, a revolving platform carries a pendulum with one

degree of freedom [16]. Second, double and triple inverted pendulums have more than one degree of freedom and are driven by an external force acting on a cart. Third, a pendulum with two degrees of freedom is mounted on a robot with weakly coupled links [17]. Monitoring and stabilization of the cart-based inverted pendulum system involve two stages: the swing-up stage and the stabilization stage [18]. The swing-up stage takes the real-time pendulum angle and cart position as inputs and generates a control voltage along with a switching signal. The stabilization stage compares the cart position and pendulum angle with their reference values using the control signal [19]. The design and performance of FOPID and FOIPD controllers are tested to maintain the equilibrium of the TRMS (Twin Rotor Multiple Input Multiple Output system). [20]. Performance evaluation as well as the Execution of the FO-DOF Controller over a Cart-Inverted based Pendulum System [21]. In this research study, both a PID controller and a fuzzy-logic-based PID controller are developed and modeled to achieve optimal control of the inverted pendulum system. The ultimate objective of this work is to ensure that the pendulum remains in a stable, upright standing position, even in the presence of external disturbances [22]. Researchers employed linear and nonlinear PID controllers to stabilize and regulate the Gantry Crane System [23]. Numerous combinations of both PID and LQR controllers are implemented to verify the robustness of the controller, while the cart-based inverted pendulum system is evaluated both in the presence and in the absence of external disturbances [24].

1.3.1 Review of PID Controller

PID controllers are extensively utilized in control applications because of their simple design, intuitive structure, and reliable effectiveness in linear systems, which makes them a preferred choice across a wide range of engineering domains, including motor control, power systems, and industrial automation [25] [26]. Their ability to provide satisfactory performance and a simple structure makes them highly practical. However, the literature highlights significant limitations when applied to nonlinear, underactuated systems such as the cart inverted pendulum (CIP) system, where system instability and coupling effects dominate [27] [28].

A major challenge associated with PID controllers lies in the tuning of their three gain parameters. Classical tuning methods, such as Ziegler–Nichols, are mainly developed for linear systems and frequently result in poor transient performance when applied to nonlinear environments [29]. Consequently, tuning frequently relies on heuristic or trial-and-error approaches, which are inefficient and lack reproducibility. To overcome this limitation, optimization techniques such as Artificial Bee Colony and Particle Swarm Optimization are used for improving convergence characteristics and disturbance rejection capabilities [30] [31]. These metaheuristic approaches enable efficient gain tuning, thereby improving controller performance [32].

A critical issue emphasized in the literature is parametric uncertainty. In situations where variations in system parameters, such as cart mass, pendulum mass and length, as well as damping and related factors, significantly influence the overall system dynamics and stability [29]. In CIP systems, this challenge becomes more severe due to strong coupling between a cart position and pendulum angle [27]. Even minor parameter variations can result in performance degradation, oscillations, or instability [34]. Therefore, incorporating parametric analysis is essential to ensure robustness, stability, and reliable control performance under varying operating conditions.

In conclusion, while PID controllers remain fundamental in control engineering, their limitations in handling nonlinearities and parametric uncertainties necessitate the adoption of advanced control frameworks.

1.3.2 Review of FOPID Controller

To address these limitations, modern control techniques have been developed to enhance system performance. Fractional Order PID (FOPID) controllers offer additional tuning flexibility via fractional calculus, enabling improved frequency-domain performance and robustness [30]. FOPID controllers offer greater degrees of freedom than traditional PID controllers, enabling improved control performance and robustness. This improvement arises from the inclusion of fractional-order integral and derivative terms. This additional tuning flexibility allows more precise shaping of system dynamics, improved frequency response, and noise attenuation [22] [23]. Such flexibility is particularly beneficial in systems affected by external disturbances, model

uncertainties, and nonlinearities [21]. FOPID enhances the plant's transient and steady-state responses [15]. A proportional-derivative (PD-type) controller can offer a quick rise time, slight overshoot, and short settling time, but it cannot achieve the desired feedback benefits [16]. Therefore, it is recommended to use standard I, P.I., or PID controllers, as well as fractional-order I (FOI)/FOPI/FOPID controllers [17] [18]. The FO controller parameters must be tuned using a variety of optimization algorithms to minimize performance criteria, such as Integral Time Absolute Error (ITAE) [19].

Furthermore, integrating control strategies with metaheuristic optimization algorithms such as PSO, GOA, and GWO significantly enhances controller tuning efficiency and convergence speed [32] [35] [36]. limitations of conventional PID controllers by improving robustness, adaptability, and transient performance. Various optimization techniques have been employed to effectively tune the parameters of FOPID controllers to achieve improved dynamic performance and robustness. For instance, the Class Topper Optimization (CTO) method has been shown to outperform traditional approaches such as Genetic Algorithm (GA) and Particle Swarm Optimization (PSO) [37], particularly in terms of convergence speed, stability, and overall control accuracy. Similarly, two-loop FOPID-based control strategies have been proposed for higher-order nonlinear inverted pendulum systems, demonstrating robust performance under a wide range of external disturbances by using advanced and adaptive tuning methods [23]. These approaches also enhance system resilience against parameter variations and modeling uncertainties. Comparative studies involving optimization algorithms such as the Grasshopper Optimization Algorithm (GOA), Water Cycle Algorithm (WCA), and PSO have further indicated that GOA-based tuning provides superior control performance in terms of faster convergence, reduced steady-state error, and improved transient response characteristics [38]. Furthermore, hybrid control approaches integrating FOPID with Linear Quadratic Regulator (LQR) and other control schemes have been explored [39]. The FOPID controllers outperform than classical PID controllers under varying operating conditions and disturbances [21] [40].

1.3.3 Review of Cascaded FOPID Controller

FOPID controllers offer enhanced flexibility and performance over integer-order PID controllers [41]. Further advancements in control strategies have led to the exploration of

cascaded controller architectures. In these advanced techniques, the FOPID controller is integrated into a multi-loop configuration, thereby improving stability and performance [42]. Cascaded controllers are generally recognized for their efficacy in rejecting disturbances and enhancing system robustness compared to classical controllers [43]. The superior performance of these controllers is evident as compared to a standalone FOPID controller [44]. The implementation of cascade controllers in Automatic Generation Control has demonstrated improvements in the frequency profile compared to classical PI and PID [45][46]. However, the design and optimization of such cascaded FOPID structures present a greater challenge due to the increased number of tunable parameters. And that requires advanced optimization algorithms for effective implementation [47]. Superior performance in handling nonlinearities and uncertainties, especially in higher-order plants or systems with significant time delays are reported in [48] [49]. These hybrid approaches effectively address the Optimal control approaches such as Linear Quadratic Regulator (LQR) offer systematic performance optimization by minimizing a cost function [50], while BLQGC further enhances robustness by incorporating stochastic estimation techniques for noise handling [51]. In [46], a novel LQR approach based on a Pareto-based Multi-objective Binary Probability Optimization Algorithm (MBPOA) is proposed. It is used to estimate optimal weighting matrices (Q and R), thereby reducing design time and improving performance. A fractional calculus-based control strategy for a rotatory inverted pendulum (RIP) was proposed in [52]. The dynamic performance of fuzzy-LQR (FLQR) and fuzzy-LQG (FLQG) controllers was compared with that of classical LQR and LQG controllers in [53] [54]. The comparative results show that the FLQR and FLQG controllers are more efficient and effective than the classical LQR and LQG controllers. A hybrid LQR and T-S fuzzy control method is proposed for stabilizing the nonlinear inverted pendulum system. Simulation results show improved stability, disturbance rejection, and swing-up performance [55]. The application of cascaded controllers in pneumatic positioning systems tuned with particle swarm optimization has shown improved performance [56]. Collectively, these studies demonstrate that cascaded FOPID controllers offer a robust, flexible solution for improving system stability and performance across various applications, outperforming both traditional PID and standalone FOPID controllers in handling complex, nonlinear, and uncertain environments [57] [58] [59] [60].

To tune the hybrid controller parameters, efficient optimization techniques are essential. The CPSO-GSA technique has been successfully used to optimize the gains and parameters of a cascaded 3DOF-FOPID-FOPI, which demonstrated superior performance compared to traditional PID controllers [61]. Similarly, the Teaching-Learning-Based Optimization (TLBO) algorithm has demonstrated better performance than Genetic Algorithm (GA) and Ant Colony Optimization (ACO) in terms of dynamic response and disturbance rejection [62] [63]. The Local Unimodal Sampling (LUS), when combined with TLBO, has been applied to optimize a complex cascaded controller, thereby improving robustness against external disturbances [64]. Additionally, the Modified Harmony Search Optimization technique has been proposed for accurate modeling and automatic tuning of nonlinear systems [65]. Various nature-inspired algorithms, including PSO, GA, and Artificial Bee Colony (ABC) etc., have been compared for FOPID design [66-69]. The PSO algorithm, in particular, has been frequently utilized due to its global search capabilities, effectively minimizing system errors and improving stability in cascade control loops [70]. These studies collectively underscore the versatility and effectiveness of optimization techniques in enhancing the performance of cascaded FOPID controllers across diverse applications [71-73].

1.3.4 Review of Neuro-Fuzzy Controller

In recent past the development of cascaded FOPID and LQR-based control strategies has focused on integrating intelligent and adaptive techniques to address the limitations posed by nonlinearities and uncertainties in inverted pendulum systems. Neuro-fuzzy systems combine the learning capability of neural networks with the reasoning ability of fuzzy logic to model and control complex nonlinear systems. Among these approaches, the Adaptive Neuro-Fuzzy Inference System (ANFIS) is widely used for its effectiveness in handling uncertainty and improving system performance [74]. A GA-tuned neuro-fuzzy logic controller (NFLC) based on an RBF neural network with Gaussian membership functions demonstrated improved performance and faster convergence compared to conventional fuzzy and GA-tuned PID controllers [75]. An adaptive neuro-fuzzy control system for a flexible manipulator with variable payload using a fuzzy logic controller and dynamic recurrent neural networks. Which demonstrates robust performance and effective handling of nonlinear system dynamics and payload variations [76]. Modeling

methods for nonlinear system identification in industrial processes with time-varying and nonlinear behavior. It highlights the balance between model accuracy and interpretability using techniques that combine neural networks and fuzzy logic [77]. An intelligent controller for underwater vehicle-manipulator systems using fuzzy PD control and a neural network compensator for dynamic approximation. The results show that improved robustness, precision, and lower energy consumption compared to conventional PD and fuzzy controllers [78].

A PID-fuzzy controller is used to stabilize the CIP system, and its design parameters are tuned using a hybrid PSO search technique that combines the Sine Cosine Algorithm (SCA) and the Levy Flight (L.F.) distribution, as proposed in [79]. It was observed that the overshoot and integral square errors were reduced by 25% and 10%, respectively, compared with the self-tuning controllers. Uni-Neuro is a unique approach that integrates uniform design with neural networks in a model built from input and response data (metamodel) [80]. A hybrid uniform multi-objective genetic algorithm was employed to obtain the optimal setup input parameters for a double inverted pendulum (DIP) [81]. This technique generated nine sets of alternative input parameter values to stabilize the DIP across 25 training datasets. Another hybrid enhanced type-2 fuzzy logic controller tuned by an RNA genetic algorithm is proposed for DIP stabilization in [82]. All of these nonlinear controllers can offer superior stabilization performance compared to conventional linear controllers. A new adaptive swing-up control algorithm design was implemented for an inverted pendulum system [83]. To eliminate the chattering effect of the fast-switching surface, the amplitude of the output function is reduced using the sigmoid function as a Signum function [84]. The results show that the method in [72] performs better in terms of robustness, adaptation to changing variables, fitness function optimization, and minimization of the angle error to zero [85]. The ANFIS was estimated to use the Sugeno fuzzy inference model in both real experiments and simulation results. The simulation results revealed that ANFIS performed better than the Sugeno-fuzzy controller, offering a flatter, more stable response and a lower error rate [86]. The modeling, design, and simulation of an Adaptive Neuro-Fuzzy Inference System (ANFIS) for controlling nonlinear systems using a hybrid neural network and fuzzy logic approach is presented in [87]. Simulation results demonstrate that the proposed ANFIS

model provides improved accuracy, learning capability, and effective performance in handling system uncertainties. The proposed intelligent control framework combines a Radial Basis Function (RBF) neural network with a Linear Quadratic Regulator (LQR) compensator [88]. In this approach, the LQR generates the nominal control signal based on the linearized model, while the neural network enhances adaptability via online learning. The stability of the closed-loop system was validated using Lyapunov analysis, and both simulation and real-time results confirmed improved performance. Deep Neuro-Fuzzy Systems (DNFS), combine deep neural networks with fuzzy inference systems to improve learning and reasoning capabilities [89]. It also analyzes different DNFS architectures and optimization methods, showing better performance with metaheuristic approaches compared to gradient-based methods [90]. The study suggests advanced fuzzy models and dynamic networks to enhance accuracy and handling of highly nonlinear problems [91]. A survey discussed the deep neural networks and their limitations, such as high computational cost, sensitivity to noise, and poor performance with incomplete data. It explores how integrating fuzzy logic systems with deep learning can improve performance and reviews various hybrid approaches and real-world applications [92]. An adaptive neuro-fuzzy PID controller using the Twin Delayed Deep Deterministic Policy Gradient (TD3) reinforcement learning algorithm for nonlinear systems, where fuzzy inference and PID control are integrated within a neural network structure for automatic tuning although computational complexity remains a challenge [93].

1.3.5 Review of Metaheuristic Optimization Techniques

Building upon such intelligent frameworks, optimization-based tuning of classical controllers has gained significant attention. In [94] utilized Differential Evolution (DE) and Constriction Coefficient Particle Swarm Optimization (CCPSO) to tune PID parameters integrated with Model Reference Adaptive Control (MRAC), demonstrating improved handling of system nonlinearities. Similarly, [95] employed a Genetic Algorithm (GA) to optimize PID controller parameters, achieving reduced settling time and overshoot compared to conventional PID control. A comprehensive study of hybrid approach combining a modified Genetic Algorithm (mGA) with a PD-like fuzzy logic controller, where mGA was used to rapidly optimize scaling factors, resulting in enhanced control performance [96]. Comprehensive review of intelligent control

techniques by integrating fuzzy logic, neural networks, and genetic algorithms into a unified hybrid framework is compiled in [97]. It provides overview of optimization methods for designing adaptive and optimized control systems for complex nonlinear applications. With the increasing complexity of control requirements, metaheuristic and hybrid optimization approaches have been further explored. A holistic optimization framework, combining Ant Colony Optimization with the Nelder–Mead method (ACO-NM), for simultaneous tuning of swing-up and stabilization controllers [98]. This approach improved both transient and steady-state performance. In a similar direction, a comparative analysis of Radial Basis Function (RBF), Fuzzy Logic (FL), and Integral Sliding Mode Control (ISMC), with parameters optimized using the Whale Optimization Algorithm (WOA), demonstrated the superior performance in terms of reduced overshoot and settling time [99]. To enhance fuzzy controller design, Genetic Algorithm (GA) is utilized to optimize membership functions, rule base, and learning parameters, resulting in improved equilibrium response and control accuracy [100]. An Integer Order Fuzzy PID (IOFPID) and Fractional Order Fuzzy PID (FOFPID) controllers are tuned using multiple optimization algorithms, including GA, Social Spider Optimizer (SSO), Parallel Ant Colony Optimization (PACO), and Pigeon Colony Optimization (PCO) [101]. A Multi-Objective Artificial Bee Colony (MOABC)- based adaptive robust control strategy combined with Decoupled Sliding Mode Control (DSMC), claims that system robustness and control efficiency are improved [102]. A hybrid control approach combining sliding mode control and feedback linearization with fuzzy logic and gradient-based adaptation is developed in [103]. It is optimized using a Multi-Objective Ant Lion Optimizer (MOALO), which demonstrates improved tracking performance and smooth control action. A Sliding Mode Controller (SMC) optimized using PSO and GA is implemented in [104], where PSO-SMC showed better performance compared to other variants. A nonlinear fuzzy control approach tuned using PSO achieved faster convergence and improved control quality [105]. A Grey Wolf Optimizer (GWO)-based adaptive super-twisting sliding mode control approach that effectively reduced chattering and enhanced robustness against disturbances and uncertainties is discussed in [106]. Adaptive PSO (APSO)-tuned nonlinear PID controllers provide improved stabilization performance with faster response, although further improvements in settling time are still required [107]. Whale

Optimization Algorithm (WOA) applications in machine learning and data mining for dimensionality reduction and performance improvement is highlighted in [108]. It compares different WOA variants and identifies key challenges, trends, and future research directions in metaheuristic-based feature selection. A detailed review of the Ant Lion Optimizer (ALO) works on the hunting behavior of ant lions used for solving optimization problems [109]. It covers various ALO variants and applications in machine learning, engineering, and image processing, showing its strong capability in diverse optimization tasks. An improved variant of the Ant Lion Optimization (ALO) algorithm, called SHALO presented in [110]. It is designed to overcome issues like slow convergence and local optima trapping in complex optimization problems. Comparative results show that SHALO significantly outperforms original ALO in terms of accuracy and success rate. A comprehensive review of swarm-based Manta Ray Foraging Optimization (MRFO) algorithm, inspired by manta ray hunting behavior, including its variants and hybrid forms summarized in [111]. It also surveys diverse applications and comparative studies, highlighting MRFO's effectiveness while suggesting future research directions for further improvement. AI-based optimization techniques using Particle Swarm Optimization (PSO) and Differential Evolution (DE) used for designing a hybrid solar PV–hydro–battery system [112]. A memetic algorithm (MA) applied to optimize the LQR controller parameters for an inverted pendulum system and compared with the traditional LQR approach, the results show that the MA-based method achieves superior control performance and effectiveness [113]. Multi-objective optimization design (MOOD) approaches for imbalanced data problems claims that improved predictive performance in both benchmark datasets and real-world applications such as anomaly detection [114]. Selection methods for ensemble systems using optimization techniques such as PSO, ACO, and GA in both mono- and bi-objective forms, show that bi-objective PSO performs best in improving feature diversity and ensemble performance on multiple data sets [115].

The literature review is in conclusion that, most of the intelligent system design approach, the primary goal is to develop efficient and feasible control architecture that satisfies the desired performance criteria. With the increasing complexity of hybrid intelligent paradigms, the fusion of neuro-fuzzy systems with nature inspired swarm-

based optimization algorithms has emerged as an effective approach for enhancing learning, adaptability, and decision-making capabilities. However, there is no universal accepted methodology that suits designing controllers. In recent years, a significant number of advanced swarm optimization techniques are widely proposed to stabilize complex dynamical underactuated systems. Hence from this through review the stabilization of underactuated systems along with controllers the following research gaps are identified.

1.4 Research Gaps

1. Consideration of non-linear effect of friction is present in limited literature. Moreover, non-linearity is majorly undertaken by converting it into linear model.
2. Cart-mass Uncertainty is not fully explored by researchers in the available literature wherein mostly work is emphasized for Time-Varying uncertainties.
3. Scope of improvement for tuning of hybrid controller using evolutionary algorithms.
4. Hybrid controller design for better system performance needs to be explored.
5. Non-linear controller design for underactuated system is limited in literature.
6. Controller's limitations in the field of optimal gain parameter setting, a lesser range of robust control, change of gain setting with time varying conditions.
7. Need of robust controllers in inverted pendulum for handling constraints and random change in motion trajectory.

1.5 Research Objectives

The present research work is primarily motivated to address the need to focus on the following aspects of under actuated systems control.

1. Underactuated system mathematical modelling considering possible non linearities and external disturbances.
2. Design of novel optimal non-linear controllers for underactuated systems.
3. Design of robust controller for performance improvement of underactuated system under uncertain environment.

4. Design of efficient controller for underactuated system using novel hybrid control techniques.

1.6 Research Contributions

The major research contributions of this work, aligned with the stated objectives, are summarized as follows:

1. Performed parametric sensitivity analysis of the CIP system to evaluate the effect of cart mass, pendulum mass, and length variations.
2. Designed a Fractional Order PID (FOPID) controller and optimized its parameters using metaheuristic algorithms (GOA, WCA, and PSO) for improved transient performance and robustness.
3. Developed a hybrid metaheuristic optimization technique for efficient tuning of controller parameters.
4. Developed a hybrid cascaded FOPI–FOPD controller integrated with BLQGC to enhance disturbance rejection, noise attenuation, and system stability.
5. Proposed an ANN-based ANFIS controller tuned using hybrid metaheuristic optimization for achieving adaptive, robust, and high-performance control of nonlinear underactuated systems.

1.7 Organization of Thesis

Chapter 1: Introduction and Motivation

This chapter begins with an introduction to under-actuated systems, discussing their fundamental characteristics, classifications, and mathematical modelling aspects. It provides a detailed analytical background to establish the Cart–Inverted Pendulum model as a classical benchmark problem in control engineering and related domains. The system's dynamic equations and inherent control challenges are thoroughly explained to highlight its practical significance. Additionally, the chapter provides a brief overview of the controllers and optimization techniques used in this research, laying the foundation for the subsequent chapters.

Chapter 2: Modelling and Dynamics of the Cart–Inverted Pendulum System

The chapter begins by introducing the various aspects of the Cart–Inverted Pendulum system and its key subcomponents, explaining its operational mechanism and dynamic behavior. It explores different approaches for stabilizing and controlling the inverted pendulum, highlighting the underlying working principles. Subsequently, a detailed mathematical model of the system is developed, and the corresponding transfer function is derived to facilitate controller design and analysis.

Chapter 3: PID-based Control and Parametric Sensitivity Analysis of Cart–Inverted Pendulum

This chapter presents a comprehensive parametric investigation of the Cart–Inverted Pendulum (CIP) system, emphasizing the control challenges associated with its nonlinear, under-actuated, and inherently unstable dynamics. The strong coupling between cart motion and pendulum angle, along with high sensitivity to system parameter variations, makes stabilization around the upright equilibrium particularly demanding. To analyze these challenges, the nonlinear mathematical model of the CIP system is derived and linearized about the unstable equilibrium point. A classical PID controller is designed and implemented to stabilize the system and to serve as a baseline for performance evaluation. The study systematically examines the effects of variations in key physical parameters—cart mass, pendulum mass, and pendulum length—on transient response characteristics, including rise time, settling time, overshoot, and stability margins. Extensive MATLAB/ Simulink simulations are performed to evaluate system behavior under different parametric conditions. The results demonstrate the sensitivity of the CIP system to parameter perturbations and highlight the limitations of conventional PID control under varying dynamics, thereby motivating the need for more robust and advanced control strategies in subsequent research.

Chapter 4: Metaheuristic Optimization of FOPID Controller for Cart–Inverted Pendulum

This chapter begins with FOPID controller design, incorporating fractional integral and derivative orders to provide additional degrees of freedom in tuning, to enhance

robustness and transient response characteristics of CIP model. Modelling of an FOPID controller includes design of three parameters k_p, k_i, k_d and two orders (μ *and* λ) which are not essentially integer, and it gives extra tunning flexibility as compared to PID controller. Then, the controller parameters are optimally tuned using three population-based metaheuristic algorithms: Particle Swarm Optimization (PSO), Water Cycle Algorithm (WCA), and Grasshopper Optimization Algorithm (GOA). A detailed comparative analysis is carried out using performance indices such as ISE, ITAE, rise time, settling time, and overshoot. Simulation results demonstrate the improved stabilization capability of metaheuristic-optimized FOPID controllers and highlight the relative effectiveness of GOA, WCA, and PSO in solving nonlinear control optimization problems. Finally, the chapter concludes that the GOA-tuned FOPID controllers outperformed the FOPID controllers tuned using PSO and WCA algorithms.

Chapter 5: Hybrid Cascaded FOPI–FOPD–BLQGC Controller for Robust Stabilization of Cart-Inverted Pendulum

This chapter builds upon the previously developed fractional and intelligent control frameworks by introducing an advanced cascaded fractional control architecture for enhanced stabilization of the nonlinear Cart–Inverted Pendulum (CIP) system. It begins by highlighting the limitations of single-loop fractional controllers in achieving simultaneous improvement in transient response, robustness, and disturbance rejection under parametric uncertainties. To address these challenges, a cascaded FOPI–FOPD–BLQGC controller structure is proposed, designed to improve dynamic compensation, noise attenuation, and stability margins. Subsequently, the controller parameters are optimally tuned using a hybrid metaheuristic to ensure global search and faster convergence. The chapter presents a detailed robustness evaluation under impulse disturbances, Gaussian noise injection, and variations in cart mass, pendulum mass, and pendulum length. Finally, comprehensive simulation studies validate the effectiveness of the proposed cascaded fractional framework, demonstrating improved gain and phase margins, reduced overshoot, faster settling time, and superior disturbance rejection compared to FOPI, FOPD, and BLQGC control strategies.

Chapter 6: Hybrid Metaheuristic-Optimized Adaptive Neuro-Fuzzy Controller for Cart–Inverted Pendulum System

This chapter begins with a brief introduction to intelligent control strategies for nonlinear and under-actuated systems, emphasizing the limitations of purely model-based fractional controllers in handling strong nonlinearities and dynamic uncertainties in the Cart–Inverted Pendulum (CIP) system. It then presents the motivation for integrating learning-based techniques with metaheuristic optimization to enhance adaptability, robustness, and control accuracy. The proposed approach develops an ANN-based ANFIS controller that combines the learning capability of Artificial Neural Networks with the rule-based inference structure of fuzzy systems. A hybrid (PSO-ACO) metaheuristic optimization technique is employed to tune the controller parameters efficiently, ensuring improved convergence and minimized training error. Finally, the chapter outlines the validation of the proposed intelligent control framework through comprehensive simulation studies, demonstrating superior transient performance, reduced steady-state error, and enhanced disturbance rejection compared to PID and FOPID controllers.

Chapter 7: Conclusions and Future Scope of Work

This chapter concludes the research work presented in the thesis by summarizing the major findings and key achievements. It highlights the effectiveness of the proposed control strategies in improving stability, robustness, and transient performance of the Cart–Inverted Pendulum system. The overall contributions of parametric analysis, fractional-order control, intelligent hybrid methods, and cascaded architecture are summarized. In addition, the chapter identifies existing limitations and open challenges associated with nonlinear and under-actuated systems. Finally, potential directions for future research are presented, including the integration of more advanced controllers and optimization techniques to further enhance system performance and address unresolved issues.

1.8 Concluding Remarks

This introduction and motivation chapter start with the background for the research work and outlines the underactuated systems, with particular emphasis on the cart–inverted pendulum (CIP) system along with the limitations of conventional control and the need for advanced, robust, and intelligent control strategies was provided to establish the research background are reviewed. Finally, the chapter outlined the key research objectives and the overall structure of the thesis, thereby laying a clear foundation for subsequent chapters focused on controller design, optimization techniques, and performance evaluation of the proposed control strategies.

Chapter 2

Modelling and Dynamics of the Cart–Inverted Pendulum System

2.1 Introduction

The Cart–Inverted Pendulum (CIP) system is widely regarded as a representative nonlinear benchmark for the design and evaluation of advanced control strategies and meta-heuristic optimization techniques [2]. Its significance arises from the complex dynamic interactions between its subsystems and its close resemblance to a variety of real-world engineering applications [6]. The system comprises a rigid pendulum mounted at the center of a cart that is free to move along a horizontal track. A single external force applied to the cart by a DC motor actuator serves as the control input, which must simultaneously regulate both the translational motion of the cart and the angular displacement of the pendulum.

The fundamental operation of the CIP system is governed by the strong coupling between the cart's linear motion and the pendulum's rotational dynamics. When the pendulum deviates from its upright position, gravitational forces generate a destabilizing torque, which must be counteracted by appropriately accelerating the cart [8]. This indirect control mechanism, in which the pendulum is stabilized through cart motion, highlights the system's underactuated nature. The interdependence between translational and rotational forces introduces significant nonlinearity, making the mathematical modelling and controller design is inherently challenging [3].

Accurate mathematical modelling of the CIP system is essential for the development of effective controllers and the reliable evaluation of optimization algorithms. The correctness and performance of control strategies depend heavily on how precisely the system dynamics are captured [5]. In this chapter, the nonlinear dynamic behaviour of the CIP system is formulated by considering the balance of horizontal forces and moments, as well as frictional effects, acting on both the cart and the pendulum. The resulting model establishes the relationship between the applied force (F) and the two primary system outputs: cart displacement $x(t)$and pendulum angular position $\theta(t)$.

Due to the complexity of the nonlinear equations, the model is subsequently linearized around the unstable equilibrium point corresponding to the upright pendulum position. This linearization simplifies the analysis while preserving the essential system dynamics required for controller design [13] [14]. Finally, the system is represented in both transfer function and state-space forms, which serve as fundamental tools for the design, implementation, and performance evaluation of the proposed control and optimization techniques in the subsequent chapters.

The chapter outline is as follows. Section 2.2 explains the internal dynamics of the CIP system, which are essential to designing efficient controllers. Section 2.3 details the system's mathematical modelling and presents its transfer function. Subsequently, Section 3.4 presents the state-space model of the CIP system. Finally, Section 2.5 presents the concluding remarks.

2.2 Internal Dynamics of CIP System

To understand the dynamic behaviour of the Cart–Inverted Pendulum (CIP) system and the interactions among various forces, a cart inverted pendulum control system experimental setup available in the laboratory, is presented in Figure 2.1.

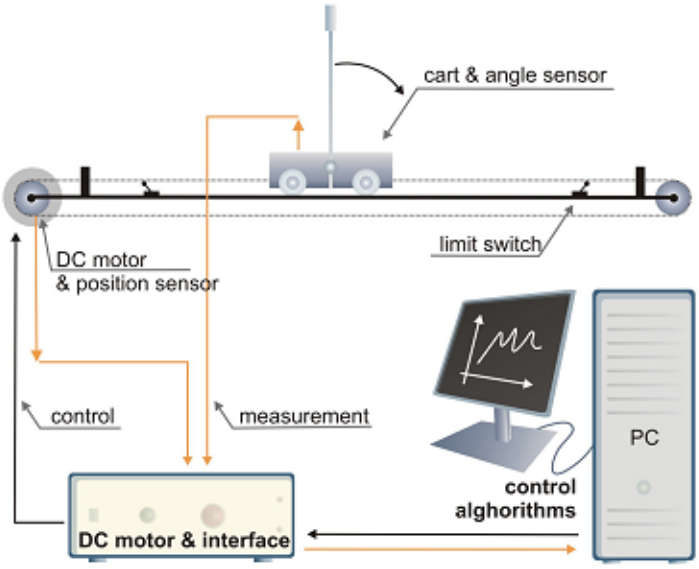

Figure 2.1 Cart Inverted Pendulum Control System

The system is modelled using the Newton–Euler approach, which is widely used to derive equations of motion from force and torque balance. The CIP system consists of a rigid pendulum of length l with a point mass m attached at its end. This pendulum is pivoted at the center of a cart of mass M, which is allowed to move horizontally along a track.

An externally applied force controls the motion of the cart F, which drives the cart forward and backward. This horizontal movement directly affects the pendulum's behaviour. When the cart accelerates, it generates an inertial effect that causes the pendulum to rotate about its pivot. Therefore, the translational motion of the cart and the rotational motion of the pendulum are strongly coupled. This coupling is the key feature that makes the CIP system complex and challenging for analysis and control.

Due to this interaction, the applied force F performs a dual role. It not only determines the position of the cart but also influences the angular displacement and velocity of the pendulum. This clearly reflects the under-actuated nature of the system, in which a single control input is responsible for two dynamic variables. The motion generated by this interaction produces the required angular velocity, which helps swing the pendulum from its stable downward position to its unstable upright position. Achieving and maintaining this upright position requires precise balancing between different forces acting within the system, including gravitational, inertial, and reaction forces.

The operation of the CIP system is primarily influenced by two main forces: the externally applied control force $u(t)$ and the gravitational force g. The gravitational force acts downward on the pendulum mass and tends to pull it away from the upright position, thereby creating instability. To counteract this effect, the control force must generate sufficient inertial force through cart acceleration. In addition to these primary forces, other forces also play an important role in the system dynamics. A normal reaction force acts at the contact interface between the cart and the ground, as well as at the pivot joint connecting the pendulum and the cart. An inertial force is generated due to the horizontal acceleration of the cart, which contributes significantly to stabilizing

the pendulum in its upright position. Furthermore, frictional forces between the cart and the ground oppose motion and can affect the system's dynamic response.

The CIP system has two equilibrium states: a stable hanging position and an unstable upright position. Initially, the pendulum remains in the stable downward position. To achieve control objectives, it must first be swung up to the upright position and then stabilized with minimum oscillations. This swing-up and stabilization process is challenging due to the strong coupling between the cart's displacement and the pendulum's angle. Any movement of the cart directly affects the pendulum motion, and vice versa, making the controller design more complex. Controller tuning becomes more monotonous due to the interdependence between the pendulum angle and the cart.

2.3 Transfer Function Representation of CIP Dynamics

The system parameters used for modelling and analysis are defined based on a Feedback (UK) make laboratory setup. The mass of the cart M is 2.4 kg, and the mass of the pendulum m is 0.2 kg. The length of the pendulum l is 0.3 m. The coefficient of friction B between the cart and the surface is 0.05 Ns/m, and the moment of inertia of the pendulum is 0.009 kg·m². The acceleration due to gravity, g, is taken as 9.8 m/s². The control input u varies within the range of ±24 N. The cart displacement x is limited to ±0.4 m, while its velocity $\dot{x}$ is expressed in m/s. The pendulum angle ϕ is measured with respect to the vertical axis, and its angular velocity $\dot{\phi}$ is expressed in rad/s. These parameters are used to accurately represent the system dynamics and facilitate subsequent modeling, simulation, and controller design.

The cart's position describes the system's motion $x(t)$ and the angular displacement of the pendulum $\theta(t)$, as illustrated in free body diagram shown in Figure 2.2.

The total external force applied to the system is balanced by the dynamic forces generated due to the motion of both the cart and the pendulum. Specifically, it is opposed by the inertial force due to the acceleration of the cart mass and the horizontal component of the pendulum's acceleration.

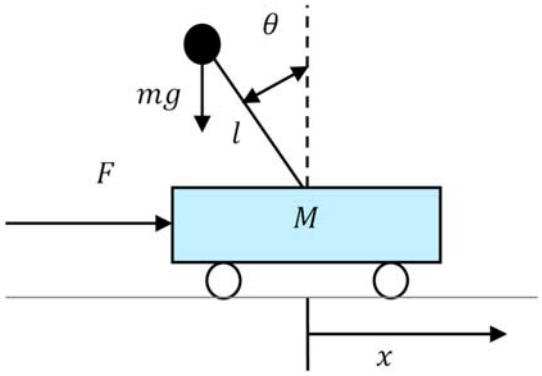

Figure 2.2 Free Body Diagram of Cart-Inverted Pendulum System

The equation 2.1 provides the force balance, which is the basis for deriving the system's equations of motion.

$$M\frac{d^2}{dt^2}x + m\frac{d^2}{dt^2}x_m = F \tag{2.1}$$

where the corresponding movement for the pendulum mass in x and y directions, is given by equation (2.2)

$$x_m = (lsin\theta + x) and,\ y_m = (lcos\theta) \tag{2.2}$$

By substituting the parameter values from equation (2.2) into the respective terms of equation (2.1), the resulting expression is obtained as equation (2.3).

$$M\frac{d^2}{dt^2}x + m\frac{d^2}{dt^2}(lsin\theta + x) = F \tag{2.3}$$

Further simplification is carried out by solving the following equations (2.4)

$$(M+m)\ddot{x} - (ml)sin\theta\dot{\theta}^2 + \left(mlcos\theta\ddot{\theta}\right) = F \tag{2.4}$$

The torque balance equations of the system can be derived by considering the moment produced by the vertical (y direction) component of the force, along with the effect of the pendulum length. These include the torque acting on the pendulum mass due to its acceleration and the torque generated by the gravitational force g. The resulting equations are given as equation (2.5).

$$(F_x \cos\theta\, l) - \left(F_y \sin\theta\, l\right) = (mg \sin\theta\, l) \tag{2.5}$$

The components of the external forces can be expressed as equations (2.6) and (2.7).

$$F_x = m\frac{d^2}{dt^2}x_m = m[\ddot{x} - l\sin\theta\,\dot{\theta}^2 + l\cos\theta\,\ddot{\theta} \tag{2.6}$$

$$F_y = m\frac{d^2}{dt^2}y_m = -m[l\cos\theta\,\dot{\theta}^2 + l\sin\theta\,\ddot{\theta}] \tag{2.7}$$

By substituting equations (2.6) and (2.7) into the torque equation (2.5), the resulting expression is obtained as equation (2.8).

$$m\ddot{x}\cos\theta + ml\ddot{\theta} = mg\sin\theta \tag{2.8}$$

Further, the transfer functions for the cart position and the pendulum angle are given by equations (2.9) and (2.10), respectively.

$$H_{cart} = \frac{X(s)}{F(s)} = \frac{0.132(s^2+0.0378\,s-12.98)}{0.339(s^3+0.058s^2-13.27s-0.253)} \tag{2.9}$$

$$H_{angle} = \frac{\theta(s)}{F(s)} = \frac{0.0874s^2}{0.339(s^3+0.058s^2-13.27s-0.253)} \tag{2.10}$$

2.4 State Space Representation of CIP Dynamics

The transfer function model establishes only the relationship between the system's input and output and does not provide information about the system's internal states. This limitation makes it less suitable for advanced controller design, particularly for nonlinear and under-actuated systems such as the Cart–Inverted Pendulum (CIP). Therefore, to design the Cascaded fractional order proportional integral- fractional order proportional derivative-backstepping linear quadratic Gaussian controller (FOPI-FOPD-BLQGC) and intelligent controller, a state-space model is developed.

The state-space representation provides a complete description of the system by including all relevant internal states, such as cart position, cart velocity, pendulum angle, and angular velocity. These states play a crucial role in maintaining the pendulum in its upright position. In intelligent control, the controller's performance depends on learning the relationship between these system states and the required control action. Hence,

access to internal state variables becomes essential for accurate training and effective control.

Moreover, the state-space model is well-suited to represent the nonlinear, coupled dynamics of the under-actuated CIP system. It enables better observation and control of internal behaviour, which supports the development of adaptive and intelligent control strategies. As a result, the state-space approach offers greater flexibility and effectiveness for the design of hybrid and intelligent controllers than the transfer function model. The force balance dynamics from Figure 2.2 are given as equations (2.11) and (2.12).

$$m\frac{d^2}{dt^2}\,(x - lsin\theta) = -F_y \tag{2.11}$$

$$m\frac{d^2}{dt^2}\,(lcos\theta) = F_x - mg \tag{2.12}$$

The torque (moment) balance equation about the pendulum's center of mass with P_i (Moment of inertia of the pendulum (pole) about its center of gravity) and τ_{net}(net torque acting on the pendulum about its center of gravity), given in equations (2.13)

$$\tau_{net} = P_i\frac{d^2\theta}{dt^2} \tag{2.13}$$

The rotating dynamic equation of the pendulum is further derived as equation (2.14), where Pen_d represents the damping coefficient of the pendulum.

$$-F_y cos\theta + F_x sin\theta - Pen_d\dot{\theta} = P_i\ddot{\theta} \tag{2.14}$$

From equations (2.11) and (2.12), the pole equation is derived as equation (2.5).

$$(-mlcos\theta)\ddot{x} + (P_i + ml^2)\ddot{\theta} + Pen_d\ddot{\theta} - mglsin=0 \tag{2.15}$$

The net horizontal force in the cart's dynamic equation is denoted as equation (2.16).

$$F_{xnet} = M\ddot{x} \tag{2.16}$$

The net force could be written in expanded form as equations (2.17) and (2.18), where C_b is the cart damping coefficient.

$$F + F_y - C_b\dot{x} = M\ddot{x} \tag{2.17}$$

$$(M+m)\ddot{x} + C_b\dot{x} - (mlcos\theta)\ddot{\theta} + (mlsin\theta)(\dot{\theta})^2 = F \tag{2.18}$$

Equations (2.15) and (2.18), which denote the nonlinear system behavior, are combined and stated as equation (2.19) in the state-space model.

$$\begin{bmatrix}\ddot{x}\\ \ddot{\theta}\end{bmatrix} = \frac{1}{\Delta}\begin{bmatrix}-mlcos\theta & -(P_i+ml^2)\\ -(M+m) & -mlcos\theta\end{bmatrix}\begin{bmatrix}mglsin\theta - Pen_d\dot{\theta}\\ F-(mlsin\theta)(\dot{\theta})^2 - C_b\dot{x}\end{bmatrix} \tag{2.19}$$

Where, $\Delta = m^2l^2cos\theta - (M+m)(P_i+ml^2)$;

The state attributes of the linear dynamical method are selected as $X, \dot{X}, \theta, \dot{\theta}$, where x is the cart position and θ is the pendulum angle that is denoted in the following equations (2.20) and (2.21).

$$\dot{X} = AX + Bu \tag{2.20}$$

$$Y = X^T \tag{2.21}$$

The state trajectory is considered $X = [x_1, x_2, x_3, x_4]^T = [x, \dot{x}, \theta, \dot{\theta}]$ and linearizing the non-linear differential equation for the CIP system at the unstable balance position $\theta = 0$ and by assuming $sin\,\theta \approx \theta, cos\,\theta \approx 1, \dot{\theta}^2 \approx 0$. Therefore, the linearized state-space model can be expressed as equation (2.22).

$$\dot{X} = \begin{bmatrix}0 & 1 & 0 & 0\\ 0 & \frac{(P_i+ml)C_b}{\Delta} & \frac{-m^2l^2g}{\Delta} & \frac{mlPen_d}{\Delta}\\ 0 & 0 & 0 & 1\\ 0 & \frac{mlC_b}{\Delta} & \frac{-mlg(M+m)}{\Delta} & \frac{Pen_d(M+m)}{\Delta}\end{bmatrix}\begin{bmatrix}x_1\\ x_2\\ x_3\\ x_4\end{bmatrix} + F\begin{bmatrix}0\\ -\frac{(P_i+ml^2)}{\Delta}\\ 0\\ -\frac{ml}{\Delta}\end{bmatrix} \tag{2.22}$$

Now, substitute the Feedback (UK) make laboratory CIP system parameter values given in Section 2.3 into equation (2.22). The final state-space matrices are calculated as in equations (2.23), (2.24), (2.25), and (2.26).

$$A = \begin{bmatrix}0 & 1 & 0 & 0\\ 0 & -0.02 & 0.22 & -0.0013\\ 0 & 0 & 0 & 1\\ 0 & -0.013 & 6.632 & -0.034\end{bmatrix} \tag{2.23}$$

$$B=\begin{bmatrix}0\\0.388\\0\\0.257\end{bmatrix} \tag{2.24}$$

$$C=\begin{bmatrix}1 & 0 & 0 & 0\\0 & 0 & 1 & 0\end{bmatrix} \tag{2.25}$$

$$D = [0] \tag{2.26}$$

The controllability analysis confirms that the CIP system is fully controllable, as the controllability matrix satisfies the full-rank condition. Similarly, the output matrix, including cart position and pendulum angle, is necessary to ensure full observability for effective state estimation and implementation of Backstepping Linear Quadratic Gaussian Controller (BLQGC). The derived state-space model provides a compact, systematic representation of the system dynamics, enabling the efficient implementation of modern control strategies.

2.5 Concluding Remarks

This chapter presented the modelling and dynamic analysis of the Cart–Inverted Pendulum (CIP) system. The interaction between cart motion and pendulum dynamics was explained by considering the effects of gravitational, inertial, and frictional forces. A nonlinear mathematical model was developed using the Newton–Euler approach, highlighting the system's coupled, unstable nature. The model was then linearized around the upright equilibrium position to simplify analysis. Both transfer function and state-space representations were derived, providing a basis for controller design. The controllability analysis confirms that the CIP system is fully controllable, as the controllability matrix satisfies the full-rank condition. Similarly, the output matrix, including cart position and pendulum angle, is necessary to ensure full observability for effective state estimation and implementation of BLQGC. The derived state-space model provides a compact, systematic representation of the system dynamics, enabling the efficient implementation of modern control strategies.

The developed mathematical model will be used in subsequent chapters to design and evaluate advanced control strategies.

Chapter 3

PID-based Control and Parametric Sensitivity Analysis of Cart–Inverted Pendulum*

3.1 Introduction

A nonlinear, unstable inverted pendulum system exhibits real-time issues when implemented in industrial applications, for example, behaviour that changes with varying operational conditions, external disturbances, and physical constraints on some variables [11].

The system dynamics of the inverted pendulum-based nonlinear plant can cause instability if the load mass undergoes a sudden change. This load mass could exhibit constant or time-dependent changes (i.e., changes that vary with time) [116]. The cart's mass can also be changed by adding a load to it, even after the system becomes stable. These cart mass changes could also vary with time [117]. There are two more dominating factors, pendulum length and rail length, which can modify swing-up accuracy and stability of the cart-inverted pendulum [118]. In this chapter, the variation in the parameters of a cart-inverted pendulum system, such as pendulum mass, pendulum length, and cart mass, which can alter the system's dynamics, is analysed. The mathematical modeling of the Cart–Inverted Pendulum (CIP) system used for this controller analysis presented in this chapter has already been discussed in detail in Chapter 2.

The brief outline of the chapter is as follows. Section 3.2 provides an overview of the PID control techniques implemented for parametric uncertainty analysis. Section 3.3 presents results and discussion of detailed cases involving model parameter variation, including cart mass, pendulum mass, and pendulum length. Finally, Section 3.4 presents the concluding remarks of the chapter.

---

* *This chapter was published in Modern Electronics Devices and Communication Systems: Select Proceedings of* MEDCOM 2021, in the *Lecture Notes in Electrical Engineering* series, Vol. 948, pp. 217–230, *Springer Singapore, doi: h10.1007/978-981-19-6383-4_17*

3.2 Implemented Control Model

The implemented control model for the Cart–Inverted Pendulum (CIP) system uses a dual-loop PID control structure, as illustrated in Figure 3.1. The objective of this control architecture is to regulate the cart position simultaneously $\boldsymbol{x(t)}$ and stabilize the pendulum angle $\boldsymbol{\theta(t)}$ in its upright position.

The control system consists of two independent PID controllers. The first PID controller is responsible for tracking the reference cart position, where the error is generated by comparing the desired cart position with the actual output ($\boldsymbol{t}$). This error signal is processed through the PID controller to generate a corrective control action.

Similarly, the second PID controller regulates the pendulum angle, ensuring it remains balanced around the vertical equilibrium position. The error between the reference pendulum angle and the measured angle $\boldsymbol{\theta(t)}$ is fed to the second PID controller, which produces another control signal. The outputs of both PID controllers are combined by a summation block, yielding a unified control input to the CIP system. This combined control effort ensures coordinated action between position tracking and pendulum stabilization.

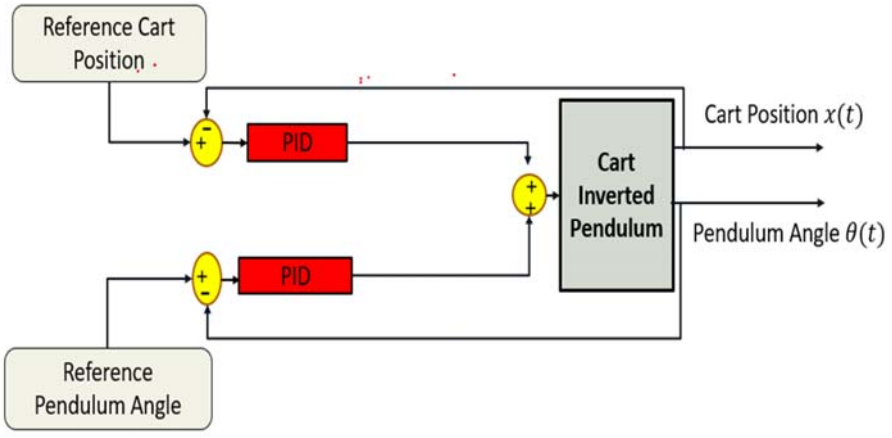

Figure 3.1 Implemented Dual Loop PID Controllers for CIP System

The PID controller implemented for both loops is described by equations (3.1) and (3.2).

$$u(t)_{p=} k_{p1} e_p(t) + k_{i1} \int e_p(t) + k_{d1} \frac{d}{dt} e_p(t) \tag{3.1}$$

$$u(t)_{\emptyset} = k_{p2}e_{\emptyset}(t) + k_{i2}\int e_{\emptyset}(t) + k_{d2}\frac{d}{dt}e_{\emptyset}(t) \quad (3.2)$$

Where $e_{\emptyset}(t)$ is angle error and $e_p(t)$ is cart position error , $u(t)_p$ and $u(t)_{\emptyset}$ are the control signals from the position and angle loops, respectively. k_{p1} and k_{p2} are proportional coefficients for the position and angle, k_{i1} and k_{i2} are integral coefficients for the position and angle, k_{d1} and k_{d2} These are derivative coefficients for the position and angle.

The controller tuning becomes more tedious because the dynamics of the pendulum angle and cart displacement are interdependent. Any alteration to a controller parameter will modify the cart's position and the pendulum angle.

3.3 Results and Discussion

The performance of the Cart–Inverted Pendulum (CIP) system is evaluated based on time-domain response, including rise time ($\boldsymbol{t_r}$), peak time, maximum overshoot ($\boldsymbol{M_p}$), settling time ($\boldsymbol{t_s}$), and steady-state error ($\boldsymbol{e_{ss}}$). The three cases of parameter variation are also evaluated by varying the cart mass ($\boldsymbol{m}$), pendulum mass ($\boldsymbol{M}$), and length ($\boldsymbol{l}$). These variations can significantly influence system stability and control performance. The PID controller gains for the pendulum angle and cart position loop are given below in Table 3.1.

Table 3.1 PID Controller's Gain Parameters

PID1 (Cart Position Loop)			**PID2 (Pendulum Angle Loop)**		
$\boldsymbol{k_{P1}}$	$\boldsymbol{k_{I1}}$	$\boldsymbol{k_{D1}}$	$\boldsymbol{k_{P2}}$	$\boldsymbol{k_{I2}}$	$\boldsymbol{k_{D2}}$
167	100	70	170	100	65

This analysis will provide valuable insight into the controller's robustness and reliability under real-time operating conditions. It will also justify the need for advanced control strategies over a simple, trusted PID controller in uncertain situations.

3.3.1 Transient Response of PID Controller CIP System

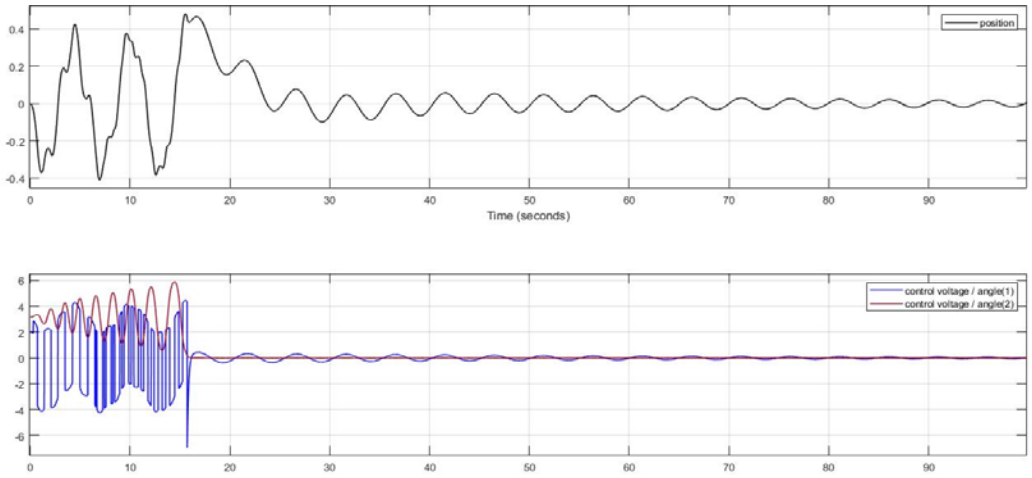

Figure 3.2 Transient Response of PID-Tuned CIP System

Table 3.2 Transient Parameters of PID-Tuned CIP System

Parameter	Cart Position	Control Voltage	Pendulum Angle
Rise Time $(t_r)sec$	8	3	4
Peak Time $(t_p)sec$	12	16	14
Max Overshoot (M_p)	~45%	~5 (abs.)	~6 (abs.)
Settling Time $(t_s sec)$	40	25	25
Steady-State Error (e_{ss})	≈ 0	≈ 0	≈ 0

The dynamic response of the CIP system, shown in Figure 3.2 and summarized in Table 3.2, exhibits underdamped behaviour. The position response rise time of approximately 7 seconds and a peak overshoot of nearly 45%. The system reaches its peak around 11 seconds and settles within 40 seconds, while maintaining negligible steady-state error. In contrast, the pendulum angle (angle 2) shows a slightly slower rise time of 4 seconds with a higher peak magnitude (≈6), reflecting increased sensitivity in pendulum stabilization. The controller effort (angle 1) demonstrates a faster initial response with a rise time of about 3 seconds. Still, it exhibits significant oscillations and high control peaks (approx. 5), indicating aggressive control action during the transient phase. Overall, although stability is achieved, high oscillations and overshoot highlight the need for improved control strategies.

3.3.2 Parametric Variation Sensitivity Analysis

In real-time applications, parameters such as the cart pendulum ($\boldsymbol{m}$), are not always constant and may undergo sudden or time-varying changes, leading to instability in the nonlinear plant dynamics. Similarly, the cart mass ($\boldsymbol{M}$), can vary due to the addition or removal of payloads, even after the system has achieved a stable operating condition, thereby affecting the overall system response. In addition to mass variations, the pendulum length ($\boldsymbol{l}$) also plays a crucial role in determining the system's swing-up characteristics and stabilization capability. These parameters directly impact the system's inertia and dynamic response, making the control task more challenging.

3.3.2.1 Variable Pendulum Mass ($\boldsymbol{m}$)

Five different values of pendulum mass (0.15kg, 0.205kg, 0.215kg, 0.22kg, 0.225kg, and 0.25kg) are considered here to evaluate the effectiveness of the PID controller in CIP stabilization. The corresponding cart position, pendulum angle, and controller effort signal are depicted in Figures 3.3-3.7 and summarized in Tables 3.3-3.5.

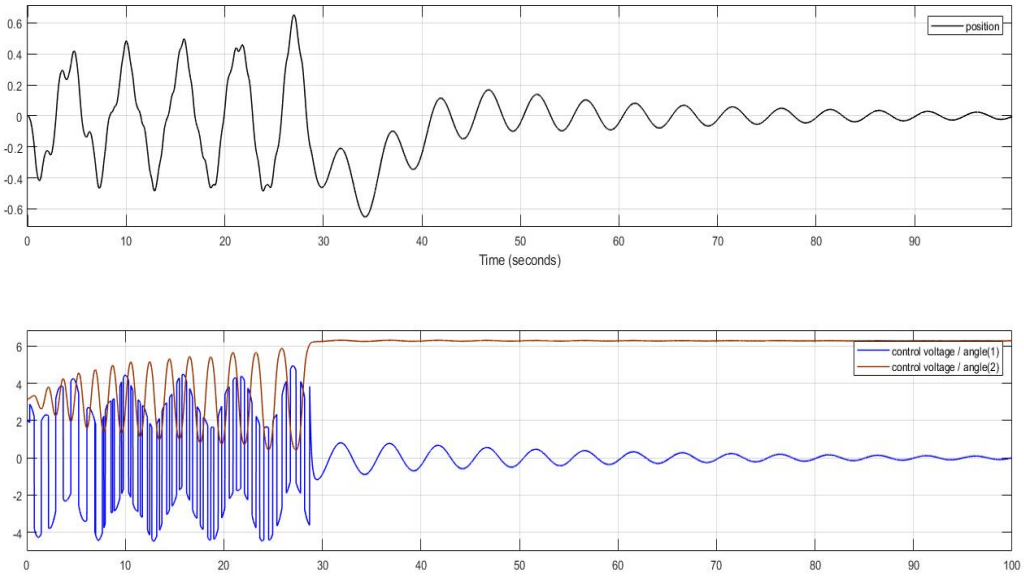

Figure 3.3 Transient Response of PID-Tuned CIP System with $m = 0.15kg$

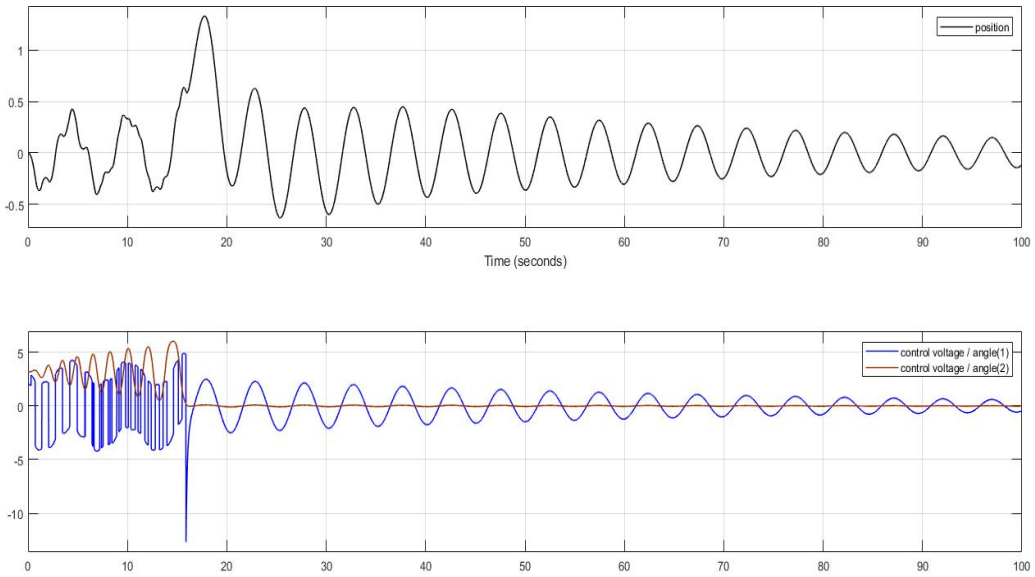

Figure 3.4 Transient Response of PID-Tuned CIP System with $m = 0.205kg$

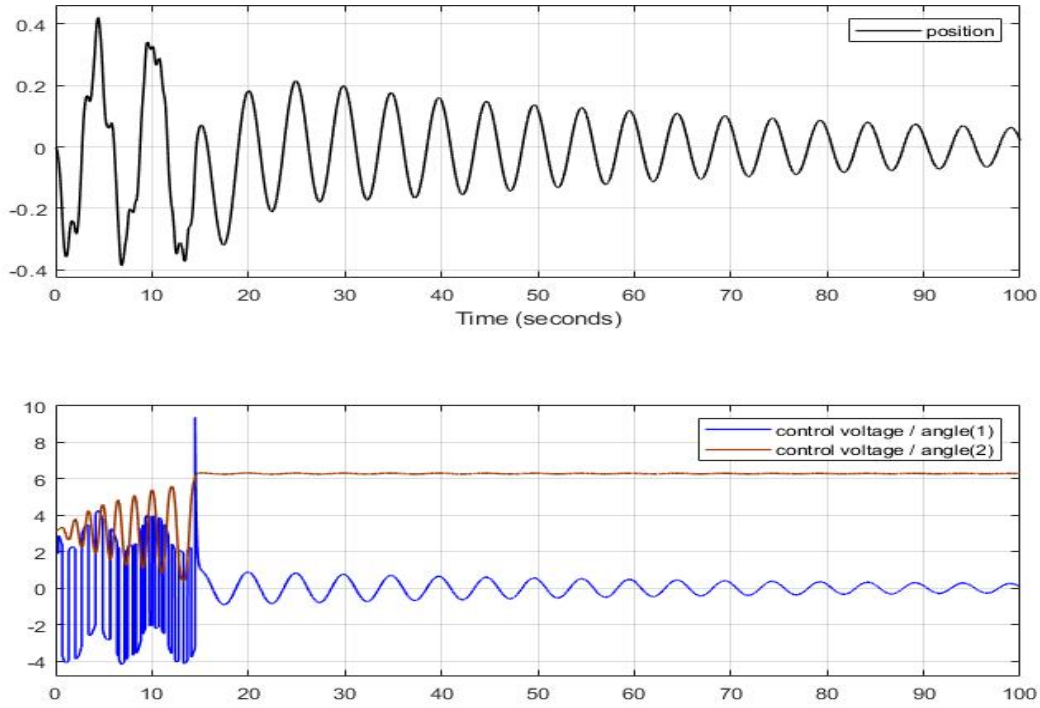

Figure 3.5 Transient Response of PID-Tuned CIP System with $m = 0.215kg$

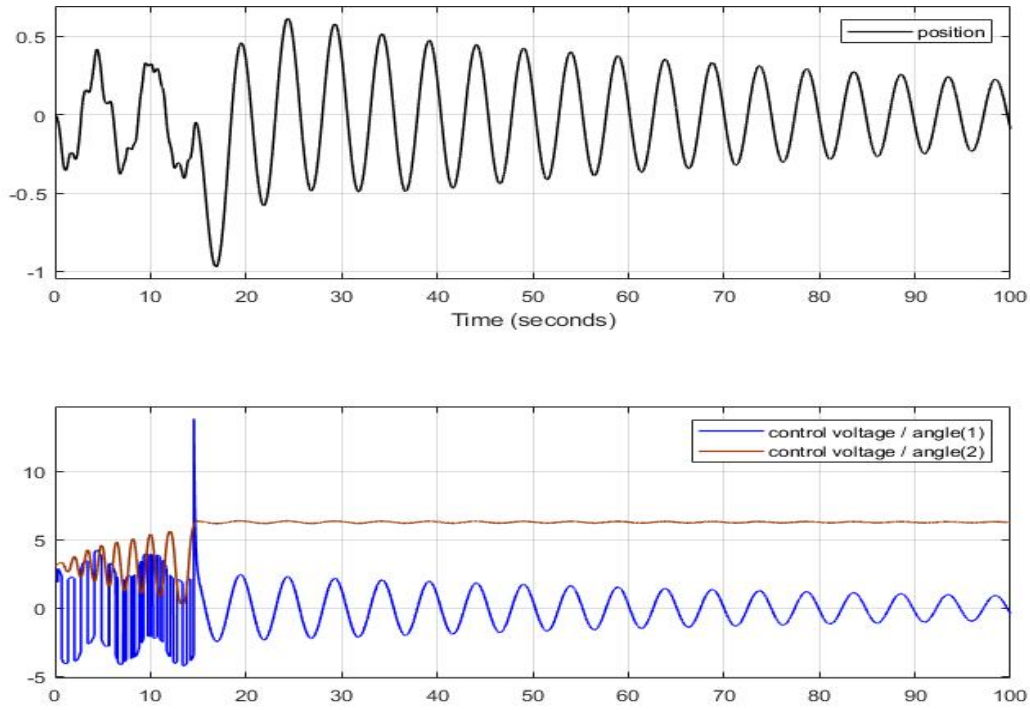

Figure 3.6 Transient Response of PID-Tuned CIP System with $m = 0.22kg$

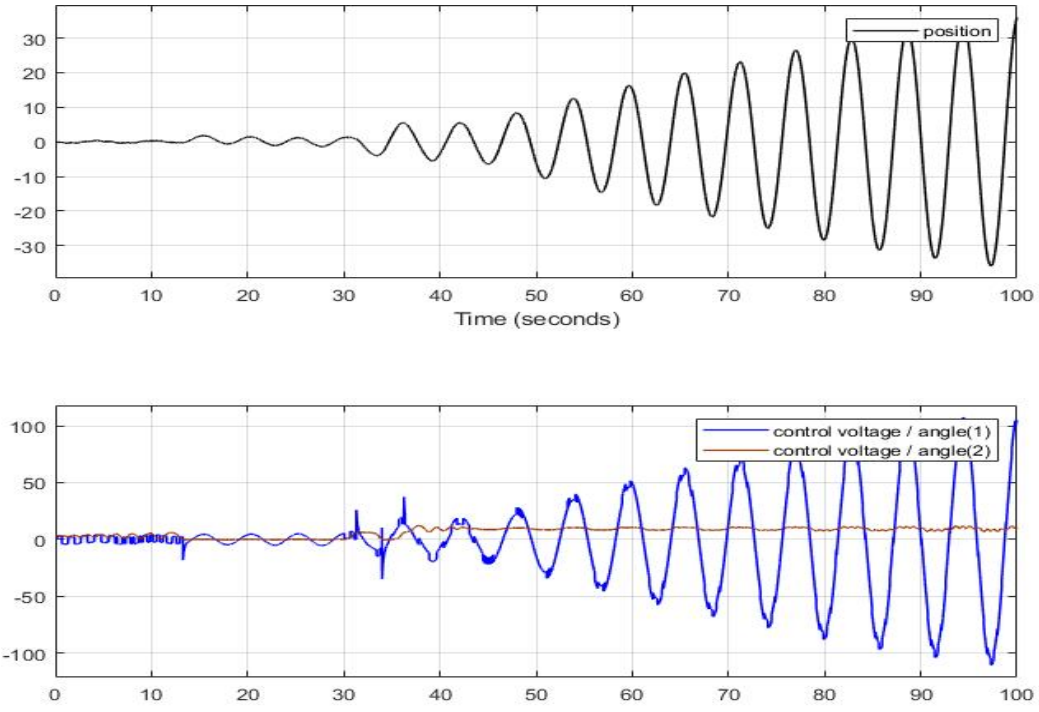

Figure 3.7 Transient Response of PID-Tuned CIP System with $m = 0.225kg$

Table 3.3 Cart Position Response Comparison of Five Values Pendulum Mass

Case	t_r **sec**	t_p **sec**	M_p	t_s **sec**	e_{ss}	**Stability**
Case 1 ($\boldsymbol{m = 0.15\ kg}$)	8	12	45%	40	≈ 0	Stable (oscillations decay)
Case 2 ($\boldsymbol{m = 0.205\ kg}$)	9	18	70%	50	≈ 0	Stable (slow) (high oscillations)
Case 3 ($\boldsymbol{m = 0.215\ kg}$)	8	25	80%	Not fully settled	Small	Marginally Stable (sustained oscillations)
Case 4 ($\boldsymbol{m = 0.22\ kg}$)	10	20	60%	Not settled	Large	Unstable (oscillations not decaying)
Case 5 ($\boldsymbol{m = 0.225\ kg}$)	—	—	Very high	Not applicable	Large	Highly Unstable (diverging response)

Table 3.4 Pendulum Angle Response Comparison of Five Values Pendulum Mass

Case	t_r **sec**	t_p **sec**	M_p	t_s **sec**	e_{ss}	**Stability**
Case 1 ($\boldsymbol{m = 0.15\ kg}$)	3–4	12–14	6	20–25	≈ 0	Stable
Case 2 ($\boldsymbol{m = 0.205\ kg}$)	3–4	14	6	25–30	≈ 0	Stable
Case 3 ($\boldsymbol{m = 0.215\ kg}$)	3–4	12	6	Settles	≈ 0	Stable
Case 4 ($\boldsymbol{m = 0.22\ kg}$)	4–6	15	6	Not settled	Large	Marginal/ Unstable
Case 5 ($\boldsymbol{m = 0.225\ kg}$)	—	—	Increasing	Not applicable	Infinite	Highly Unstable

Table 3.5 Control Signal Response Comparison of Five Values Pendulum Mass

Case	t_r **sec**	t_p **sec**	M_p	t_s **sec**	e_{ss}	**Stability**
Case 1 ($\boldsymbol{m = 0.15\ kg}$)	2–3	14–16	5	20–25	≈ 0	Stable
Case 2 ($\boldsymbol{m = 0.205\ kg}$)	2–3	16	5–6	25–30	≈ 0	Stable
Case 3 ($\boldsymbol{m = 0.215\ kg}$)	2–3	15	4–5	Not fully settled	Small	Marginally Stable
Case 4 ($\boldsymbol{m = 0.22\ kg}$)	3–5	15	>10	Not settled	Large	Unstable (large spike)
Case 5 ($\boldsymbol{m = 0.225\ kg}$)	—	—	>100	Not applicable	Infinite	Highly Unstable (diverging)

The transient response of the Cart–Inverted Pendulum (CIP) system varies significantly with parameter changes, highlighting the PID controller's sensitivity. In Case 1, the system shows stable behavior with moderate overshoot and acceptable settling time. As the parameter increases (Case 2), overshoot and oscillations increase, though stability is maintained. Case 3 exhibits marginal stability with sustained oscillations, while Case 4 becomes unstable as oscillations do not decay. In Case 5, the system exhibits complete instability, with divergent responses. These results demonstrate that PID control is not robust to variations in system parameters.

3.3.2.2 Variable Pendulum Length (l)

The pendulum length is varied to five values (0.25m, 0.28m, 0.29m, 0.32m, and 0.34m) to test the PID controller's robustness to it. The corresponding responses of cart position, pendulum angle, and controller effort signal are depicted in Figures 3.8-3.12 and summarized in Tables 3.6-3.8.

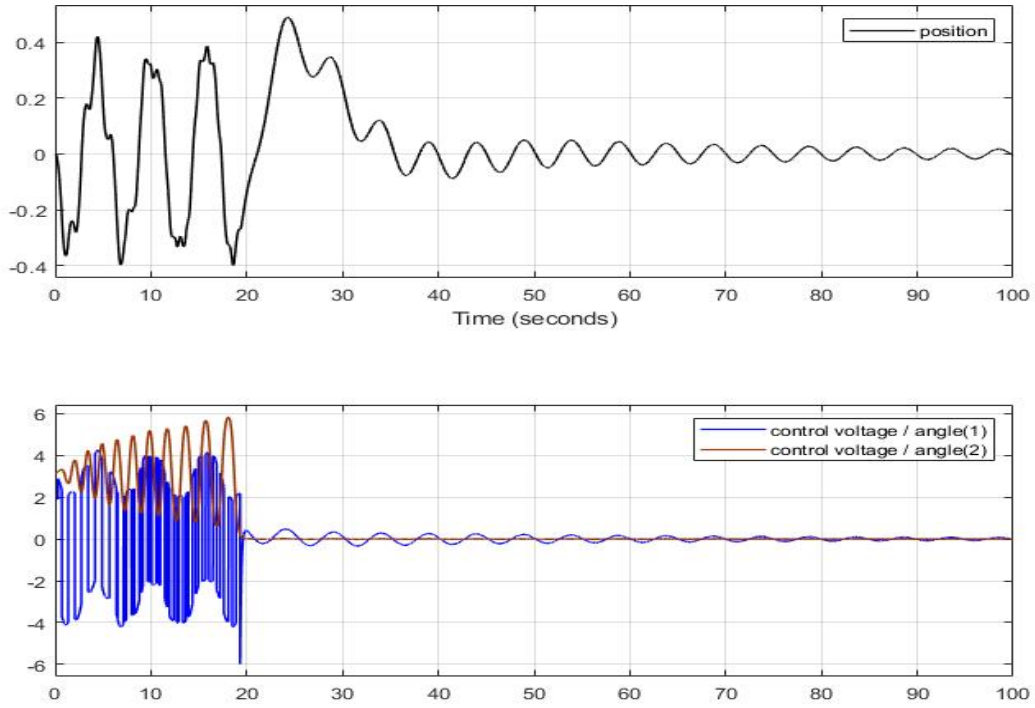

Figure 3.8 Transient Response of PID-Tuned CIP System with $l = 0.27m$

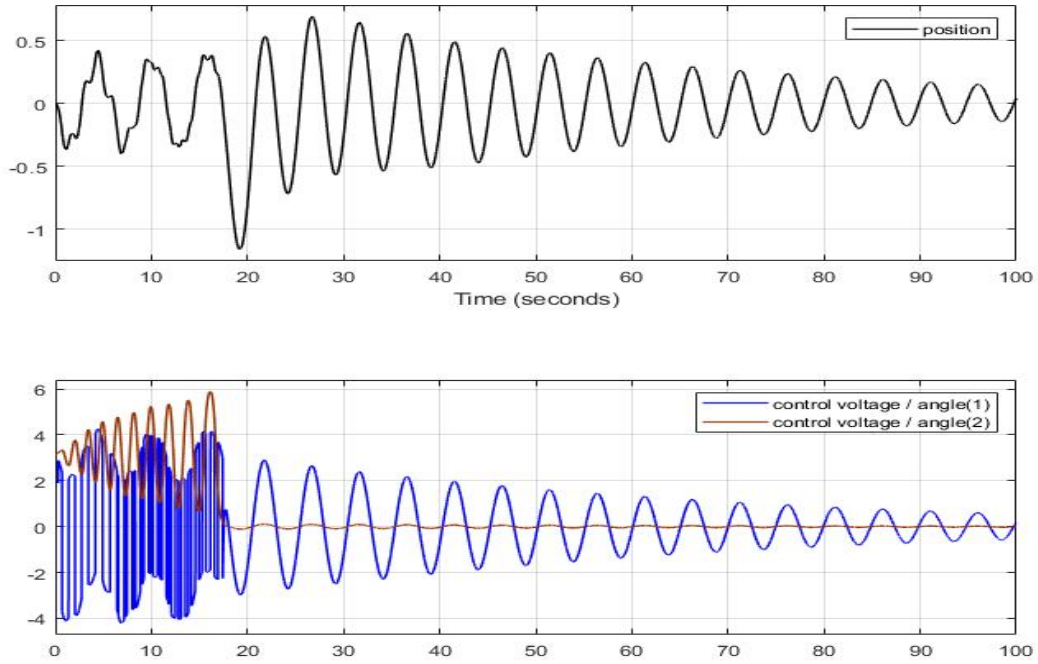

Figure 3.9 Transient Response of PID-Tuned CIP System with $l = 0.28m$

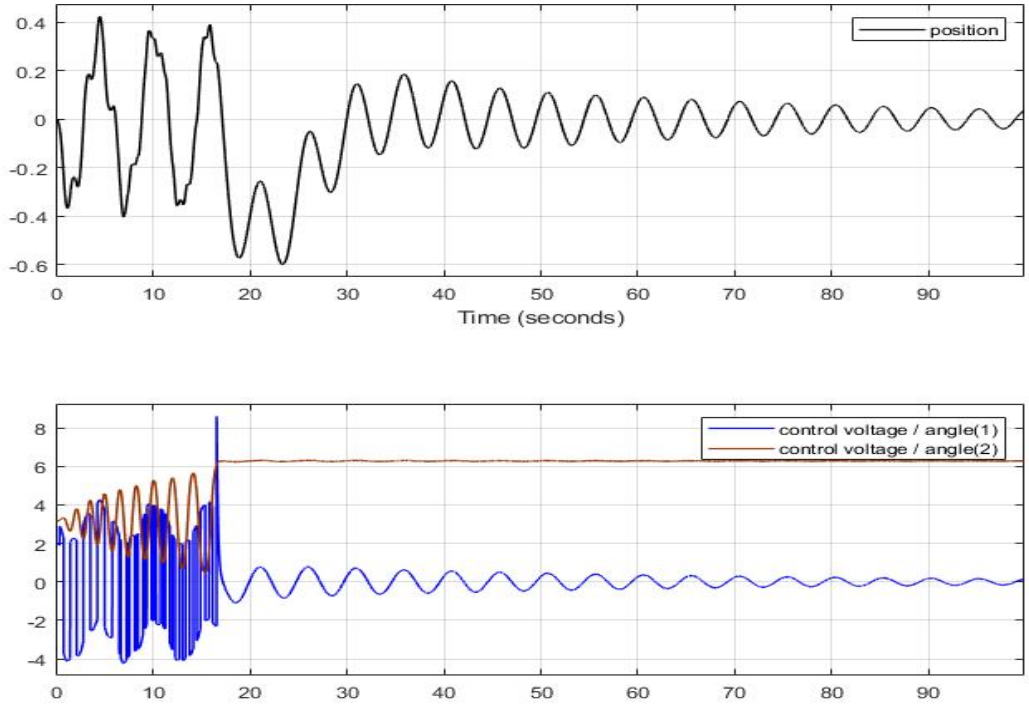

Figure 3.10 Transient Response of PID-Tuned CIP System with $l = 0.29m$

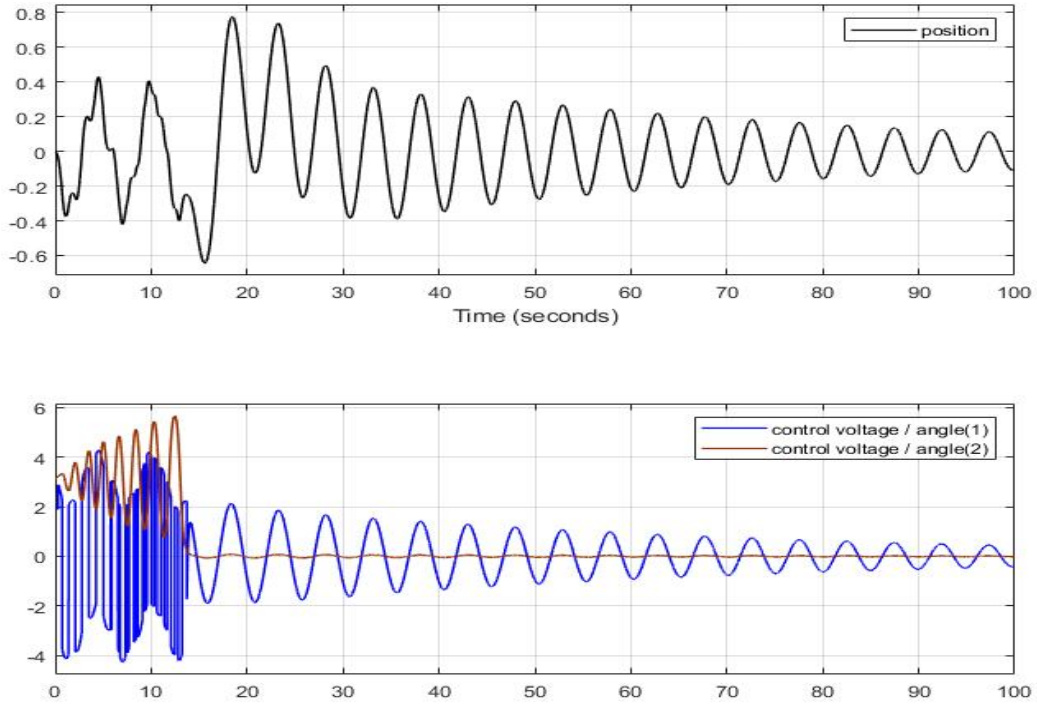

Figure 3.11 Transient Response of PID-Tuned CIP System with $l = 0.32m$

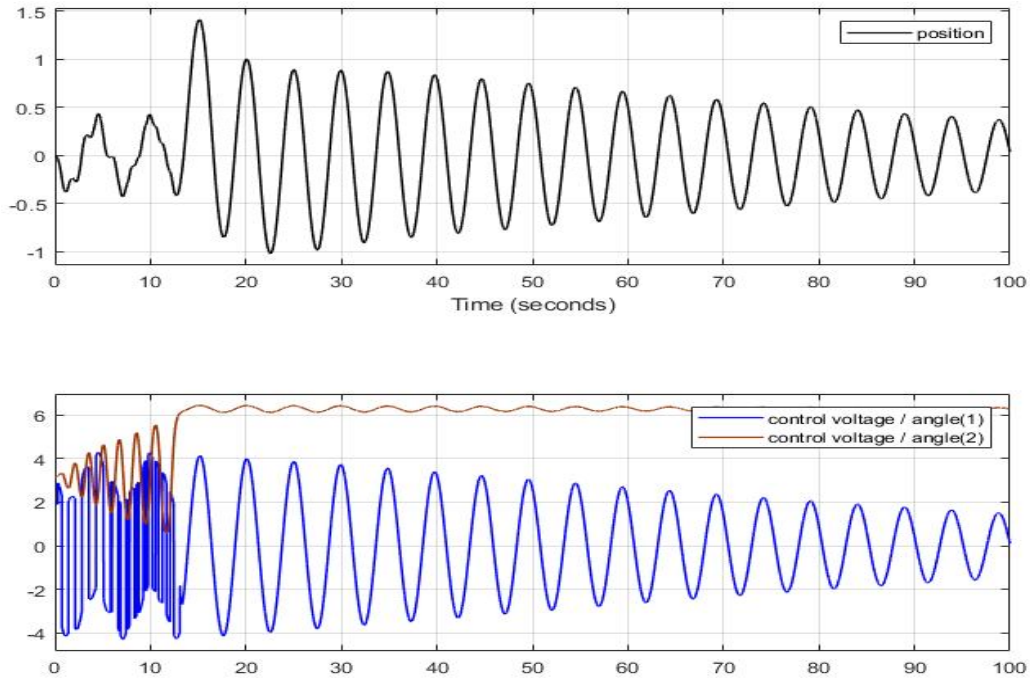

Figure 3.12 Transient Response of PID-Tuned CIP System with $l = 0.34m$

Table 3.6 Cart Position Response Comparison of Five Values Pendulum Length

Case	t_r **sec**	t_p **sec**	M_p	t_s **sec**	e_{ss}	**Stability**
Case 1 ($\boldsymbol{l = 0.25m}$)	6–8	28–30	55	Not fully settled up to 100 s	Small	Marginally stable (oscillations decay slowly, but response does not fully settle within the shown interval)
Case 2 ($\boldsymbol{l = 0.28m}$)	6–8	18–20	100	Not fully settled up to 100 s	Small	Marginally stable (bounded response, but long-lasting oscillations remain)
Case 3 ($\boldsymbol{l = 0.29m}$)	6–8	20–22	50	65–75	≈ 0	Stable (oscillations gradually decay and response converges)
Case 4 ($\boldsymbol{l = 0.32m}$)	7–9	18–20	75	Not fully settled up to 100 s	Small	Marginally stable (sustained oscillatory response with slow decay)
Case 5 ($\boldsymbol{l = 0.34m}$)	8–10	14–16	140	Not settled	Large	Unstable / near unstable (very large oscillations persist with poor damping)

Table 3.7 Pendulum Angle Response Comparison of Five Values Pendulum Length

Case	t_r **sec**	t_p **sec**	M_p	t_s **sec**	e_{ss}	**Stability**
Case 1 ($\boldsymbol{l = 0.25m}$)	2–3	26–28	6.2	Not fully settled up to 100 s	Small	Marginally stable (controller effort remains oscillatory for a long duration)
Case 2 ($\boldsymbol{l = 0.28m}$)	2–3	18–20	5.8	Not fully settled up to 100 s	Small	Marginally stable (bounded but slowly decaying oscillations)
Case 3 ($\boldsymbol{l = 0.29m}$)	2–3	16–18	8.5	55–65	≈ 0	Stable (despite spike, response decays and converges)
Case 4 ($\boldsymbol{l = 0.32m}$)	2–3	12–14	5.6	Not fully settled up to 100 s	Small	Marginally stable (persistent oscillations remain in the control signal)
Case 5 ($\boldsymbol{l = 0.34m}$)	2–3	14–16	6.3	Not settled	Large	Unstable / near unstable (high-amplitude oscillations persist without acceptable decay)

Table 3.8 Control Signal Response Comparison of Five Values Pendulum Length

Case	t_r **sec**	t_p **sec**	M_p	t_s **sec**	e_{ss}	**Stability**
Case 1 ($\boldsymbol{l = 0.25m}$)	3–4	26–28	~6.3	Does not settle to zero	Large	Unstable in tracking sense (signal remains around a nonzero value near 6.3)
Case 2 ($\boldsymbol{l = 0.28m}$)	3–4	18–20	~5.8	35–45	≈ 0	Stable (angle converges close to zero)
Case 3 ($\boldsymbol{l = 0.29m}$)	3–4	18–20	~5.8	30–40	≈ 0	Stable (bounded and converges close to zero)
Case 4 ($\boldsymbol{l = 0.32m}$)	3–4	12–14	~5.6	25–35	≈ 0	Stable (angle response converges to zero)
Case 5 ($\boldsymbol{l = 0.34m}$)	3–4	14–16	~6.3	Does not settle to zero	Large	Unstable in tracking sense (persistent offset and oscillation remain)

From the above results, it is clear that as the pendulum length increases, the system becomes more oscillatory and harder to stabilize. Among the given cases, $\boldsymbol{l = 0.28m}$ and, $\boldsymbol{l = 0.29m}$ show comparatively better position stabilization, while $\boldsymbol{l = 0.34m}$ exhibits the poorest response with very high oscillations and no proper settling. The controller effort remains bounded in all cases but becomes increasingly oscillatory as the length increases. However, the pendulum angular movement in some cases converges to zero, whereas others settle around a nonzero value, indicating loss of accurate pendulum-angle regulation.

3.3.2.3 Variable Cart Mass ($\boldsymbol{M}$)

The cart mass is varied to four values (2.42kg, 2.45kg, 2.25kgm and 2.25kg). The corresponding responses of cart position, pendulum angle, and controller effort signal are depicted in Figures 3.13 to 3.16 and summarized in Tables 3.9-3.11.

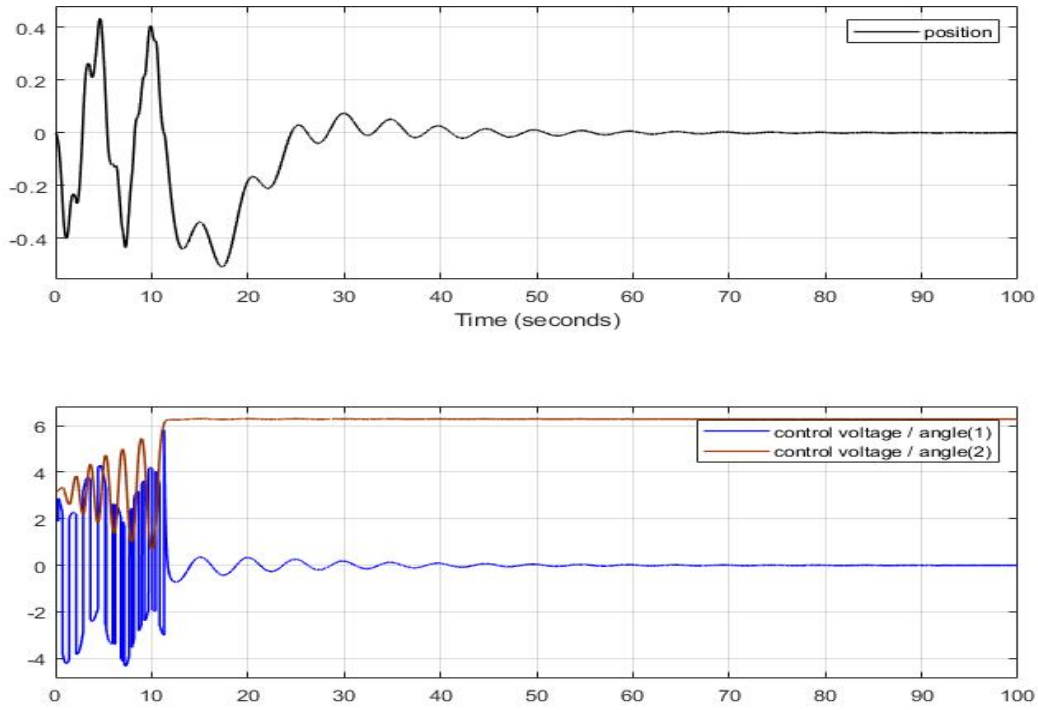

Figure 3.13 Transient Response of PID-Tuned CIP System with $M = 2.42kg$

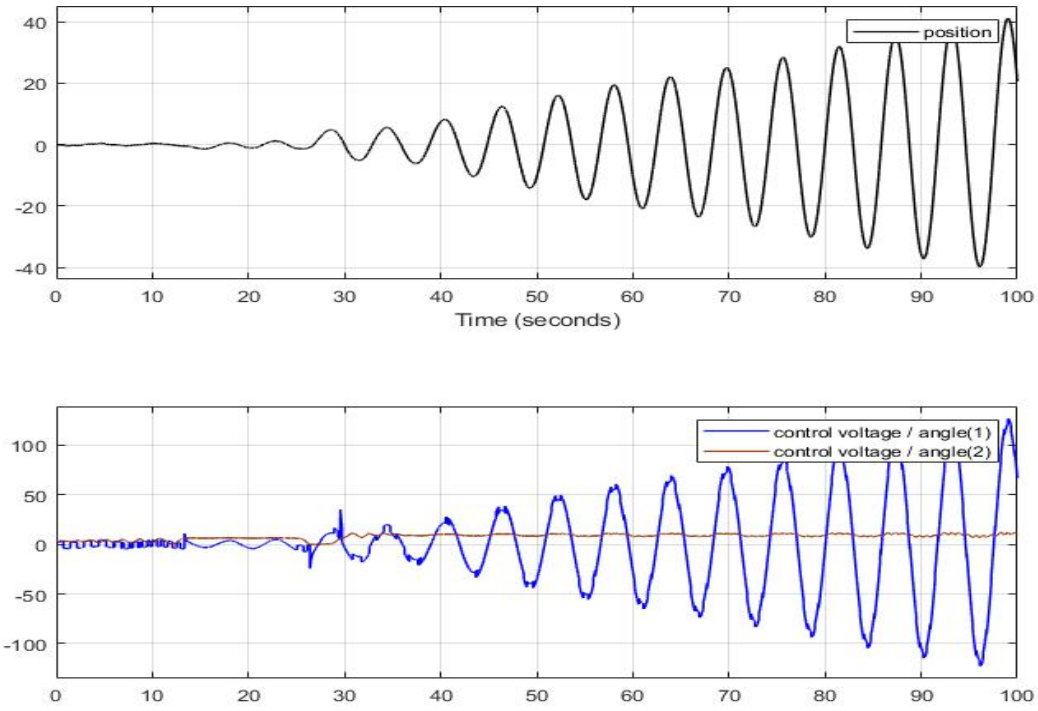

Figure 3.14 Transient Response of PID-Tuned CIP System with $M = 2.45kg$

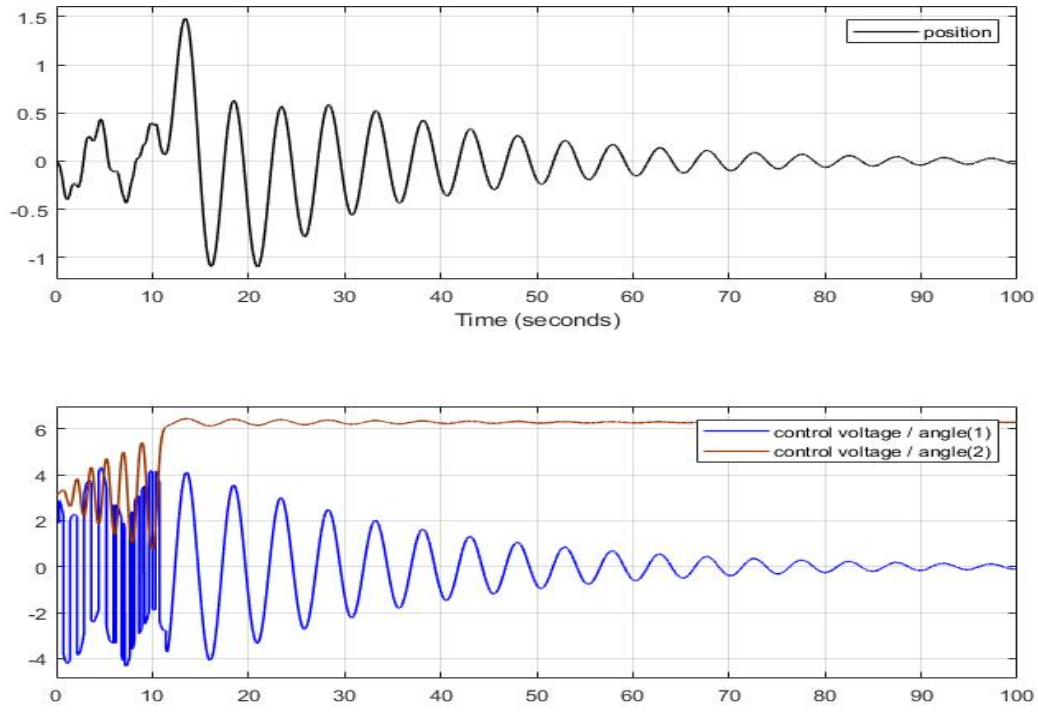

Figure 3.15 Transient Response of PID-Tuned CIP System with $M = 2.25kg$

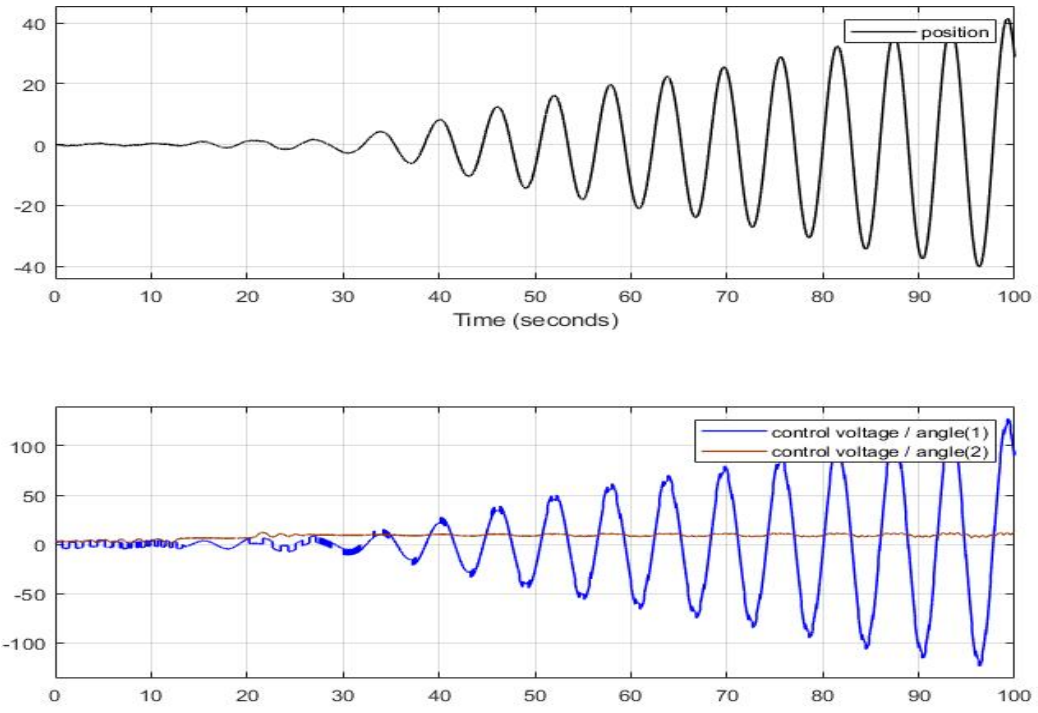

Figure 3.16 Transient Response of PID-Tuned CIP System with $M = 2.22kg$

Table 3.9 Cart Position Response Comparison of Four Values Pendulum Mass

Case	t_r **sec**	t_p **sec**	M_p	t_s **sec**	e_{ss}	**Stability**
Case 1 ($\boldsymbol{M = 2.42kg}$)	5–7	10	40%	30–35	≈ 0	Stable (oscillations decay)
Case 2 ($\boldsymbol{M = 2.45kg}$)	—	—	Very high	Not applicable	Large	Highly Unstable (diverging response)
Case 3 ($\boldsymbol{M = 2.25kg}$)	6–8	15	~60–70%	40–50	≈ 0	Stable (slow damping)
Case 4 ($\boldsymbol{M = 2.22kg}$)	—	—	Very high	Not applicable	Large	Highly Unstable (rapid divergence)

Table 3.10 Pendulum Angle Response Comparison of Four Values Pendulum Mass

Case	t_r **sec**	t_p **sec**	M_p	t_s **sec**	e_{ss}	**Stability**
Case 1 ($\boldsymbol{M = 2.42kg}$)	3–4	10–12	6	20–25	≈ 0	Stable
Case 2 ($\boldsymbol{M = 2.45kg}$)	—	—	Increasing	Not applicable	Large	Unstable (no convergence)
Case 3 ($\boldsymbol{M = 2.25kg}$)	3–4	12–14	6	30–40	≈ 0	Stable (slow)
Case 4 ($\boldsymbol{M = 2.22kg}$)	—	—	Increasing	Not applicable	Large	Unstable

Table 3.11 Control Signal Response Comparison of Four Values Pendulum Mass

Case	t_r **sec**	t_p **sec**	M_p	t_s **sec**	e_{ss}	**Stability**
Case 1 ($\boldsymbol{M = 2.42kg}$)	2–3	10–12	~6	20–25	≈ 0	Stable
Case 2 ($\boldsymbol{M = 2.45kg}$)	—	—	>100	Not applicable	Infinite	Highly Unstable (diverging control effort)
Case 3 ($\boldsymbol{M = 2.25kg}$)	2–3	15	~4–5	30–40	≈ 0	Stable (oscillatory)
Case 4 ($\boldsymbol{M = 2.22kg}$)	—	—	>100	Not applicable	Infinite	Highly Unstable

The results clearly indicate that the Cart–Inverted Pendulum system is highly sensitive to variations in cart mass. For lower values (2.25kg), the system maintains stability,

although oscillations and settling time increase slightly. However, a small increase (2.4kg and above) leads to rapid divergence in both position and control signals, indicating loss of stability. The controller effort exhibits extremely large peaks, while the pendulum angle fails to converge. This behavior demonstrates that the conventional PID controller lacks robustness and cannot effectively handle significant parametric variations.

3.4 Concluding Remarks

Experimentations are conducted to investigate the influence of key system parameters, including pendulum mass, cart mass, and pendulum length, on the performance of the Cart–Inverted Pendulum (CIP) system. The results indicate that variations in mass-related parameters significantly affect system stability, where small changes can lead to unstable and diverging responses. In particular, the cart mass is found to have a strong impact on the transient behaviour, often causing rapid oscillation growth under certain conditions. The variations in pendulum length exhibit a more gradual influence on system performance. Hence, to enhance the stability of the CIP system, conventional PID controllers need to be modified or replaced with advanced alternative controller variants.

Chapter 4

Metaheuristic Optimization of FOPID Controller for Cart–Inverted Pendulum*

4.1 Introduction

The Cart Inverted Pendulum (CIP) system remains the most widely researched system for designing advanced controllers and metaheuristic algorithms [2]. The Proportional-Integral-Derivative (PID) controller is utilized, and its robustness against parametric variations is comprehensively analyzed in Chapter 2. Despite its extensive application in both academic research and practical real-time settings, the PID controller imposes significant constraints when used with underactuated and higher-order nonlinear systems.

The literature shows that advanced Fractional-Order PID (FOPID) controllers perform better than conventional PID, especially for nonlinear systems [15], [119]. The FOPID controllers extend the PID controller by incorporating two additional fractional order tuning parameters (λ and μ) to the basic gains $k_p, k_i \; and \; k_d$ [120]. These fractional-order parameters improve system performance and robustness against gain variations and parameter uncertainty [121]. Comparative studies in [122], [123], and [124] clearly show reductions in settling time and overshoot, and lower values of IAE, ISE, and ITAE error metrics compared to the conventional PID. This controller also demonstrates its superior capability through frequency-domain analysis against system uncertainty, and enhanced disturbance rejection [125]. Meta-heuristic optimization techniques overcome the limitations of complex parameter tuning for FOPID and efficiently provide optimal controller gains, revolutionizing controller design to achieve the desired system performance [126-128]. Even in the CIP experimental setup, these controllers demonstrate their effectiveness in stabilizing the pendulum in its upright

* *This chapter was published in the proceedings of the 2022 IEEE International Power and Renewable Energy Conference (IPRECON), held in Kollam, 2022, pp. 1–7. DOI: 10.1109/IPRECON55716.2022.10059474*

position [47] [129]. The increased computational complexity of FOPID controllers is well handled by modern digital technology. These literature reviews conclusively demonstrate that the FOPID controller outperforms the PID controller, particularly in terms of improved transient response and frequency-domain performance.

This chapter introduces a FOPID controller design for simultaneously regulating the cart position and stabilizing the pendulum angle. The mathematical modeling of the CIP system is already explained in Chapter 1. To further enhance its performance and optimize the tuning of controller parameters efficiently, three metaheuristic techniques, particle swarm optimization (PSO), water cycle algorithm (WCA), and grasshopper optimization algorithm (GOA), are employed. A comparative transient analysis is performed to validate their effectiveness in stabilizing the pendulum in its unstable upright position and returning the cart to its center position.

The brief outline of the chapter is as follows. Section 4.2 provides an overview of FOPID control techniques. Section 4.3 explains three meta-heuristic optimization techniques, GOA, WCA, and PSO. The proposed control model is discussed in Section 4.4. Results and Discussion in Section 4.5. Finally, Section 4.6 presents the final concluding remarks.

4.2 FOPID Controller Design

Fractional-order control systems are described by differential equations based on fractional calculus, in which the orders of differentiation and integration can take any real value rather than only integers. In simple terms, this means the system can be modelled more flexibly compared to traditional methods, allowing better representation of real-world dynamics that involve memory and past behaviour. The extension of the conventional Proportional–Integral–Derivative (PID) controller using this concept is known as the Fractional-Order PID (FOPID) controller.

Unlike the classical PID controller, which has three parameters (k_p, k_i, k_d), the FOPID controller introduces two additional parameters, namely the fractional integral order (λ)

and fractional derivative order (μ). This results in five design parameters, providing greater tuning flexibility.

These additional degrees of freedom help improve system performance, robustness, and adaptability to uncertainties. The Laplace domain FOPID implementation model is shown in Figure 4.1.

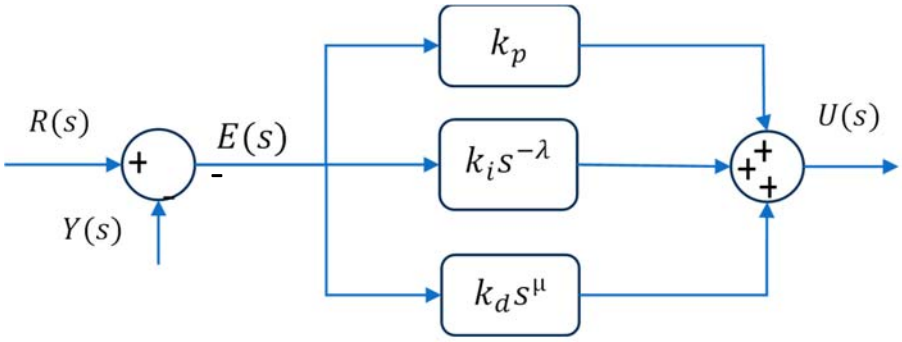

Figure 4.1 Architecture of FOPID Controller

Equation (4.1) describes the controlling signal $u(t)$ generated by the FOPID controller in response to the error signal $e(t)$ between the reference signal $r(t)$ and the real-time output signal $y(t)$.

$$u(t) = k_P e(t) + k_i D_t^{-\lambda} e(t) + k_d D_t^{\mu} e(t) \tag{4.1}$$

Where, the $D^{-\lambda}$ and D^{μ} represent the fractional order integral and derivative operators. The λ and μ are additional degrees of tuning provided by FOPID as compared to the PID controller. In the PID method, their values are restricted to integer numbers, but in the FOPID method, they can also take real values. In most cases, they are kept between 0 and 1.

Implementation of an FOPID controller for any system involves tuning the basic gains (k_p, k_i, k_d), and two fractional orders (λ, μ). PID, PI, PD, and FOPID controllers are closely related to each other and can be converted from one form to another by setting the value of fractional orders (λ, μ), as shown in Figure 4.2.

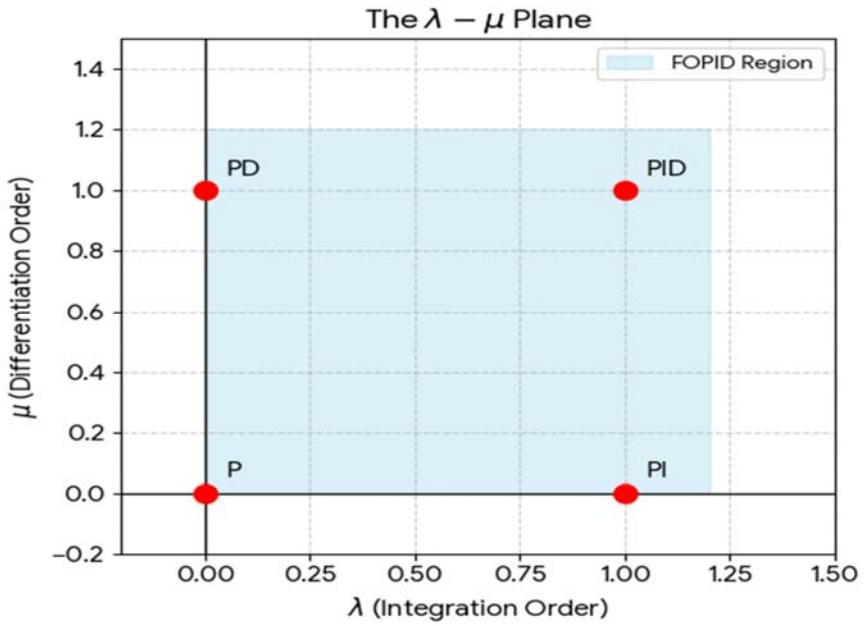

Figure 4.2 λ–μ Plane with FOPID Region and PID Family

4.3 Metaheuristic Optimization Technique Used for FOPID Tuning

Three optimization techniques are implemented in this chapter to tune the FOPID controller parameters, as manual tuning is difficult and often inefficient. The selection of PSO, WCA, and GOA for optimization in this work is motivated by their effectiveness in handling nonlinear and unstable systems. Particle Swarm Optimization (PSO) is widely used in control applications because of its simple implementation, fast convergence, and strong capability to solve multidimensional optimization problems, making it suitable for FOPID tuning. The Water Cycle Algorithm (WCA) is selected for its strong global search and its effectiveness at avoiding local minima. The Grasshopper Optimization Algorithm (GOA), a relatively recent technique, has gained attention for its balanced exploration and exploitation capabilities. The ITAE (Integral Time Absolute Error) criterion is preferred over other indices like ISE and IAE as it gives more importance to errors that persist for a longer time. While ISE emphasizes large initial errors and IAE treats all errors equally, ITAE focuses on reducing errors over time, leading to improved settling performance. In the optimization problem, the best controller parameters are obtained by minimizing the objective function, also known as the cost function. In each iteration, the set of parameters that gives the lowest

cost value is selected. The mathematical expression of the ITAE is given in equation (4.2).

$$J(t) = \int_0^t t|e(t)|dt \tag{4.2}$$

Here, $\boldsymbol{J(t)}$ represents the cost function, and $\boldsymbol{e(t)}$ is the error obtained by subtracting the system output from the set-point.

4.3.1 Grass-Hopper Optimization Technique

The Grasshopper Optimization Algorithm (GOA) is a nature-inspired optimization technique that mimics the swarming behavior of grasshoppers. It moves like a grasshopper searching for food in the best direction. There are two tasks they perform: exploration (searching for food over large areas) and exploitation (converging on a target). The forward-moving group has two stages: a slow-moving nymph stage, which represents local search, and an adult stage, which makes long-range, sudden movements, representing global search or the exploitation of the best solutions. These two characteristics help the algorithm maintain a balance between exploration and exploitation, making it effective for solving complex optimization problems. In GOA, each grasshopper represents the possible solution whose new position will be kept updated based on three factors: social interaction, gravitational force, and wind effect. GOA's strong global search capability makes it an effective solution for complex, nonlinear problems such as CIP control.

The search agents lean towards passage shortly in exploration, while the actions become local displacement during exploitation, which is mathematically modelled as equation (4.3).

$$X_i = r_1 S_i + r_2 G_i + r_3 A_i \tag{4.3}$$

where X_i signifies the location of the ith grasshopper, S_i and G_i are communal interaction as well as the gravitational force on the ith grasshopper, correspondingly, and A_i signifies wind advection. S_i, G_i as well as A_i can be considered by equations (4.4), (4.5), and (4.6) respectively.

$$S_i = \sum_{j=1, j\neq i}^{N} s(d_{ij})\hat{d}_{ij} = \sum_{j=1, j\neq 1}^{N} s(|x_i - x_j| \frac{x_i - x_j}{d_{ij}} \tag{4.4}$$

$$s(r) = f e^{-r/l} - e^{-r} \tag{4.5}$$

where $d_{ij} = |x_i - x_j|$ is the distance within the ith and j^{th} grasshopper. $s(r)$ It is employed to express social forces, such as attraction and repulsion, in grasshoppers. $\hat{d}_{ij} = (x_i - x_j)/d_{ij}$ signifies a unit vector within the ith and j^{th} grasshopper. f and l are the strengths of attraction as well as the attractive length, correspondingly. Normally, $f = 1.5$ and $l = 0.5$ are chosen. The position of ith grasshopper is written as equation (4.6).

$$G_i = -g\hat{e}_g \tag{4.6}$$

Where g signifies the gravitational constant, and $\hat{e}_g$ signifies a unity vector in the direction of the center of earth. The wind advection (or drift) component acting on the ith grasshopper is modelled as equation (4.7)

$$A_i = u\hat{e}_w \tag{4.7}$$

where u signifies a constant drift. $\hat{e}_w$ is a unity vector in the direction of the wind. The final version of equation (4.3) can be obtained by substituting S_i, G_i, and A_i into it and represented as equation (4.8).

$$X_i = \sum_{j=1, j\neq i}^{N} s(|x_j - x_i|)\frac{x_i - x_j}{d_{ij}} - g\hat{e}_g + u\hat{e}_w \tag{4.8}$$

The constraint N signifies the number of grasshoppers.

In the GOA, optimization complications are addressed using an improved equation (4.9) that can be obtained without considering gravity and the wind direction, is always aligned with the tuning target.

$$X_i^d = c\left(\sum_{j=1, j\neq i}^{N} c\,\frac{ub_d - lb_d}{2} s(|X_j^d - X_I^d|)\frac{x_j - x_i}{d_{ij}}\right) + \hat{T}_d \tag{4.9}$$

where ub_d and lb_d are the upper and lower bounds in the Dth dimension, correspondingly. $\hat{T}_d$ signifies the optimization target, and the constraint c is a diminishing coefficient derived from equation (4.10).

$$c = c_{max} - l\frac{c_{max} - c_{min}}{L} \tag{4.10}$$

where $l\ and\ L$ signify the current iteration and total number of iterations correspondingly, c max and c min signify the supreme and mean values of constraint c. Figure 4.3 shows the logical flowchart of the GOA.

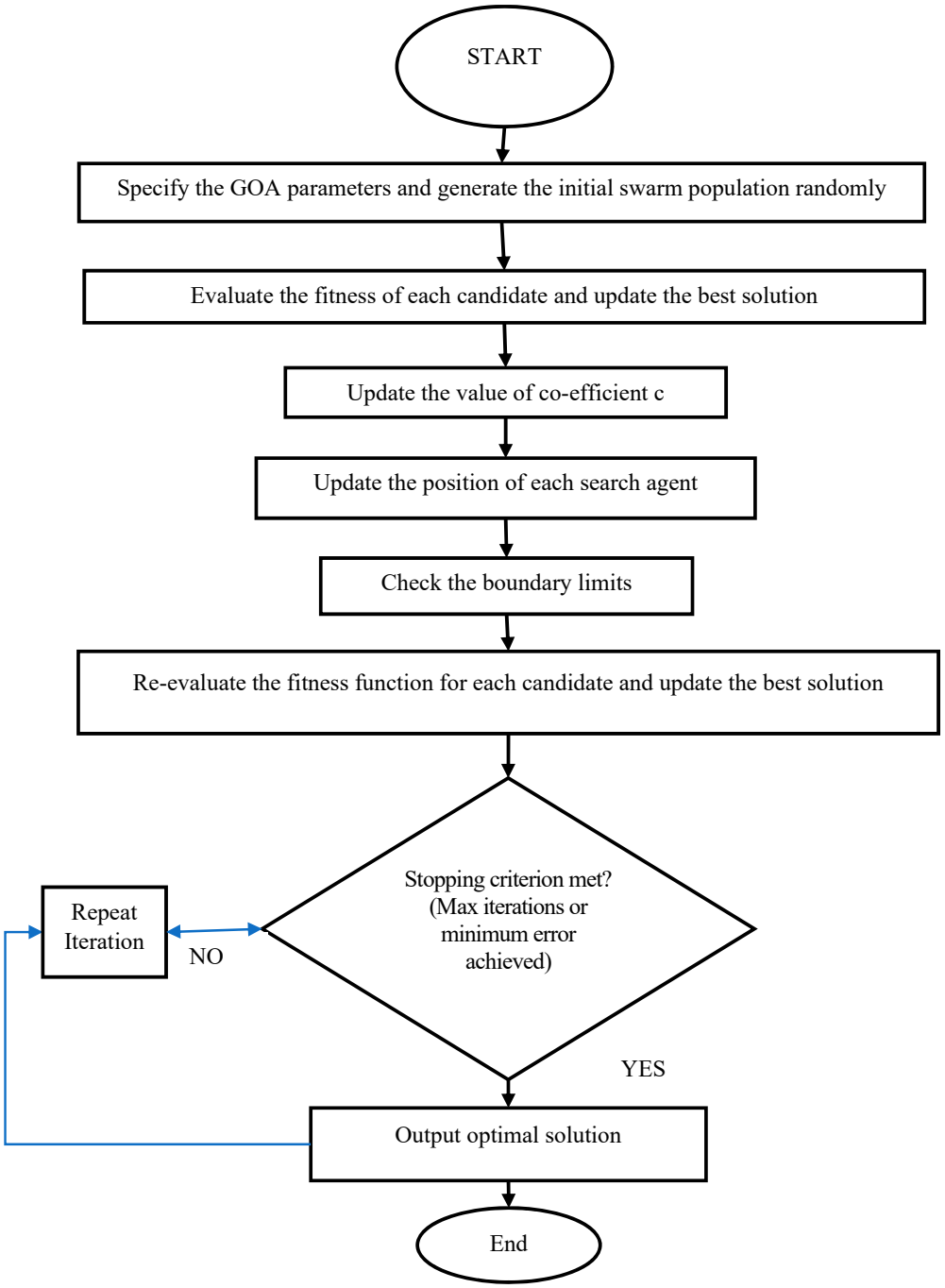

Figure 4.3 GOA Algorithm Flow Diagram

4.3.2 Particle Swam Optimization

The PSO algorithm is very popular among researchers across various fields due to its simplicity of implementation and fewer parameters to tune. In this algorithm, each particle represents a possible solution. It has two main attributes, position and velocity. Position represents the current solution, while velocity represents the direction and speed of movement. As the particle moves through the search space, it continues to learn and adjust its path based on its own experience and that of its neighbors. The logical flowchart of the PSO is given in Figure 4.4. The velocity of each particle will keep on updating as per equation (4.11), and it is based on three factors: particle inertia (wv_i^k), a cognitive component $c_1 r_1 (p_i^k - x_i^k)$ which pulls it towards the best position found so far, and the social component $c_2 r_2 (g_i^k - x_i^k)$ which tells the particle to move towards the best solution found by the entire population.

$$v_i^{k+1} = \left(wv_i^k\right) + c_1 r_1 \left(p_i^k - x_i^k\right) - c_2 r_2 (g^k - x_i^k) \tag{4.11}$$

Here g^k and p_i^k is the global best position and the personal best position.

The position of each particle will be updated as per equation (4.12)

$$x_i^{k+1} = x_i^k + v_i^{k+1} \tag{4.12}$$

where x_i^k presents the previous position, v_i^{k+1} represent the updated velocity and v_i^k velocity of ith particle at k iteration. There is an inertia sensitivity factor, a personal learning factor, and a social learning factor as w, c_1 and c_2 respectively. r_1 and r_2 are random numbers between 0 and 1.

To enhance the convergence capability of PSO techniques, the inertia weight is updated as per the equation (4.13)

$$w = w_{max} - \frac{(w_{max} - w_{min})}{iter_{max}} \times iter \tag{4.13}$$

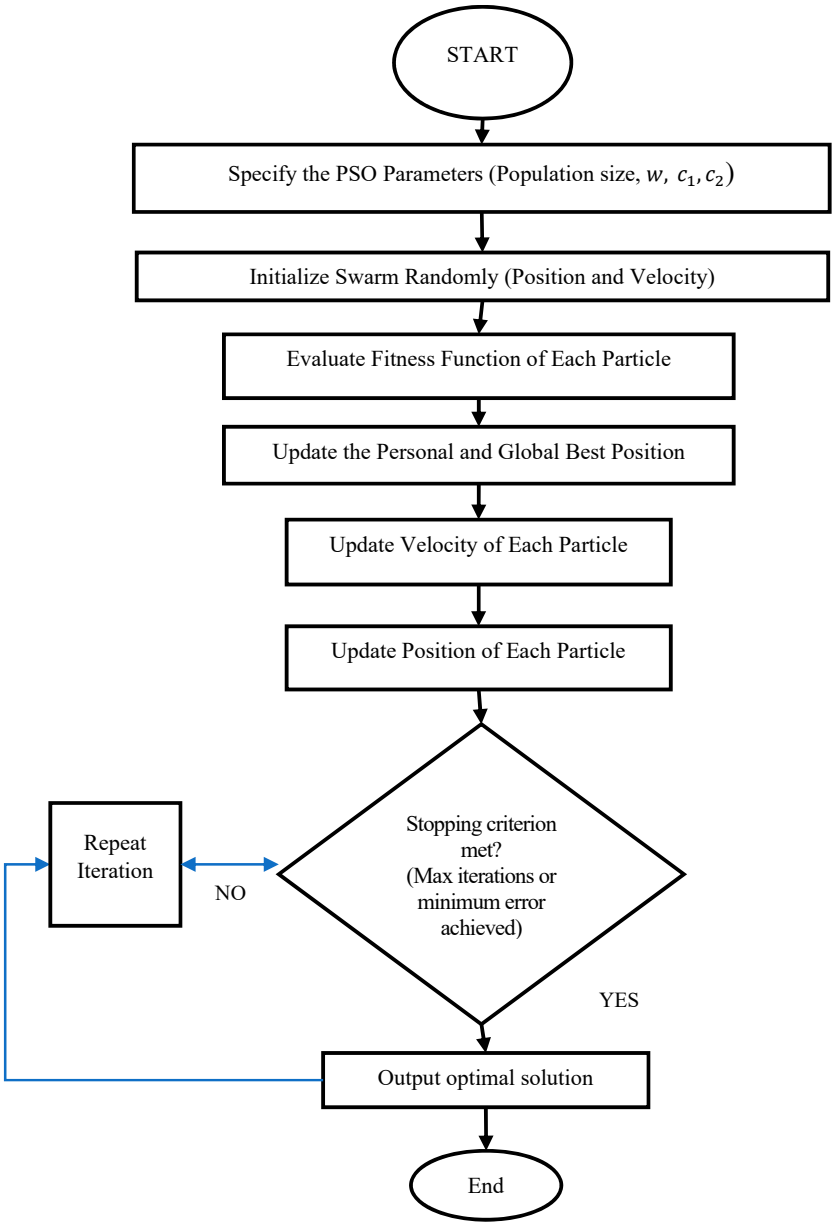

Figure 4.4 Flowchart of PSO Algorithm

4.3.3 Water Cycle Algorithm

A nature-inspired Water Cycle Algorithm (WCA) is based on the real-world water cycle and is specifically designed to solve constraint-based problems. This hydrological process has three phases: evaporation, condensation, and precipitation. Each raindrop represents a possible solution, and when a few highly eligible drops are grouped together, they form a river. The best raindrop (solution) is considered the sea, and the

remaining are streams that flow towards rivers and the sea. This streamed movement enables both the global exploration and local exploitation of the search space.

Initially population of N The solution is assigned, and the fitness function will be evaluated. According to the fitness value, sea (X_{sea}), rivers (X_{river}) and streams (X_{stream}) will be assigned.

Movement of each stream towards the assigned river will be governed by the equation (4.14)

$$X_{\text{stream}}^{(t+1)} = X_{\text{stream}}^{(t)} + r \cdot C \cdot (X_{\text{river}}^{(t)} - X_{\text{stream}}^{(t)}) \tag{4.14}$$

Similarly, river's movement towards the sea will be following equation (4.15)

$$X_{river}^{(t+1)} = X_{river}^{(t)} + r \cdot C \cdot (X_{sea}^{(t)} - X_{river}^{(t)}) \tag{4.15}$$

where r is a random number between 0 and 1, and C is the movement intensity control factor varying between 1 and 2.

This flow will continue until the distance between the river, and the sea becomes less than the assigned threshold value $d_{\max}$, given in equation (4.16)

$$\| X_{\text{sea}} - X_{\text{river}} \| < d_{\max} \tag{4.16}$$

A new random solution will be generated when the river reaches the threshold distance, to prevent stagnation and the trapping of local minima, given in equation (4.17)

$$X_{\text{new}} = l_b + rand \cdot (u_b - l_b) \tag{4.17}$$

where l_b and u_b represent the lower and upper bounds, respectively, and rand $\in [0,1]$ is a random number.

This process redistributes solutions across the search space, thereby enhancing exploration. The equation (4.18) denotes a gradual shift from exploration to exploitation, ensuring a finer search near the optimal region in subsequent iterations.

$$d_{\max}^{(t+1)} = d_{\max}^{(t)} - \frac{d_{\max}^{(t)}}{MaxIter} \tag{4.18}$$

The algorithm will generate its best solution and stop the iteration when either it reaches its maximum value or the possibility of further improvement in the best function is negligible. The final flow chart of the WCA algorithm is given in Figure 4.5.

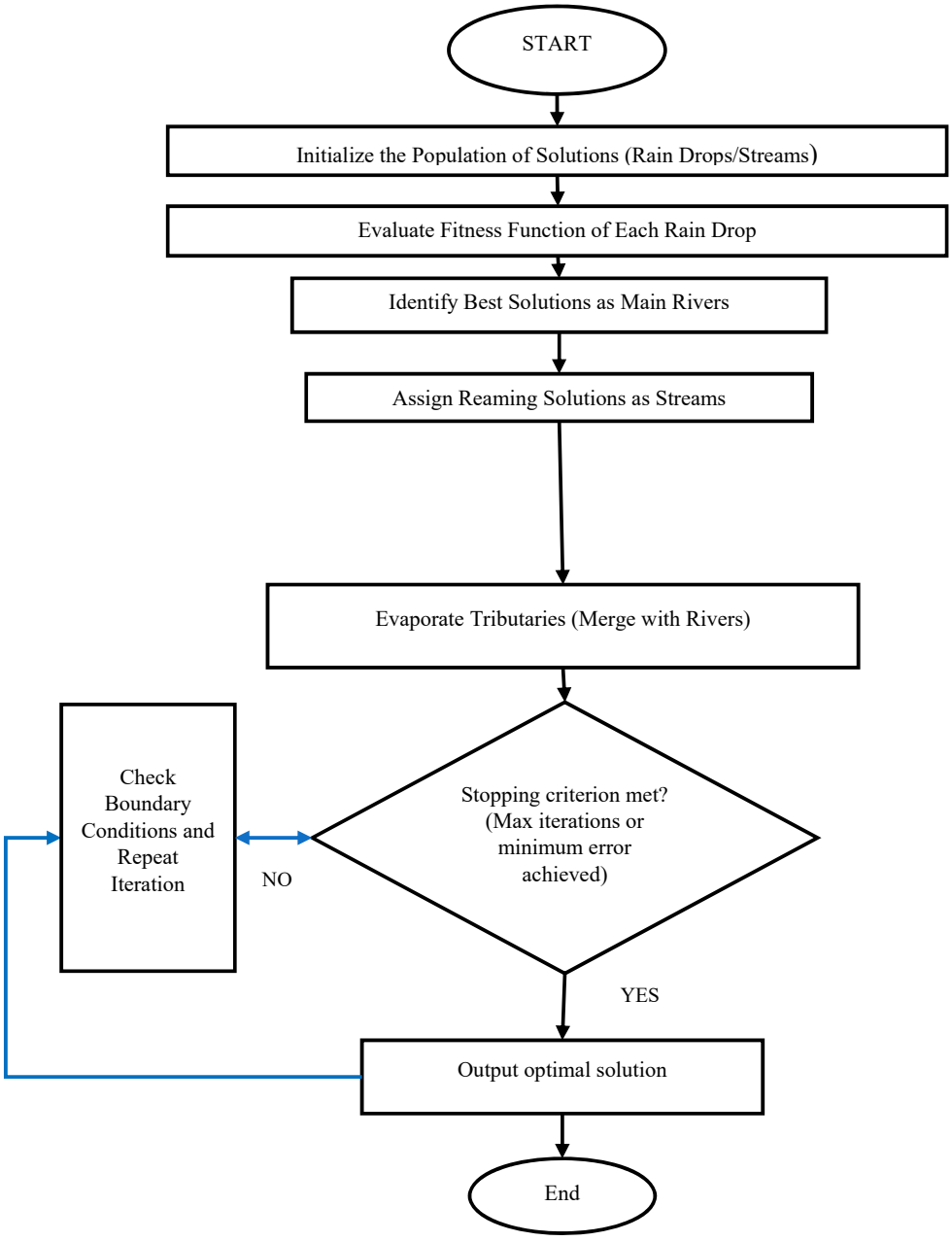

Figure 4.5 Flowchart of WCA Algorithm

4.4 Design of Implemented FOPID Controller for CIP Model

Most of the existing literature on CIP control focuses only on the pendulum angle while designing the controller. However, the cart position is directly related to the stabilization of the pendulum, as discussed in Chapters 1 and 2. Therefore, in this work, both the cart position and pendulum angle are considered simultaneously in the control design. The FOPID controller is used in the control loop to provide better flexibility and improved response compared to a conventional controller. To further improve performance, optimization algorithms are applied to effectively tune the set of five controller parameters. The main objective is to achieve stable operation and accurate tracking of the desired position with minimum error.

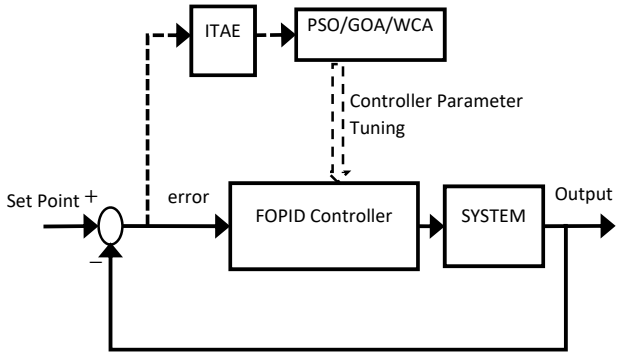

Figure 4.6 Control Structure of the CIP System using an Optimized FOPID Controller

The main idea behind the control structure design is to appoint an FOPID controller in the desired control loop, shown in Figure 4.6. This controller will receive an error signal, the difference between the set point and the actual system's output, as input. The same error signal will also be fed to the ITAE block and, ultimately, to the optimization algorithm (PSO, GOA, and WCA), based on which the controller's five parameters will be tuned for optimal performance of the cart position and pendulum stabilization.

The above idea is extended to control both the degree of freedom, the cart position and pendulum angle, depicted in Figure 4.7. So, two FOPID controllers are implemented in the control structure. One controller is used to regulate the cart position, while the other is responsible for stabilizing the pendulum angle. This dual-loop control approach is adopted because the two variables are closely related and must be controlled simultaneously for proper system operation. The use of FOPID controllers provides

additional flexibility due to their fractional-order nature, helping achieve better dynamic performance than conventional PID controllers.

The search space for these parameters has lower bound, and an upper bound for different parameters is as follows: $(-2000) \leq k_{P1}, k_{P2} \leq (2000), (-2000) \leq k_{I1}, k_{I2} \leq (2000), (-2000) \leq k_{D1}, k_{D2} \leq (2000), 0 \leq \lambda_1, \lambda_2 \leq 2, 0 \leq \mu_1, \mu_2 \leq 2.$

These bounds ensure that the optimization algorithms explore a wide range of possible solutions while maintaining system stability and feasibility.

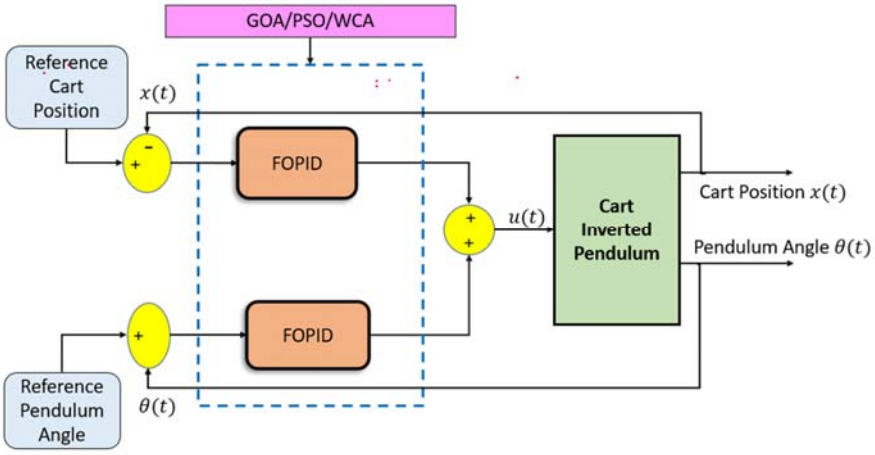

Figure 4.7 Implemented FOPID-controlled CIP System

However, these advantages come at the cost of increased tuning complexity, as a total of ten controller parameters need to be adjusted for both controllers. To solve this issue, three metaheuristic optimization algorithms, Particle Swarm Optimization (PSO), Water Cycle Algorithm (WCA), and Grasshopper Optimization Algorithm (GOA), are employed to tune the controller parameters. Each algorithm is applied separately to obtain the optimal controller parameters, including proportional gains (k_{P1}, k_{P2}), integral gains (k_{i1}, k_{i2}), derivative gains (k_{d1}, k_{d2}), and fractional orders (λ_1, λ_2) and (μ_1, μ_2).

To evaluate the robustness of the system, a step disturbance of 0.1 radian is applied to the pendulum angle. This disturbance introduces a sudden deviation in the pendulum's position, which helps assess how effectively the controller can bring the system back to its desired state.

In addition to the system response, the ITAE (Integral Time Absolute Error) performance index is also computed within the model. The ITAE criterion is selected because it accounts for both the magnitude of the error and the time over which it persists. A lower ITAE value indicates better control performance, as it reflects faster error reduction and improved system stability.

4.5 Results and Discussion

The control structure implemented in the previous section aims to bring the cart back to its reference position and stabilize the pendulum in the upright position. The controller's performance is evaluated in this section based on its transient behavior and ITAE. The controller gains achieved with three optimization techniques are given in Table 4.1.

Table 4.1 Tunned FOPID Controller Parameters and ITAE

Optimization	FOPID1					FOPID2					ITAE
	k_{P1}	k_{I1}	k_{D1}	λ_1	μ_1	k_{P2}	k_{I2}	k_{D2}	λ_2	μ_2	
WCA	42.17	1377	1693.5	1.18	0.23	-1415	-225.8	-2000	1.54	0.24	6.5591
PSO	1263.4	1177.7	-57.06	1.52	0.22	-216.5	-2000	-2000	0.74	0.01	6.048
GOA	2000	2000	-1159.7	1.66	0.054	-928.4	-1380	64.99	0.543	0.099	5.415

4.5.1 Transient Analysis of GOA-FOPID for CIP System

The cart position response is shown in Figure 4.8. The initial overshoot and undershoot are approximately +1.6m and -1.4m, respectively, which characterizes the highly unstable nature of the inverted pendulum model. Despite this transient behavior, the oscillations are quickly damp, and the cart settles to the steady state value of zero in 3 to 4 seconds. This rapid stabilization and reduced oscillations validate the effectiveness of the proposed GOA-tuned FOPID in maintaining stable cart motion.

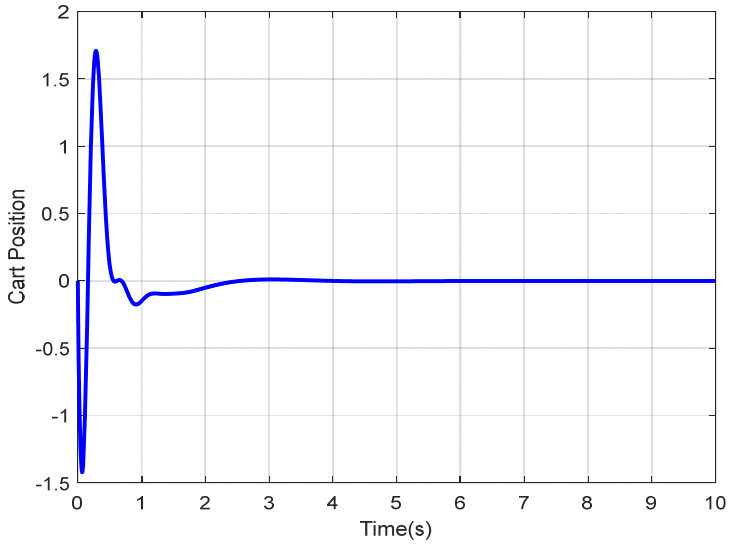

Figure 4.8 Cart Position Response for the GOA-tuned FOPID Controller

The angular pendulum response is depicted in Figure 4.9, also conforming to the effectiveness of the proposed GOA-FOPID controller. Initially, the pendulum angle reaches a peak of approximately +1.0 rad and a minimum deviation of approximately 0.85 rad, which shows the inherent instability of the CIP system. Finally, the controller settles to zero steady-state error within 2 to 3 seconds. The controller stabilizes the pendulum first, rather than the cart, and this priority is essential for the pendulum's upright control.

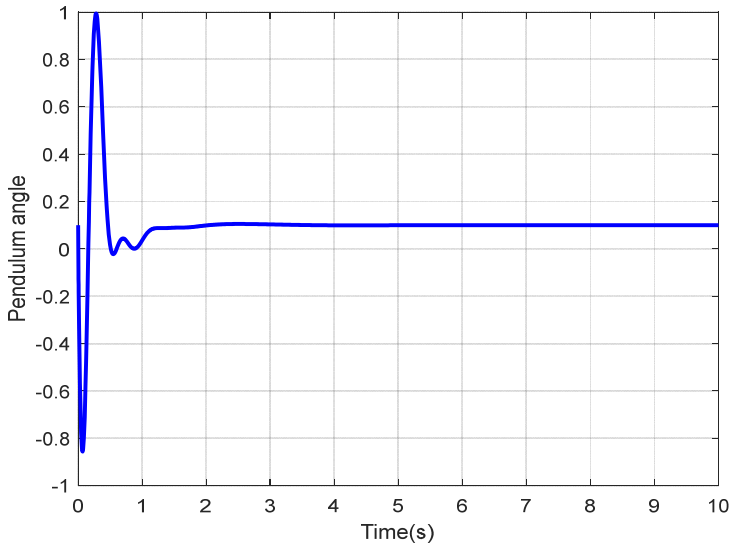

Figure 4.9 Pendulum Angle Response for the GOA-tuned FOPID Controller

The ITAE error functions are 6.5591, 6.048, and 5.415 for WCA, PSO, and GOA, respectively. The GOA algorithm provides 17.4% and 10.5% greater reductions in ITAE than WCA and PSO, respectively, confirming GOA-FOPID's superiority among the three methods. The time-domain analysis shows that GOA-FOPID exhibits fewer oscillations and faster stabilization compared to PSO and WCA. The initial peak of GOA and PSO is almost the same, ±1.5 m, but is significantly less than that of WCA. Moreover, the GOA-based system settles in approximately 2 to 3 seconds, whereas PSO requires around 3 to 4 seconds, and WCA shows comparatively slower settling with longer oscillations. The improved damping characteristics of GOA indicate better control over system instability.

4.5.2 Comparative Analysis of FOPID Tuned with GOA, PSO and WCA

The FOPID controller is tuned with GOA, PSO and WCA algorithm and their comparative cart position and pendulum angle response are given in Figure 4.10 and Figure 4.11 and summarized in Table 4.3 and Table 4.4.

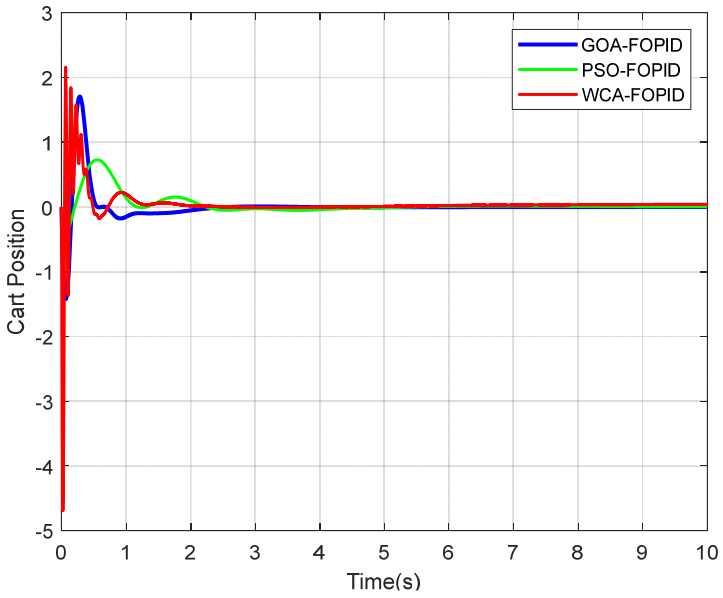

Figure 4.10 Cart position control with GOA-FOPID, PSO-FOPID and WCA-FOPID

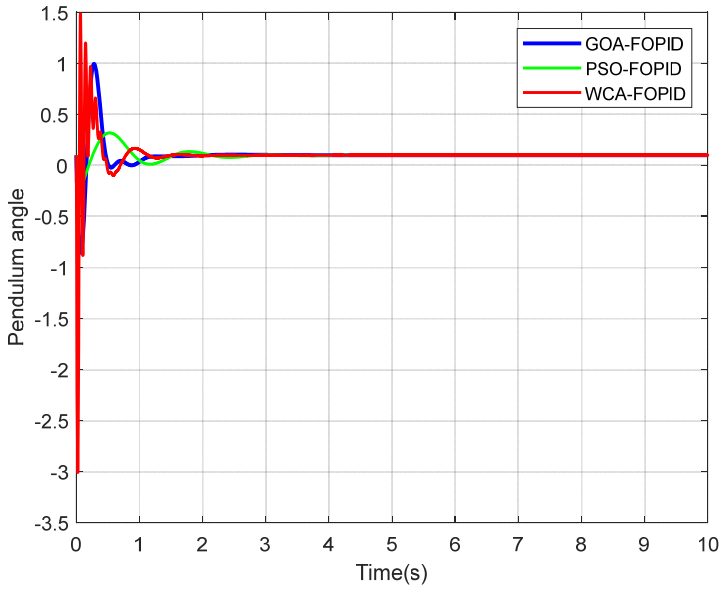

Figure 4.11 Pendulum Angle Control with GOA-FOPID, PSO-FOPID, and WCA-FOPID

Table 4.2 Comparative Analysis of Pendulum Angle

Controller	Rise Time (sec)	Peak Time (sec)	Maximum Overshoot	Settling Time (sec)	Steady-State Error
GOA-FOPID	0.12	0.18	0.95	1.10	0
PSO-FOPID	0.28	0.42	0.32	1.80	0
WCA-FOPID	0.06	0.10	1.50	1.45	0

The cart position response demonstrates the superior performance of the GOA-FOPID controller in achieving stable and efficient system behavior. The GOA-FOPID controller shows a rise time of 0.10 s and settling time of 1.20 s, which is significantly faster than PSO-FOPID with 0.35 s rise time and 2.10 s settling time. Although WCA-FOPID exhibits the fastest rise time of 0.05 s, it results in the highest overshoot. In contrast, GOA maintains a controlled overshoot with zero steady-state error, confirming better stability and overall performance.

Table 4.3 Comparative Analysis of Cart Position

Controller	Rise Time (sec)	Peak Time (sec)	Maximum Overshoot	Settling Time (sec)	Steady-State Error
GOA-FOPID	0.10	0.16	1.75	1.20	0
PSO-FOPID	0.35	0.52	0.70	2.10	0
WCA-FOPID	0.05	0.08	2.15	1.60	0

Similarly, the pendulum angle response highlights the effectiveness of GOA in maintaining system balance. The GOA-FOPID controller shows a maximum deviation of approximately ±1.2 rad, while PSO exhibits slightly higher oscillations and WCA demonstrates the largest deviations, exceeding ±1.5 rad. In addition, the settling time for GOA is approximately 2 seconds, which is faster than both PSO and WCA. The reduced oscillations and faster convergence to zero angle confirm that GOA ensures superior stabilization of the pendulum in its upright position.

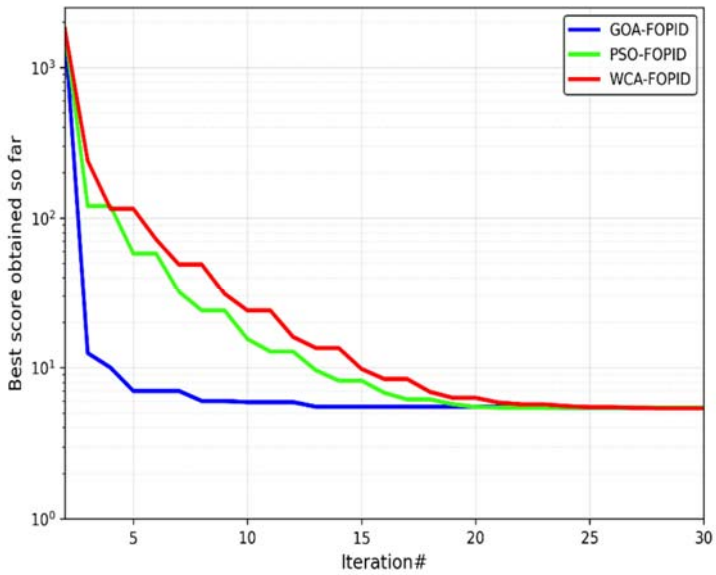

Figure 4.12 Comparative Convergence Curve

The comparative convergence analysis of GOA, PSO, and WCA-tuned FOPID controllers for stabilizing the Cart–Inverted Pendulum (CIP) system is presented in Figure 4.12 Among all three, GOA exhibits the fastest convergence rate with an effective exploration–exploitation balance. Initially, the fitness value is nearly 10^3, which rapidly decreases to approximately 10^1 within the first 3–5 iterations. Thereafter, the convergence becomes gradual and stable, and the fitness value settles around 5–6 within nearly 15–20 iterations, indicating efficient exploitation capability and stable convergence without oscillations.

The PSO-tuned FOPID controller also shows satisfactory convergence performance. However, its convergence rate is slower than GOA, with stabilization achieved near the 20th iteration. In contrast, the WCA-tuned FOPID controller demonstrates the slowest

convergence behavior, requiring nearly 28 iterations for stabilization. Therefore, GOA provides the best optimization performance, followed by PSO and WCA, respectively.

The improved performance of GOA can be attributed to its adaptive exploration and exploitation mechanism, which allows efficient search of the solution space and avoidance of local minima. In contrast, PSO tends to suffer from premature convergence, limiting its ability to refine solutions in later stages, while WCA exhibits slower convergence due to its structured flow mechanism.

Furthermore, the optimized controller parameters obtained using GOA exhibit balanced tuning of proportional, integral, derivative, and fractional orders, resulting in improved dynamic response and reduced error indices. The consistency between convergence characteristics, time-domain performance, and error metrics validates the robustness of the GOA-based approach.

Overall, the comparative analysis confirms that the GOA-FOPID controller outperforms PSO-FOPID and WCA-FOPID in terms of accuracy, stability, and convergence speed. Therefore, GOA can be considered a highly effective optimization technique for tuning FOPID controllers in nonlinear systems such as the cart-inverted pendulum.

4.6 Concluding Remarks

This chapter presents the dual-loop FOPID controllers design of the cart–inverted pendulum (CIP) system by considering both the cart position and pendulum angle, which improves system stability, coordination, flexibility and dynamic performance. However, it increases the number of parameters, making tuning more complex. To address this, three optimization algorithms, Particle Swarm Optimization (PSO), Water Cycle Algorithm (WCA), and Grasshopper Optimization Algorithm (GOA), are applied for parameter tuning. The system performance is evaluated using the ITAE criterion. The results show that all methods improve performance, but the GOA-based FOPID controller provides better results with lower errors, faster response, and improved stability compared to PSO and WCA. Finally, it is concluded that the GOA technique is more effective than the PSO and WCA techniques for tuning FOPID parameters in the CIP system.

Chapter 5

Hybrid Cascaded FOPI–FOPD–BLQGC Controller for Robust Stabilization of Cart–Inverted Pendulum*

5.1 Introduction

In preceding chapters, PID and FOPID controllers were implemented for CIP stabilization. PID showed simplicity but significant sensitivity to parametric uncertainties, especially cart mass variations, which critically affected transient performance. To overcome these limitations, the FOPID controller was introduced, offering enhanced flexibility through fractional tuning. When optimized using metaheuristic algorithms such as GOA, PSO, and WCA, the FOPID improved robustness and transient response, with GOA-tuned FOPID achieving the best overall performance.

Despite these improvements, FOPID controllers in cart position control loop as well as pendulum angle control loop may not be sufficient to effectively handle the coupled dynamics of the CIP system. To further enhance control performance, this work explores the use of a cascaded FOPI–FOPD controller in each loop, which is relatively underexplored in the literature. However, its effectiveness has been demonstrated in both simulation and experimental studies for CIP systems. For instance, the study in [130] reported that cascaded FO PI–PD control improves transient and frequency-domain performance, simplifies controller tuning, and enhances disturbance rejection [131].

Additionally, advanced nonlinear control techniques, such as backstepping, have been widely recognized for their ability to ensure Lyapunov-based stability in nonlinear systems [132]. When integrated with optimal control frameworks such as Linear Quadratic Gaussian (LQG), the resulting Backstepping Linear Quadratic Gaussian Controller (BLQGC) structure further enhances performance by incorporating optimal state estimation and noise-rejection capabilities, making it well-suited for complex,

* *This chapter was published in Mechanics & Industry, Vol. 27, 14(2026), pp. 1-14, EDP Sciences, doi: https://doi.org/10.1051/ meca/2026009*

uncertain dynamic systems. Furthermore, the BLQGC component mitigates the effects of external disturbances, including Gaussian white noise, thereby enhancing the overall system's robustness [15].

In most existing control designs, either error-based or state-based control strategies are employed. In contrast, the proposed control architecture integrates both approaches by combining a cascaded FOPI–FOPD feedback controller with a Backstepping Linear Quadratic Gaussian Controller (BLQGC). The cascaded FOPI–FOPD controller generates control action based on the tracking error, while the BLQGC incorporates state estimation and nonlinear control principles to improve system stability and robustness. The interdependence between cart motion and pendulum dynamics is explicitly considered, as the cart displacement provides the necessary momentum to stabilize the pendulum in its upright position. Two parallel control loops are designed to simultaneously regulate both cart position and pendulum angle.

In the context of fractional-order control of CIP systems, robustness analysis has primarily focused on controller parameter sensitivity and disturbance rejection. However, comprehensive parametric robustness analysis that accounts for simultaneous variations in physical parameters, such as cart mass (M), pendulum mass (m), and pendulum length (l), remains limited. This aspect is explicitly addressed in the present work.

To optimally tune the parameters of the cascaded FOPI–FOPD controller, a hybrid optimization approach based on the Grasshopper Optimization Algorithm and Firefly Algorithm (GOA–FA) is employed. The proposed hybrid cascaded FOPI–FOPD–BLQGC controller is then evaluated through comparative analysis with FOPI, FOPD, and BLQGC controllers. Performance is assessed based on transient response, frequency-domain characteristics, and robustness to parametric uncertainties. The state-space model of the Cart Inverted Pendulum (CIP) system utilized in this chapter is derived in Chapter 2.

The brief outline of the chapter is as follows. Section 5.2 provides an overview of cascaded FOPI-FOPD control techniques, and Section 5.3 explains the mathematical implementation architecture of the BLQGC controller. The hybrid GOA-FF

optimization technique is presented in Section 5.4. The proposed control model is discussed in Section 5.5. Results and Discussion in Section 5.6. Finally, Section 5.7 presents the final concluding remarks.

5.2 Cascade FOPI-FOPD Controller Design

The cascaded FOPI–FOPD controller structure differs from the conventional FOPID controller in that the fractional-order integral (FOPI) and fractional-order derivative (FOPD) components are arranged in a series (cascaded) configuration, whereas in a FOPID controller, the proportional, integral, and derivative actions are combined in a parallel structure, shown in Figure 5.1. The controller gain for the suggested structure is as equation (5.1).

$$C_{FOPI-FOPD} = k_p(1 + \frac{k_i}{s^\lambda})(1 + k_d s^\mu) \tag{5.1}$$

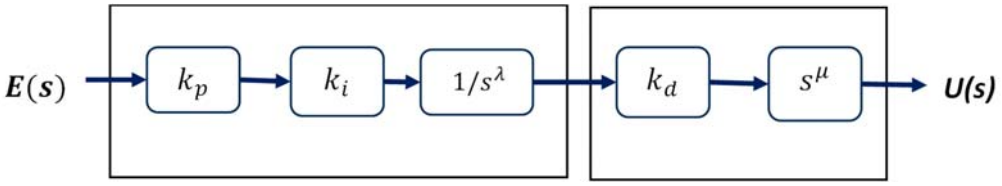

Figure 5.1 Cascaded FOPI-FOPD Controller

5.3 Backstepping Linear Quadratic Gaussian Controller (BLQGC)

Backstepping–Linear Quadratic Gaussian Control (BLQGC) is an advanced control strategy that combines the advantages of backstepping design with Linear Quadratic Gaussian (LQG) control [51]. This hybrid approach is particularly effective for nonlinear systems with uncertainties, as it integrates nonlinear stabilization with optimal state estimation. Compared to conventional control techniques, BLQGC offers improved robustness and enhanced performance in the presence of disturbances and modelling inaccuracies. The BLQGC framework has been widely applied in domains that require high precision and reliability, such as aerospace systems, automotive control, robotics, and the process industries. Unlike the Linear Quadratic Regulator (LQR), which relies on full-state feedback and assumes all system states are directly measurable, the BLQGC incorporates a state estimator (Kalman filter) to reconstruct

unmeasurable states. This enables the controller to operate effectively even when complete state information is not available.

Furthermore, integrating backstepping with LQG enhances the controller's ability to handle nonlinear dynamics while maintaining optimal performance. The Kalman estimator accounts for measurement noise and external disturbances, whereas the LQR component ensures optimal control action based on the estimated states. As a result, the BLQGC structure provides improved stability, better disturbance rejection, and greater robustness than conventional LQR-based approaches. The overall architecture of the BLQGC system, including the interaction between the estimator and controller, is illustrated in Figure 5.2.

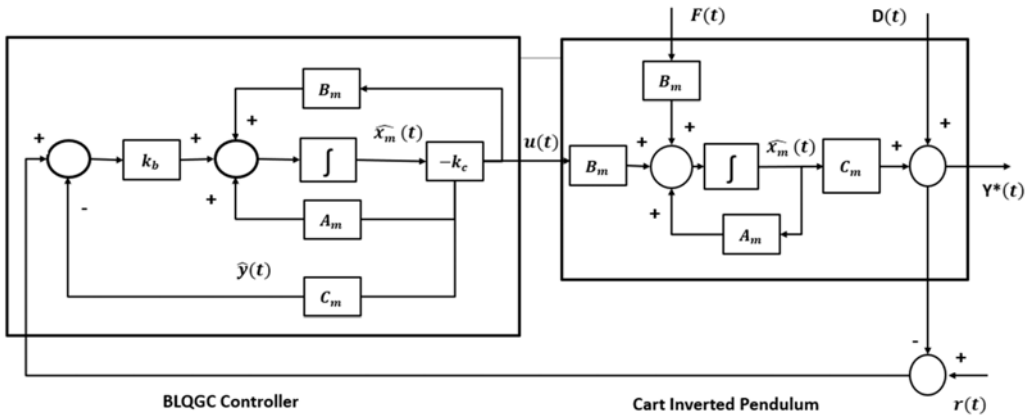

Figure 5.2 BLQGC Controller Design for Cart Inverted Pendulum

To achieve effective control and stabilization, the BLQGC design is based on the state-space model of the Cart-Inverted Pendulum (CIP) system, as presented in Chapter 2. In the implemented control architecture, both process disturbances and measurement noise are explicitly considered. The process disturbance, denoted as $F(t)$, is modeled as a constant external force of 1 (N) applied to the cart, while the measurement noise, represented by $D(t)$. It is characterized as additive white Gaussian noise affecting the output signals.

The Kalman filter's state estimation enables the controller to operate effectively even when not all states are directly measurable. The resulting CIP state-space model,

incorporating both process disturbance and measurement noise, is formulated with additive noise terms and is represented by equations (5.2) -(5.3).

$$\dot{x_m}(t) = Ax_m(t) + Bu(t) + BF(t) \tag{5.2}$$

$$y(t) = C_m x_m(t) + D(t) \tag{5.3}$$

Where $x_m(t)$ and $u(t)$ denote the system state vector and control input, respectively, while $y(t)$represents the measured output. Figure 5.2 illustrates the BLQGC design, which incorporates the LQR gain. $K_c$and the backstepping control gain K_b. The LQR gain $K_c$is determined by minimizing the objective (cost) function defined in equation (5.4) and is computed using the relation given in equation (5.5).

$$j(t) = \int_0^\infty [x_m(t)^T Q\, x_m(t) + u(t)^T R u(t) \tag{5.4}$$

$$K_c = R^{-1}B^T \prod \tag{5.5}$$

Where $Q = C^T qC$ is a positive semi-definite state weighting matrix, and R is a positive definite input weighting matrix. The matrices Q and R are used to regulate the relative importance of state deviations and control effort in the performance index. Specifically, Q penalizes deviations in the system outputs (cart position and pendulum angle), while R penalizes excessive control input $u(t)$. Controller performance can be tuned by appropriately adjusting the weighting matrices to achieve the desired dynamic response.

The positive semi-definite matrix $\prod$ is obtained by solving the Continuous-time Algebraic Riccati Equation (CARE), as given in equation (5.6).

$$A^T \prod + \prod A - \prod B R^{-1} \prod + \prod C^T qC = 0 \tag{5.6}$$

Equations (5.7) – (5.9), represent the state-space formulation of the Cart-Inverted Pendulum (CIP) system using the states estimated by the backstepping-based controller.

$$\dot{\hat{x}}(t) = A\hat{x}(t) + Bu(t) + K_b[r(t) - y(t) - \hat{y}(t)] \tag{5.7}$$

Where

$$u(t) = -K_c \hat{x}(t) \tag{5.8}$$

$$\hat{y}(t) = C\,\hat{x}(t) \tag{5.9}$$

So, equation (5.9) will get modified as equation (5.10).

$$\dot{\hat{x}}(t) = \hat{x}(t)(A - BK_c - K_bC) + K_b[r(t) - y(t)] \tag{5.10}$$

Where K_b denotes the backstepping controller gain, $\hat{x}(t)$represents the estimated state vector, and $\hat{y}(t)$denotes the estimated output vector. The gain $K_b$is computed as given in equation (5.11)

$$K_b = \prod_b C^T R_1^{-1} \tag{5.11}$$

Where $\prod_b$ is taken as a positive definite matrix and can be formulated as a solution of the Lyapunov function, given in equation (5.12).

$$\prod_b (A - BK_c) + (A - BK_c)^T \prod_b + B_d Q_1 {B_d}^T + I = 0 \tag{5.12}$$

Where the closed-loop matrix $(A{-}BK_c)$ must be Hurwitz (i.e., all eigenvalues have negative real parts) to ensure system stability while computing the LQR gain K_c. The matrix Idenotes the $(n \times n)$identity matrix, where $n$is the order of the system matrix A, and B_d represents the disturbance (or noise) input weighting matrix. Finally, the transfer function of the BLQGC is derived using the LQR gain $K_c$and the Kalman filter gain, as expressed in equation (5.13).

$$K(s) = K_c(sI - A + BK_c + K_bC)^{-1}K_b \tag{5.13}$$

Table 5.1 includes the estimated BLQGC controller parameters (Q, R, Q_1, R_1) used in this work, whereas Table 5.2 provides the estimated controller gains.

Table 5.1 Proposed BLQGC Controller Parameter Values

Q	R	Q_1	R_1
Diag(1.0e+04*[1.0,0.001,0.001,0.001,0.001,0.001])	0.01	0.01	0.002

Table 5.2 Proposed Controller Gain Value of BLQGC Controller

K_b	K_c
[1.123,0.234,1.892,0.456,3.681,2.1356]	[1.103,0.214,1.792,0.216,1.890,2.777]

5.4 Hybrid Meta-Heuristic (GOA-FA) Algorithm

The Grasshopper Optimization Algorithm (GOA) and the Firefly Algorithm (FA) are nature-inspired metaheuristic techniques widely used to solve complex optimization problems [133][134]. The swarming behaviour of grasshoppers inspires GOA, whereas FA is based on fireflies' bioluminescent communication. GOA is known for its strong exploration capability and its ability to balance exploration and exploitation; however, it may occasionally converge to local optima. To address this limitation, hybridization of GOA with FA is introduced, as FA exhibits strong local search capabilities that help escape suboptimal solutions and refine the search process. On the other hand, FA alone may face challenges when dealing with highly nonlinear and complex systems such as the Cart-Inverted Pendulum (CIP), particularly in achieving fast convergence for real-time control applications. In this context, GOA's global search capability complements FA's local search strength, enabling more efficient exploration of the solution space.

Therefore, the hybrid GOA–FA approach effectively balances global exploration and local exploitation, leading to faster convergence and improved optimization performance. This balance is particularly important for the CIP system, where both optimal selection of the control parameter and precise fine-tuning are required to ensure stability and accurate tracking performance.

5.4.1 Phase 1: Grass-Hopper Optimization Algorithm (GOA)

The Grasshopper optimization algorithm is inspired by swarm life cycle and has three phases: egg, nymph, and adulthood, but the important phases for determining the grasshopper's life span are the nymph and adulthood. The nymph depicts immature agents with slow movement and small steps, while the adult phase shows the swarm's aggressive nature, with longer steps and randomized movement in all directions in search of the best. These two phases of food seeking can be modeled as exploration (nymph) and exploitation (adulthood) [135]. The current location of the grasshopper is modeled as equation (5.14).

$$L(i) = r_1 S_o(i) + r_2 G_f(i) + r_3 A_w(i) \quad (5.14)$$

where $L(i)$ depicts the ith grasshopper location, $S_o(i)$ and $G_f(i)$ are communal interaction as well as the gravitational force on the ith grasshopper, correspondingly, and $A_{w(i)}$ signifies wind advection. The detailed explanation of GOA algorithm is already discussed in Chapter 4.

5.4.2 Phase 2: Firefly Algorithm (FA)

The Firefly Algorithm is a metaheuristic optimization technique characterized by its automatic population subdivision capability. It possesses a natural capability to handle multimodal optimization problems, exhibits high ergodicity, and maintains diversity in the generated solutions [136]. This algorithm models the attractiveness between current and subsequent flies in a forward direction. This attractiveness decreases with increasing distance between flies and increases with increasing brightness level of the flies. Flies follow the random walk if the brightness of two flies is equal to a uniform or non-uniform step size [137]. So, new positions could be modeled as a function of the current position, brightness level, and random walk step size. This algorithm has two loops to generate the new solution: an inner loop for population size 'n'and outer loop for number of iterations. 't'. The complexity of the algorithm is linear $(n \times t)$ for a smaller population and is non-linear $(n \times log(nt))$ for a larger population. The initial population will be generated according to equations (5.15) - (5.16).

$$Position = Lower\ Bound + (Lower\ Bound - Lower\ Bound) \times rand(1, problem_Dimension) \quad (5.15)$$

$$F(x_i) =: \sum_{i=1}^{n} x(i-1)^2 \quad (5.16)$$

The flight's new position will be modified between the ith and jth location based on the brightness criterion and updated according to the position equations (5.17) – (5.18).

$$New\ position = Current\ position + Attractiveness * (x_i - x_j) + Step\ size \quad (5.17)$$

$$x_i(t+1) = x_i(t) + \beta_0 e^{-\gamma r^2}(x_i - x_j) + \alpha \varepsilon_i(t) \quad (5.18)$$

Where, α is a random no between (0,1), $\varepsilon_i(t)$ is a random variable drawn from a uniform distribution, a Gaussian distribution, or any other distribution form and β_0 The attractiveness control function is typically set to 1.

5.4.3 Hybrid GOA-FA Algorithm

In the proposed sequential hybrid GOA–FA algorithm, the Grasshopper Optimization Algorithm is first employed to perform global exploration of the search space and identify promising candidate solutions. Thereafter, the best solutions obtained from the GOA phase are used as the initial population for the Firefly Algorithm, which performs local refinement to further improve solution quality. Thus, hybridization is sequential in nature, where FA operates on the output of GOA rather than running independently. This arrangement combines GOA's strong exploration capability with FA's effective local search, resulting in improved convergence accuracy and a reduced risk of local-optima trapping.

Finally, by combining the above-discussed algorithm, the implemented hybrid (GOA-FA) algorithm is depicted in Figure 5.3.

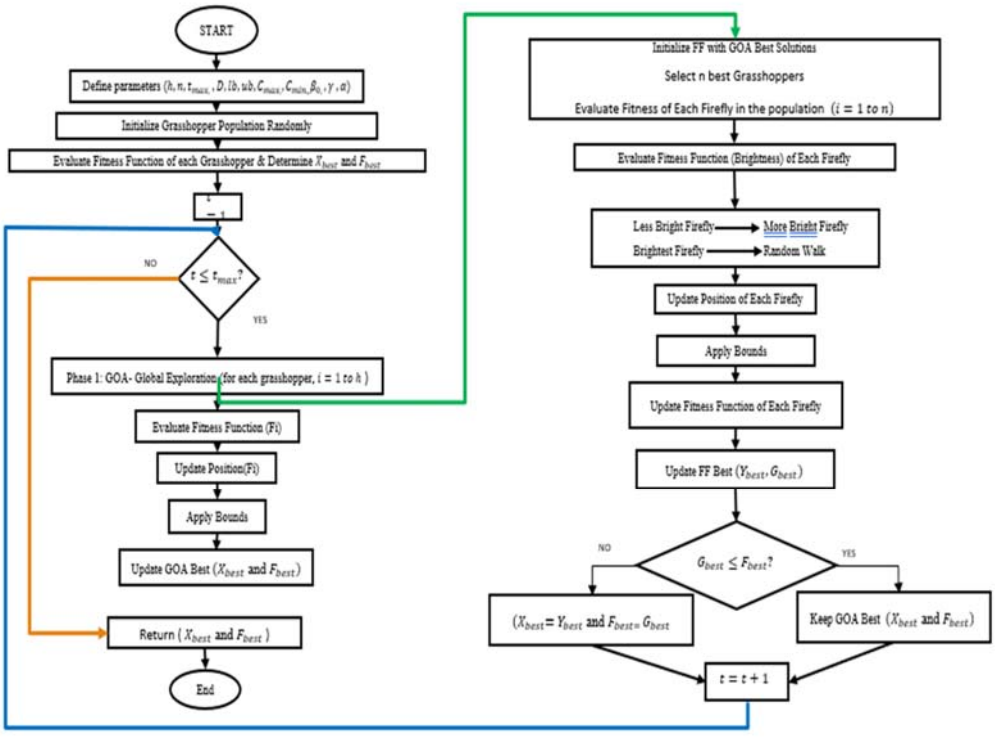

Figure 5.3 GOA-FA Algorithm Flowchart

5.5 Proposed Cascaded FOPI-FOPD-BLQGC Controller

The proposed control architecture integrates a cascaded (FOPI–FOPD) controller with a Backstepping Linear Quadratic Gaussian Controller (BLQGC) to effectively stabilize the Cart-Inverted Pendulum (CIP) system, depicted in Figure 5.4. The overall structure consists of two parallel control loops that simultaneously regulate the cart position and pendulum angle. In each loop, the cascaded FOPI–FOPD controller operates in the feedback path to generate control actions based on the tracking error, ensuring improved transient response and steady-state performance.

In addition, the BLQGC is incorporated as an auxiliary control component to enhance system robustness and stability. It uses a Kalman filter for state estimation to handle measurement noise and external disturbances, including white Gaussian sensor noise. The control signals generated from both controllers are combined and applied to the CIP system, enabling coordinated control of both states.

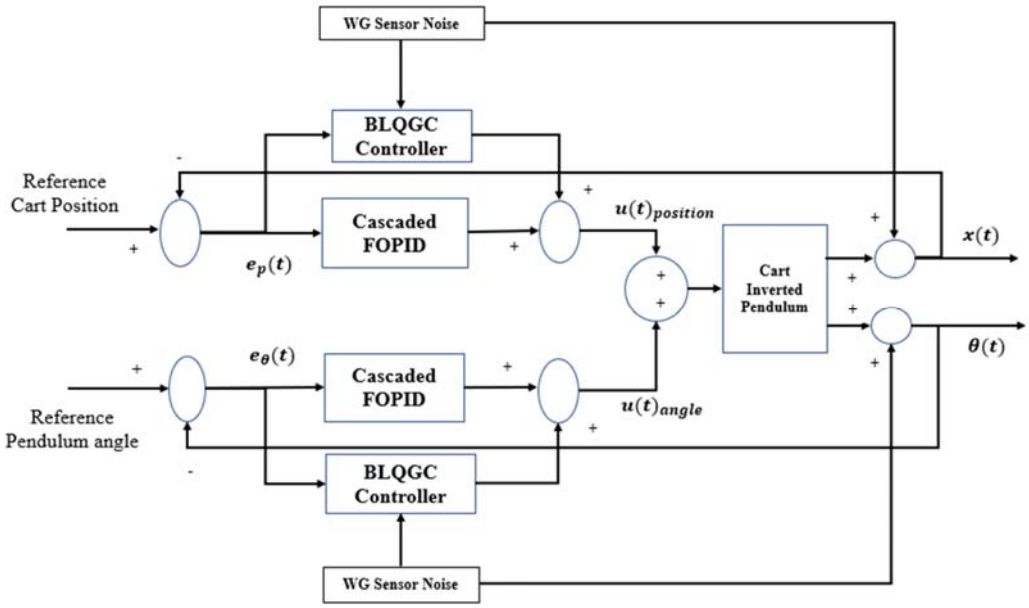

Figure 5.4 Proposed Cascaded FOPI-FOPD-BLQGC Controlled CIP Model

This hybrid configuration leverages the advantages of fractional-order control for flexibility and fine-tuning, along with the optimal and nonlinear control capabilities of BLQGC. As a result, the proposed controller achieves improved disturbance rejection, faster convergence, and enhanced robustness compared to conventional control

approaches. It uses the Cascaded FOPI-FOPD technique as the feedback controller and the BLQGC as the feedforward controller, respectively.

5.6 Results and Discussion

The capability and effectiveness of the suggested cascaded FOPI-FOPD-BLQGC controller are examined for CIP system. The efficient control of CIP systems needs fast responses to maintain balance and eliminate steady-state error for perfect stabilization. The ITAE criterion minimizes time-weighted absolute error, penalizing errors that persist longer. This improves stability and reduces oscillations. Hence, ITAE is selected as the cost function J_{ITAE}, as defined in equation (5.19).

$$J_{ITAE} = \int_0^{ts} t * |e(t)|\mathrm{dt} \tag{5.19}$$

The hybrid Grasshopper and Firefly optimization algorithm (GOA-FA) is employed to search for optimal parameter values that achieve high stability and robust error handling for the proposed controller. The adjusted cascaded FOPI-FOPD controller parameters are displayed using the hybrid (GOA-FA) optimization method. The comparative tuned parameters of all controllers are summarized in Table 5.3.

Table 5.3 Optimized Cascaded FOPI-FOPD Controller Parameters

Gain / Controller	kp_1	kd_1	ki_1	kp_2	kd_2	ki_2	μ	λ
Proposed cascaded FOPI-FOPD-BLQGC	2.4	1.5	3.8	3.4	1.9	3.2	0.95	0.98
FOPD	1.53	1.55	-	2.53	2.63	-	0.88	-
FOPI	1.85	-	2.58	-	2.45	1.99	-	0.47

The transient performance analysis, stability analysis, and robust analysis of a parametric uncertain CIP system subjected to impulse disturbance are compared for FOPI, FOPD, and BLQGC methods by evaluating the rise time (t_r), settling time (t_s), maximum peak overshoot (M_p), and steady-state error (e_{ss}) parameters.

5.6.1 Transient Performance Analysis

Transient analysis provides information on how the system responds to disruptions or setpoint changes. The comparative performance of the proposed controller with FOPD, FOPI, and BLQGC controllers has been analyzed for pendulum angle, cart position, and controller effort responses, as shown in Figures 5.4(a-c), and quantitatively summarized in Table 5.4. This analysis is carried out based on t_r, t_s, M_p, and e_{ss} parameters.

As shown in Figure 5.5(a), the pendulum-angle response has steady state error (e_{ss}) values of 0, 0.05, 0.05, and 0.07 with settling time (t_s) of 3sec, 13sec, 19sec, and 20sec with the proposed cascaded FOPI-FOPD-BLQGC, FOPD, FOPI, and BLQGC controllers, respectively. Further, M_p values obtained are 1.3, 0.4, 0.5, and 0.7, and t_r, values are 0.1sec, 0.4sec, 0.5sec and 0.7sec, respectively for these controllers. Similarly, from Figure 5.5(b), the steady state error (e_{ss}) values obtained for cart-position are 0, 0.05, 0.05, and 0.07, and settling time (t_s) are 3.2sec, 19sec, and 20sec, respectively, for the above-mentioned controllers. Further, M_p values obtained are 0.3, 0.8, 0.8, and 0.7, and t_r values are 0.2sec, 0.5sec, 0.6sec, and 0.7sec, respectively, for these controllers. Thus, the proposed hybrid controller results in the best e_{ss} t_s, M_p and t_r values are also shown in Table 5.4. The control signals for the different controllers considered are shown in Figure 5.5(c). The control signal for the proposed cascaded FOPI-FOPD-BLQGC exhibits a relatively smooth response, with minimal overshoot and settling time, compared to other controllers. The FOPI shows a more oscillatory response, indicating less stable behavior than the proposed controller. The FOPD controller exhibits significant overshoot and undershoot and takes longer to settle than the other controllers. The BLQGC controller shows a relatively smooth response but a slower settling time than the proposed control scheme. It also exhibits overshoot and undershoots, indicating a less stable behaviour than the cascaded controller. Hence, the proposed cascaded FOPI-FOPD-BLQGC controller gives the least overshoot, undershoot, settling time, and minimum control effort as compared to FOPI, FOPD, and BLQGC controllers.

Thus, the best transient performance and control signal are achieved with the proposed cascaded FOPI-FOPD-BLQGC controller compared to FOPD, FOPI, and BLQGC controllers.

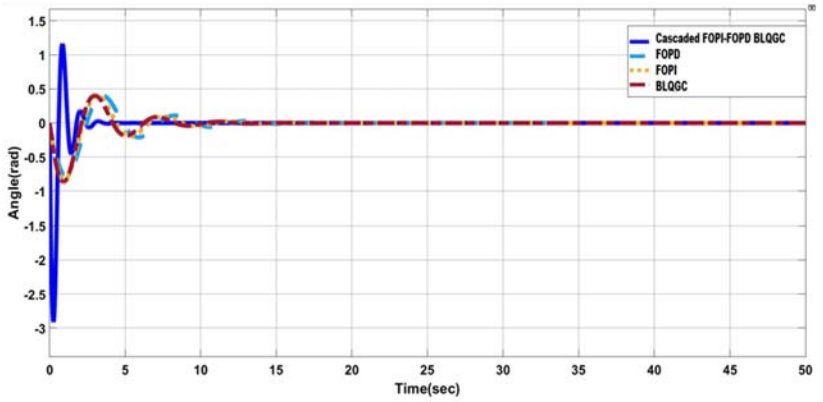

(a)

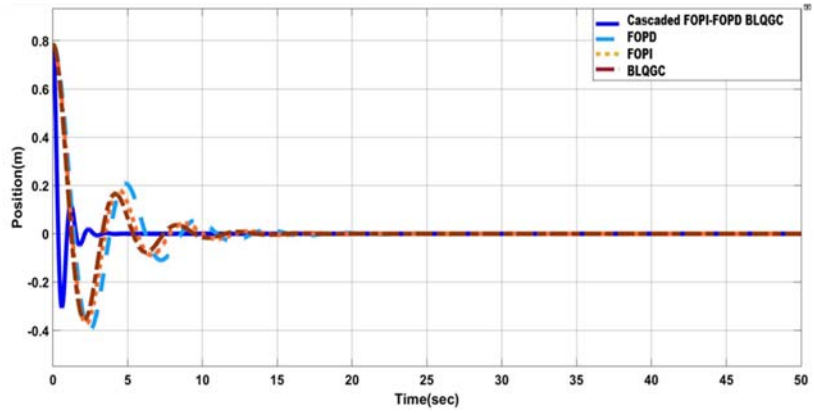

(b)

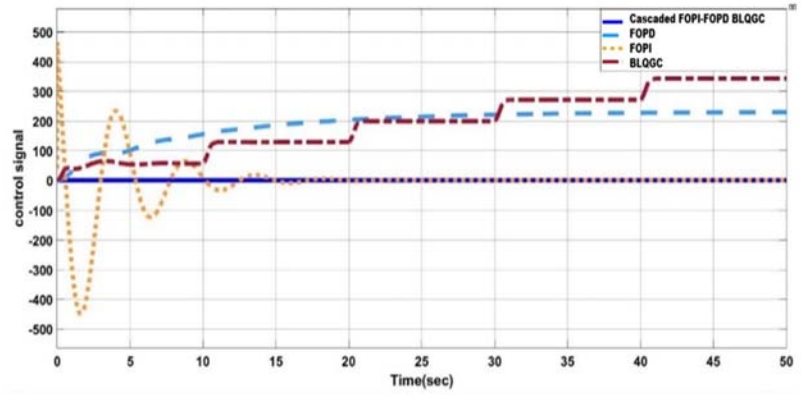

(c)

Figure 5.5 Proposed (FOPI-FOPD-BLQGC) Controller Response Tuned with GOA-FA Algorithm (a) Pendulum Angle Response, (b) Cart Position Response, (c) Controller Effort Response

Table 5.4 Comparative Transient Analysis

Parameters / Controller	Pendulum Angle (θ)				Cart Position (x)			
	t_r (sec)	M_p	t_s (sec)	e_{ss}	t_r (sec)	M_p	t_s (sec)	e_{ss}
Proposed cascaded FOPI-FOPD-BLQGC	0.1	1.3	3	0	0.2	0.3	3.2	0
FOPD	0.4	0.4	13	0.05	0.5	0.8	19	0.05
FOPI	0.5	0.5	19	0.05	0.6	0.8	19	0.05
BLQGC	0.7	0.7	20	0.07	0.7	0.7	20	0.07

5.6.2 Closed-Loop Stability Analysis under Impulsive Disturbances

Stability is a crucial aspect to consider while designing any system, as an unstable system can result in adverse behavior, ranging from poor performance to system damage. This is particularly important when designing systems with life-critical applications, such as spacecraft, underwater vehicles, and human-driven transportation. The FOPD, FOPI, BLQGC and Cascaded FOPI-FOPD-BLQGC controllers are tested on CIP system. An external force of 1(N) applied to the pendulum arm, causing a deviation in the pendulum angle, and the proposed Cascaded FOPI-FOPD-BLQGC controller stabilizes the pendulum at the upright position very quickly. Figures 5.6 (a-c) depicts the stability response of the pendulum angle, cart position, and controller effort. The CIP system can recover from the disturbance and attain an upright position within 3.5 seconds. Furthermore, with the aid of the proposed Cascaded FOPI-FOPD-BLQGC controller, the cart returns to its reference position in 3.2 seconds, demonstrating satisfactory performance despite the sudden disruption.

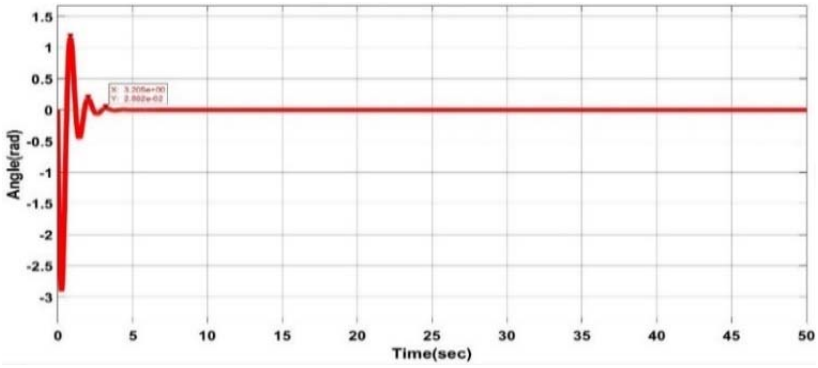

(a)

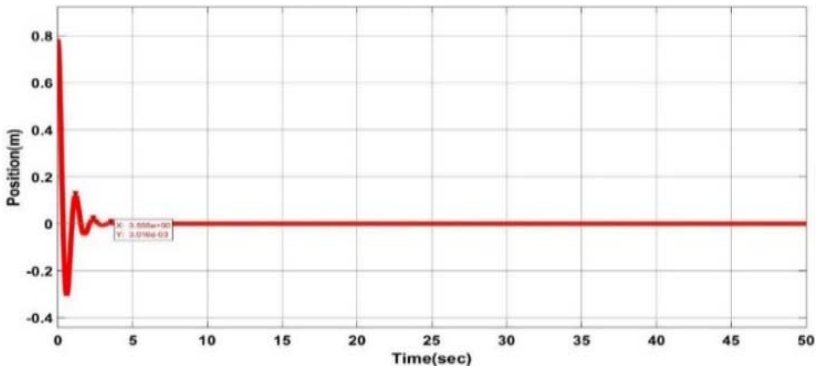

(b)

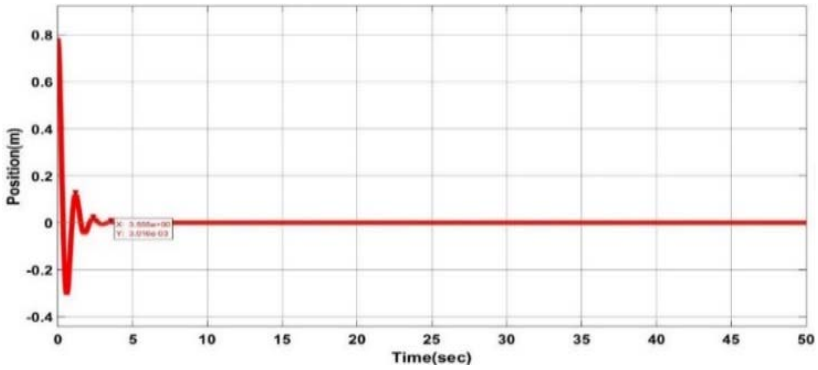

(c)

Figure 5.6 Stability Response of Proposed Controller with Application of 1(N) Impulse Force (a) Pendulum Angle Response (b) Cart Position Response (c) Controller Effort

5.6.3 Robustness Analysis under Parametric Uncertainties

Robust analysis of any controller is crucial in controller design, as it ensures the model's satisfactory behavior even in the presence of uncertainties. The pendulum mass

(m) variation could alter the torque required to swing and stabilize the pendulum in the upright position. Change in Cart-mass (M) could be a result of a modified system parameter or a disturbance parameter, with additional weight added during operation. And this will change the requirements for external force input. Similarly, Pendulum length (l) will affect the total torque experienced by the pendulum and ultimately result in angle displacement [27] [28] [26]. So, it explains the interdependence of the pendulum mass, cart mass, and pendulum length, and their importance in any controller design. To evaluate the robustness of the proposed controller, three varied sets of cart mass (2.1kg-2.3kg), pendulum mass (0.1kg-0.3kg), and pendulum length (0.1m-0.3m), are considered as demonstrated in *cases 1-3* in the following section.

Case 1: The system parameters are changed to $M = 2.1kg\ (12.5\%), m = 0.1kg\ (56.52\%)\ and\ l = 0.1m\ (73.68\%)$, from the initial values and their pendulum-angle and cart-position responses are shown in Figures 5.7(a-b) and quantitatively compared in Table 5.5.

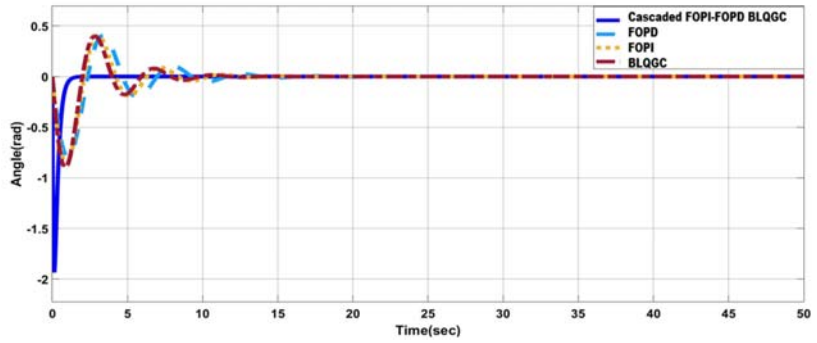

(a)

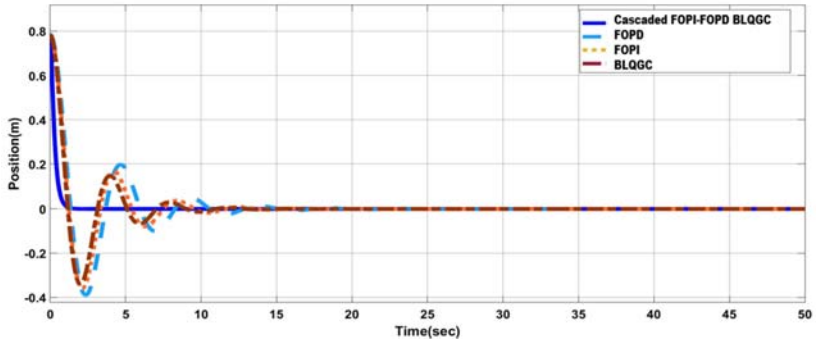

(b)

Figure 5.7 Comparative Responses with $M = 2.1kg, m = 0.1kg$ and $l = 0.1m$ (a) Pendulum Angle Response (b) Cart Position Response

Table 5.5 Comparative Transient Parameters for Case 1

Parameters / Controller	Pendulum Angle (θ)				Cart Position (x)			
	t_r (sec)	M_p	t_s (sec)	e_{ss}	t_r (sec)	M_p	t_s (sec)	e_{ss}
Proposed cascaded FOPI-FOPD-BLQGC	0.1	0.8	2	0	0.1	0.1	2	0
FOPD	1.5	0.2	20	0.06	1.6	0.3	20	0.05
FOPI	1.8	0.2	19	0.05	1.7	0.3	19	0.05
BLQGC	2.0	0.18	20	0.07	2.0	0.2	20	0.07

As shown in Table 5.5, t_r time obtained with proposed controller, FOPD, FOPI and BLQGC are 0.1sec, 1.5sec, 1.8sec and 2.0sec respectively to stabilize the pendulum and 0.1sec, 1.6sec, 1.7sec and 2.0sec respectively for cart-position control. Similarly, Mp recorded for these controllers is 0.8, 0.2, 0.2, and 0.18 respectively for pendulum-control and 0.1, 0.3, 0.3, and 0.2 respectively for cart-position control. Further, the proposed controller also attained the zero e_{ss} value in 2sec of t_s time for both pendulum stabilization and cart stabilization. The FOPD, FOPI and BLQGC controllers are settling to e_{ss} value of 0.06, 0.05 and 0.07 for pendulum-angle and of 0.05, 0.05 and 0.07 for cart-position in 20sec, 19 sec and 20sec of t_s time respectively. The results show that the implemented controller can stabilize the CIP with minimum values of t_r, e_{ss}, M_p and t_s.

Case 2: The system parameters are changes to $M = 2.2kg$ $(8.33\%), m = 0.2kg$ (13.04%) and $l = 0.2m$ (47.36%), from the initial setting and its pendulum-angle and cart-position responses are given in Figures 5.8(a-b) and the respective transient parameters are interpreted in Table 5.6.

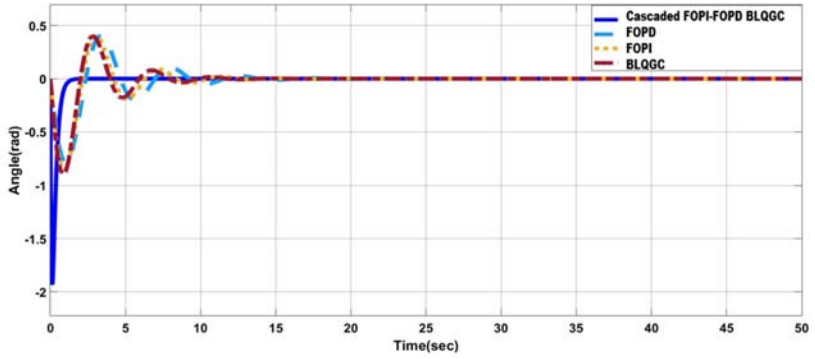

(a)

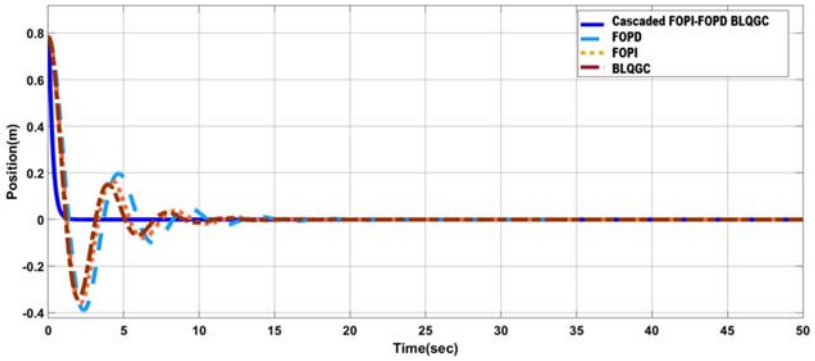

(b)

Figure 5.8 Comparative Responses with $M = 2.2kg$, $m = 0.2kg$ and $l = 0.2m$ (a) Pendulum Angle Response (b) Cart Position Response

As given in Table 5.6, the proposed controller, FOPD, FOPI, and BLQGC are getting t_r of 0.1sec, 2 sec, 3sec and 3sec respectively to pendulum-angle and are 0.1sec, 3sec, 3 sec and 3 sec respectively for cart-position. The M_p recorded for these controllers is 0.3, 0.7, 0.8, and 0.3, respectively, for pendulum control and 0.5, 0.4, 0.6, and 0.7, respectively, for cart control. Similarly, the proposed cascaded FOPI-FOPD-BLQGC controller reaches the zero e_{ss} value in 3sec for pendulum stabilization as well as cart stabilization, while FOPD, FOPI, and BLQGC are reaching to e_{ss} value of 0.05, 0.05, and 0.08 for pendulum control and of 0.07, 0.05, and 0.07 for cart control in 18sec, 19sec, and 20sec of settling time, respectively.

Table 5.6 Comparative Transient Parameters for Case 2

Parameters / Controller	Pendulum Angle (θ)				Cart Position (x)			
	t_r (sec)	M_p	t_s (sec)	e_{ss}	t_r (sec)	M_p	t_s (sec)	e_{ss}
Proposed cascaded FOPI-FOPD-BLQGC	0.1	0.3	3	0	0.1	0.5	3	0
FOPD	2	0.7	18	0.05	3	0.4	18	0.07
FOPI	3	0.8	19	0.05	3	0.6	19	0.05
BLQGC	3	0.3	20	0.08	3	0.7	20	0.07

Case 3: The system parameters are changed to $M = 2.3kg$ (4.2%), $m = 0.3kg$ (30.43%) and $l = 0.3m$ (21.05%), from the initial setting and its pendulum-angle and cart-position responses are given in Figures 5.9(a-b) and the respective transient parameters are interpreted in Table 5.7.

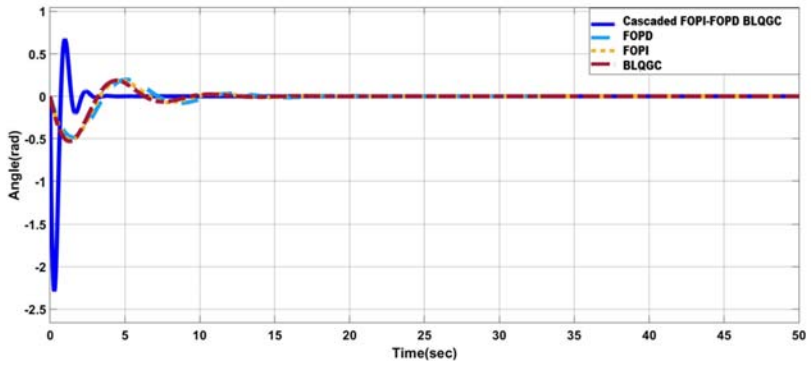

(a)

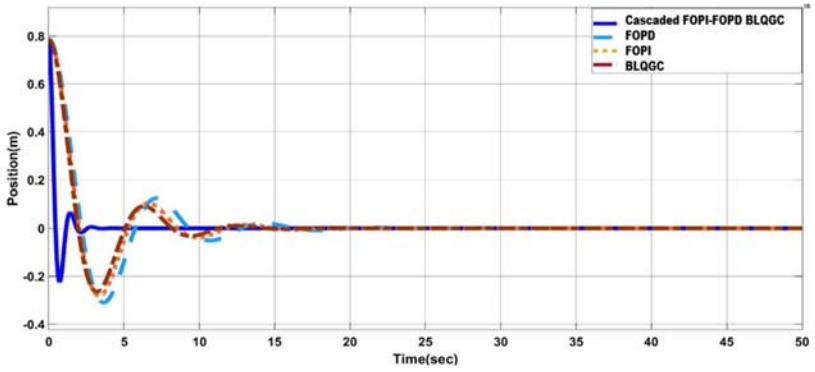

(b)

Figure 5.9 Comparative Responses with $M = 2.3kg$, $m = 0.3kg$ and $l = 0.3m$ (a) Pendulum Angle Response (b) Cart Position Response

As given in Table 5.7, the proposed controller is getting zero e_{ss} value in 3 seconds, and FOPD, FOPI, and BLQGC are reaching e_{ss} value of 0.05, 0.05, and 0.07 in 19 sec, 19 sec, and 20 sec of t_s time, respectively, for both pendulum stabilization and cart stabilization. Furttime for these controllers is 1 sec, 7 sec, 7 sec, and 7 sec, respectively, to stabilize the pendulum, and 2sec, 7 sec, 7 sec, and 7 sec, respectively, for cart control. Similarly, the M_p for these controllers, the values are 0.6, 0.5, 0.5, and 0.7, respectively, for pendulum control and 0.3, 0.5, and 0.7, respectively, for cart control. The results again confirm the superiority of the proposed cascaded FOPI-FOPD-BLQGC, as it gives better values of t_r, M_p, t_s and e_{ss}.

Table 5.7 Comparative Transient Parameters for Case 3

Parameters / Controller	Pendulum Angle (θ)				Cart Position (x)			
	t_r (sec)	M_p	t_s (sec)	e_{ss}	t_r (sec)	M_p	t_s (sec)	e_{ss}
Proposed cascaded FOPI-FOPD-BLQGC	1	0.6	3	0	2	0.3	3	0
FOPD	7	0.5	19	0.05	6	0.5	19	0.05
FOPI	7	0.5	19	0.05	7	0.5	19	0.05
BLQGC	7	0.7	20	0.07	7	0.7	20	0.07

The responses shown in Figure 5.7, Figure 5.8 and Figure 5.9 under the prevailing test conditions of cases 1, case 2 and case 3, confirms that the proposed cascaded FOPI-FOPD-BLQGC controller is able to adopt suppression of parameter changes for CIP system successfully and stabilize quickly as compared to FOPD, FOPID and BLQGC controllers.

5.6.4 Frequency Domain Analysis

Frequency domain parameters: Gain Margin (GM), Phase Margin (PM), and Bandwidth (BW) are used for analyzing the proposed cascaded FOPI-FOPD-BLQGC controller in comparison to FOPD, FOPID and BLQGC controllers. The magnitude and phase variation against frequency are depicted in Figure 5.10, and parameter values are

summarized in Table 5.8. GM and PM represent the maximum gain and phase, respectively, up to which the system remains stable. The GMs achieved with the proposed cascaded FOPI-FOPD-BLQGC, FOPD, FOPI, and BLQGC controllers are 8.02, 6.8, and 6.5, 6 respectively. Similarly, the PM and BW recorded with cascaded FOPI-FOPD-BLQGC, FOPD, FOPI, and BLQGC controllers are 45, 45, 44, and 3.5, 3.3, 3.2, 3.1, respectively. Hence, the improved frequency response of CIP with the proposed cascaded FOPI-FOPD-BLQGC controllers, as evidenced by GM (8.02), PM (45), and BW (3.5), is confirmed over FOPD, FOPI, and BLQGC controllers.

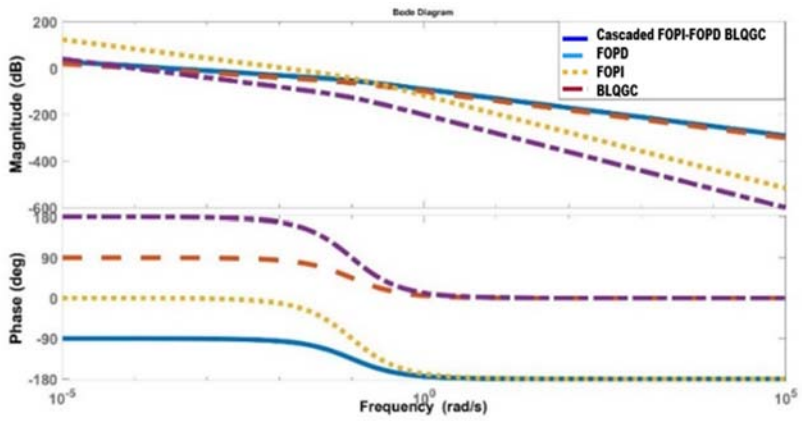

Figure 5.10 Comparative Bode Plot of Cascaded FOPI-FOPD-BLQGC, FOPD, FOPI, and BLQGC Controllers

Table 5.8 Frequency Domain (Bode Plot) Parameters

Parameters / Controller	GM (dB)	PM (Degree)	Bandwidth
Proposed cascaded FOPI-FOPD-BLQGC	8.02	45	3.5
FOPD	6.8	45	3.3
FOPI	6.5	44	3.2
BLQGC	6.0	44	3.1

5.7 Concluding Remarks

This chapter presented a hybrid cascaded FOPI–FOPD–BLQGC controller for stabilizing the cart–inverted pendulum system. The proposed structure effectively combines fractional-order feedback control with BLQGC feedforward action to handle

nonlinear dynamics and stochastic disturbances. The hybrid GOA–FA optimization technique enabled efficient tuning of controller parameters, thereby improving overall system performance. The results demonstrated enhanced transient response, robustness, and stability compared to conventional FOPI, FOPD, and BLQGC controllers. The proposed cascaded FOPI-FOPD-BLQGC controller showed better disturbance rejection and resilience under parametric uncertainties, making it suitable for real-time nonlinear control applications.

Chapter 6

Hybrid Metaheuristic-Optimized Adaptive Neuro-Fuzzy Controller for Cart–Inverted Pendulum System*

6.1 Introduction

In the preceding chapters, conventional and advanced control strategies, including PID, fractional-order PID (FOPID), and the hybrid cascaded FOPI–FOPD–BLQGC controller, were developed and analyzed for stabilizing the Cart-Inverted Pendulum (CIP) system. Although these approaches demonstrated significant improvements in transient performance, robustness, and disturbance rejection, their effectiveness largely depends on accurate mathematical modeling and proper parameter tuning. For highly nonlinear and uncertain systems such as the CIP system, model-based controllers may struggle with complex, unmodeled nonlinear dynamics. To address these challenges, artificial intelligence (AI)-based control techniques have emerged as a powerful alternative for nonlinear dynamic systems [138] [139]. The Controllers based on fuzzy logic, neural networks (NNs), and hybrid neuro-fuzzy approaches can learn system behavior from data, adapt to uncertainties, and reduce dependence on precise mathematical models [140]. Fuzzy Logic Controllers (FLCs) are particularly effective in representing system behavior using linguistic rules derived from expert knowledge, making them suitable for systems with imprecise or incomplete models [141]. However, their performance depends on the design of appropriate rule sets, which often requires prior knowledge and manual tuning. In contrast, neural networks provide strong learning and approximation capabilities, enabling them to model complex nonlinear relationships directly from data, but they lack interpretability and efficient uncertainty handling [142] [143].

In this context, the present chapter aims to develop a Nero-Fuzzy controller that combines the learning capability of a neural network with the linguistic approach of fuzzy logic systems. The controller takes the error and its rate of change as inputs, and it

* *This chapter was published in Multimedia Tools and Applica tions, Vol. 83.18 (2024): pp. 54839-54861, Springer, doi: https://doi.org/10. 1007/s11042-023-17699-3*

primarily controls the system's transient behavior. An integral loop is added in parallel with the neuro-fuzzy controller to compensate for accumulated errors and facilitate zero steady-state error. The controller parameters are optimally tuned using a hybrid PSO–ACO algorithm. The objective is to enhance system performance by minimizing pendulum angle error, angular deviation, and cart position error while ensuring improved stability and robustness. By combining intelligent control with hybrid optimization, the proposed approach seeks to achieve faster convergence, better tracking accuracy, and superior disturbance rejection compared to previously implemented controllers. The proposed technique's performance is compared with that of classical PID to stabilize the CIP model. The control objective considered in this chapter is consistent with those defined in the previous chapters, stabilizing the pendulum in the upright position and the cart at the reference position. This dual-objective control problem requires precise coordination between cart motion and pendulum dynamics due to their strong coupling. In addition, the controller must ensure fast transient response, minimal steady-state error, and robustness against disturbances and parameter variations. The detailed mathematical modelling of the CIP system has already been presented in Chapter 2 and is adopted here without modification.

The brief outline of the chapter is as follows. Section 6.2 discusses the overview of artificial intelligence-based control techniques, and Section 6.3 explains the concept of a hybrid neuro-fuzzy controller. The hybrid ACO-PSO optimization technique is presented in Section 6.4. Results and Discussion in Section 6.5. Finally, Section 6.6 presents final concluding remarks.

6.2 Overview of Artificial Intelligence-based Controllers

Artificial intelligence (AI)-based controllers have gained significant attention in recent years for controlling nonlinear and uncertain dynamic systems, such as the Cart-Inverted Pendulum (CIP) [144]. Unlike conventional model-based controllers, AI-based approaches can learn system behavior from data, adapt to uncertainties, and handle nonlinearities effectively [145] [146]. Among these, Fuzzy Logic Controllers (FLCs), Neural Networks (NNs), and hybrid neuro-fuzzy systems are widely adopted due to their flexibility and robustness [147-150]. Fuzzy Logic Controllers (FLCs) are

particularly useful for systems where precise mathematical models are difficult to obtain. They utilize linguistic rules and membership functions to represent system behavior based on human expertise, making them suitable for handling imprecision and uncertainty [151]. However, designing an effective fuzzy rule base requires prior knowledge and manual tuning, which may limit scalability and adaptability in complex systems.

On the other hand, Neural Networks (NNs) offer powerful learning and approximation capabilities, enabling them to model highly nonlinear relationships directly from input–output data [152]. NNs can be trained using historical datasets and can adapt to varying system dynamics. Despite these advantages, neural networks lack interpretability and are less effective at explicitly handling uncertainty than fuzzy systems. Additionally, they may require large training datasets and careful parameter tuning to achieve optimal performance.

To overcome the limitations of individual AI techniques, hybrid approaches that utilize neural network architectures to represent fuzzy logic systems come into play. These hybrid controllers integrate the learning capabilities of neural networks with the reasoning and knowledge representation of fuzzy logic, resulting in improved convergence speed, transient response, and steady-state accuracy [153] [154]. This combination allows the controller to automatically tune fuzzy rules based on data, reducing reliance on manual design while maintaining interpretability.

Therefore, the use of a hybrid neuro-fuzzy approach is well justified for the CIP system, where both uncertainty handling and learning capability are essential. This motivates the adoption of a hybrid neuro-fuzzy -based controller in the present work, further enhanced by hybrid optimization techniques to improve performance.

6.3 Hybrid Neuro-Fuzzy Controller Design

The Neuro-Fuzzy Inference System is a hybrid intelligent control approach that combines the learning capabilities of neural networks with a rule-based fuzzy control model. It is particularly suitable for nonlinear systems such as the Cart-Inverted Pendulum (CIP), where precise mathematical modeling of its underactuated dynamics

is a significant challenge. In the proposed work, this controller is employed to model the relationship between input (error signal and its derivative) and the corresponding control actions, thereby improving system stability and performance.

A neuro-fuzzy controller is a 6-layer network, as shown in Figure 6.1. In this architecture, circles represent fixed nodes and squares represent adaptive nodes. The controller takes X and Y as input and produces F as output.

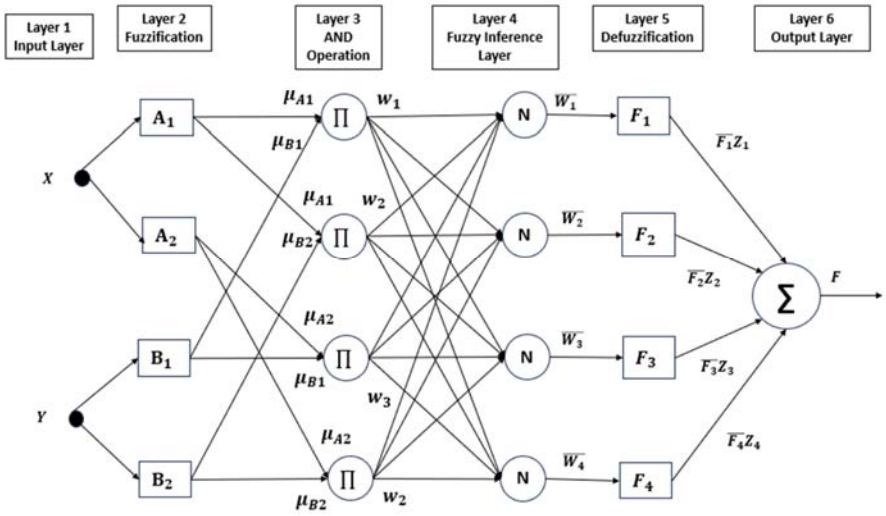

Figure 6.1 Architecture of Neuro-Fuzzy Controller

Layer 1: In this input layer, external inputs are entered through a linear transfer function.

Layer 2: This layer is adaptive, with its parameters changing during training. The parameters A_1, A_2, B_1 and B_2 represents a membership function used to design a fuzzy interface. Here, the node function associated with each node is given by equations (6.1) -(6.2).

$$O_i^1 = \mu_{Ai}(x), \qquad i = 1,2 \tag{6.1}$$

$$O_{1,i} = \mu_{Bi}(x), \qquad i = 3,4 \tag{6.2}$$

The Gaussian membership function is used in this layer to construct an FIS system because it provides a continuous, smooth transition, enhancing learning capability and stability. The mathematical representation is given in equations (6.3)

$$Gaussian\ (x; c, \sigma) = \ e^{-\frac{1}{2}\left(\frac{x-c}{\sigma}\right)^2} \tag{6.3}$$

Where (c, σ) are the premises parameters, which control the shape of the membership function.

Layer 3: Each node is a fuzzy AND operator, which multiplies the incoming membership value corresponding to the (x, y) input and produces the firing strength of the rule, given in equations (6.4)

$$O_{2,i} = W_k = \mu_{Ai}(x) \times \mu_{Bj}(x), \quad i = 1,2\ ; j = 1,2 : k = 2(i-1) + j \tag{6.4}$$

Layer 4: This layer is a normalization layer, where the ith node calculates the ratio of the firing strength of ith rule to the summation of the rule's firing strength, given in equations (6.5).

$$O_{3,i} = \overline{W_i} = \frac{W_1}{W_1+W_2+W_3+W_4} \quad , \quad i = 1,2,3,4 \tag{6.5}$$

where W_i represent the normalized firing strength.

Layer 5: This layer defuzzifies the firing strength it receives from layer 4 and produces a crisp value. Unlike Sugen's method, which utilizes the linear relationships of the consequences parameter, the Mamdani approach uses linguistic variables (e.g., "Output is Small"). Hence, Mamdani's approach allows defining membership functions on the output side, and its parameters are considered as consequence parameters. The neuro-fuzzy algorithm (such as backpropagation or nature-inspired techniques) tunes the shape parameters (Center, Width) of these output membership functions to minimize the error between the predicted and target outputs.

The output equation is given as equations (6.6)

$$F_i = \frac{\sum_1^N W_i b_i}{\sum_1^N W_i} \tag{6.6}$$

F_i is the crisp output value and W_i is the weight (firing strength) of ith rule in layer 4. Here the b_i represent the peak of the output membership function, which is considered here as a consequence parameter.

Layer 6: This is a final output layer having a summation function of all incoming signals, given by equations (6.7):

$$O_{5,i} = \sum \overline{W_i}\ F_i \tag{6.7}$$

In the learning and training phase, the premises parameter at the input side and the consequence parameters at the output side are adjusted. There are two algorithms used in this phase: Forward Pass, where premise parameters are fixed, and consequence parameters are updated, and Backward Pass, where consequence parameters are fixed, and premise parameters are updated. Working of the neuro-fuzzy controller is depicted in Figure 6.2.

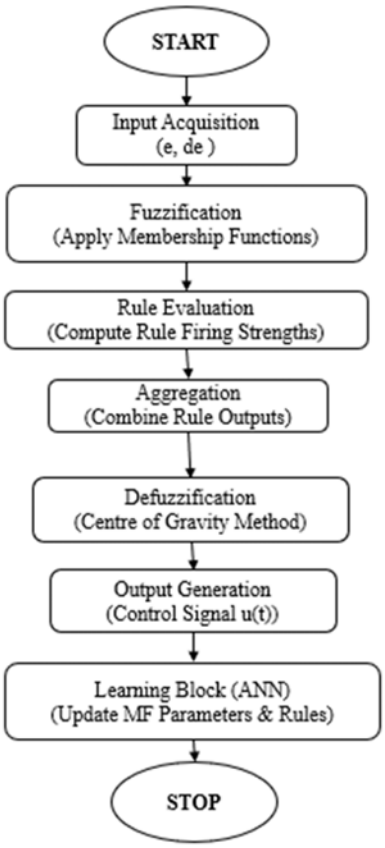

Figure 6.2 Flow Chart of Neuro-Fuzzy Controller Implementation

During the learning phase of a neural network, the ADAM (Adaptive Moment Estimation) optimizer updates the parameters of the premises and consequences. It checks the prediction error at the end of each iteration and adjusts the membership

parameters to reduce it further. The proposed model integrates a 25-rule fuzzy inference system (FIS) with Gaussian input and triangular output membership functions over the [-2, 2] range, tuned by a neural network to minimize errors. The underlying neural network architecture consists of 4 input layers, 10 hidden layers, 2 dense layers, and 2 output layers, designed to optimize the FIS parameters through training data.

6.4 Hybrid PSO-ACO Algorithm

In the proposed hybrid optimization approach, Particle Swarm Optimization (PSO) is employed to enhance the parameter selection mechanism of the Ant Colony Optimization (ACO) algorithm. Unlike conventional ACO, where parameter tuning often relies on predefined heuristic rules, the integration of PSO enables a more robust and adaptive search based on particle interactions within the solution space. This allows the optimization process to be guided by collective intelligence rather than fixed assumptions, thereby improving convergence toward optimal solutions.

Furthermore, the enhanced ACO component effectively identifies optimal paths by simulating ants' pheromone-based search behaviour. Through hybridization, the search space is efficiently reduced, eliminating redundant or less promising paths and enabling faster identification of the shortest path even in large, complex search domains. In this context, PSO provides strong global exploration, while ACO enables efficient local exploitation through pheromone updating and path selection mechanisms.

As a result, the hybrid PSO–ACO algorithm achieves a better balance between exploration and exploitation, leading to improved convergence speed and solution quality. The obtained results demonstrate that the proposed hybrid approach outperforms the standalone PSO and ACO algorithms in terms of optimization efficiency and accuracy. The workflow chart is given in Figure 6.3. The hybrid ACO-PSO algorithm operates through a three-stage hierarchical search strategy that balances global exploration with local exploitation. In the Employed Learning phase, the swarm initiates a wide-area search, updating particle velocities using exemplars generated via Biogeography-Based Optimization (BBO), thereby ensuring the population maintains diversity and avoids premature clustering. This is followed by the Onlooker Learning

phase, which mimics ant behavior by assigning pheromone-based probabilities to particles; a Roulette Wheel selection then identifies high-quality targets for local refinement and intensive search. Throughout these cycles, the algorithm tracks the progress of individual particles using a stagnation counter. If a particle fails to improve its personal best after a predefined Limit, the Scout Learning phase triggers a random re-initialization of that particle. This mechanism effectively "breaks" local optima traps, allowing the system to continuously discover new regions of the search space until the global best position is optimized.

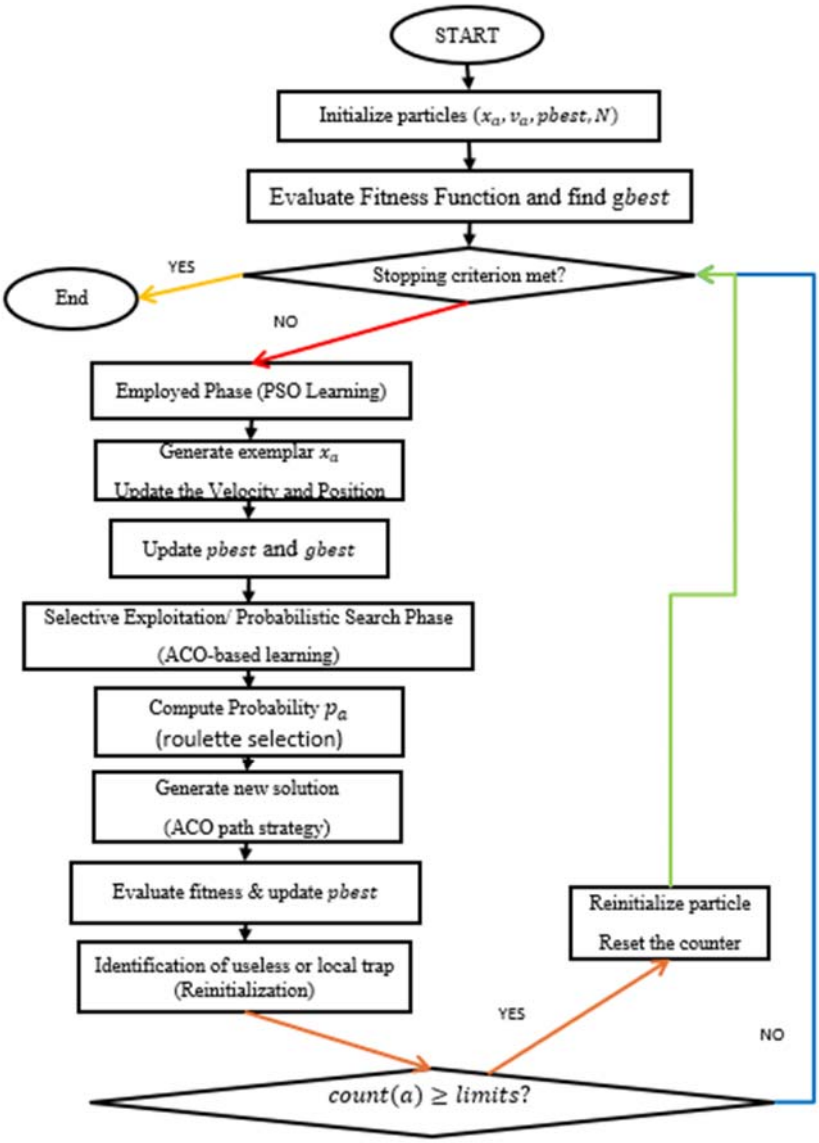

Figure 6.3 Flowchart of Hybrid PSO-ACO Algorithm

Assume that the optimization problem has N candidate solutions (particles), and each particle is represented by a D-dimensional vector. For the i^{th}particle at iteration k, the population is given as equation (6.8).

$$X_i^k = \left[x_{i1}^k, x_{i2}^k, \dots, x_{iD}^k\right] \tag{6.8}$$

and its velocity calculated from equation (6.9)

$$V_i^k = \left[v_{i1}^k, v_{i2}^k, \dots, v_{iD}^k\right] \tag{6.9}$$

where $i = 1,2, \dots, N$.

The personal best position of the ith particle is denoted by equation (6.10)

$$P_i^k = \left[p_{i1}^k, p_{i2}^k, \dots, p_{iD}^k\right] \tag{6.10}$$

and the global best position among all particles is represented as equation (6.11)

$$G^k = \left[g_1^k, g_2^k, \dots, g_D^k\right] \tag{6.11}$$

1. Fitness Evaluation

The objective function value for the ith particle is evaluated as equation (6.12)

$$f_i^k = f\left(X_i^k\right) \tag{6.12}$$

For a minimization problem, the fitness can be expressed as equation (6.13)

$$\text{Fit}_i^k = \begin{cases} \frac{1}{1+f_i^k}, & f_i^k \geq 0 \\ 1+|\, f_i^k \,|, & f_i^k < 0 \end{cases} \tag{6.13}$$

This fitness value is used in the probabilistic selection stage.

2. Personal Best and Global Best Update

The personal best of each particle is updated as equation (6.14)

$$P_i^{k+1} = \begin{cases} X_i^k, & \text{if } f(X_i^k) < f(P_i^k) \\ P_i^k, & \text{otherwise} \end{cases} \tag{6.14}$$

The global best is selected as the best personal best among all particles, following equation (6.15)

$$G^k = \arg \min_{i \in \{1,2,\ldots,N\}} f(P_i^k) \tag{6.15}$$

3. Probability Calculation for ACO-Based / Roulette Selection

To select candidate particles for further learning, the probability associated with the i^{th}particle is defined as equation (6.16)

$$p_i^k = \frac{\text{Fit}_i^k}{\sum_{j=1}^{N} \text{Fit}_j^k} \tag{6.16}$$

This probability is used in the roulette-wheel mechanism so that better particles have a higher chance of being selected.

4. Exemplar Selection

For the selected particle i, an exemplar particle $r$is chosen probabilistically according to p_i^k. The exemplar-guided learning term may be written as equation (6.17)

$$E_i^k = X_r^k \tag{6.17}$$

where $r$is the index selected using roulette-wheel sampling.

5. PSO-Based Velocity Update

The velocity of the i^{th}particle is updated using inertia, cognitive, and social learning terms as equation (6.18)

$$V_i^{k+1} = \omega V_i^k + c_1 r_1 \left(P_i^k - X_i^k\right) + c_2 r_2 \left(G^k - X_i^k\right) + c_3 r_3 \left(E_i^k - X_i^k\right) \tag{6.18}$$

where: ω is the inertia weight, c_1, c_2, c_3 are acceleration coefficients, $r_1, r_2, r_3 \in [0,1]$ are uniformly distributed random numbers.

The additional term $\left(E_i^k - X_i^k\right)$ incorporates the probabilistic learning behavior into the PSO framework.

6. Position Update

After updating the velocity, the particle position is updated as equation (6.19)

$$X_i^{k+1} = X_i^k + V_i^{k+1} \tag{6.19}$$

To keep the search within allowable limits, the updated position is bounded as equation (6.20)

$$x_{id}^{k+1} = \begin{cases} x_d^{\min}, & x_{id}^{k+1} < x_d^{\min} \\ x_d^{\max}, & x_{id}^{k+1} > x_d^{\max} \\ x_{id}^{k+1}, & \text{otherwise} \end{cases} \tag{6.20}$$

for $d = 1,2, \dots, D$.

Similarly, velocity can be bounded as equation (6.21)

$$v_{id}^{k+1} = \begin{cases} v_d^{\min}, & v_{id}^{k+1} < v_d^{\min} \\ v_d^{\max}, & v_{id}^{k+1} > v_d^{\max} \\ v_{id}^{k+1}, & \text{otherwise} \end{cases} \tag{6.21}$$

7. Reinitialization of Stagnant Particles

If a particle fails to improve for a predefined number of trials, it is reinitialized randomly to increase diversity, given in equations (6.22) -(6.23)

$$x_{id}^{k+1} = x_d^{\min} + rand(0,1)\left(x_d^{\max} - x_d^{\min}\right) \tag{6.22}$$

$$v_{id}^{k+1} = v_d^{\min} + rand(0,1)\left(v_d^{\max} - v_d^{\min}\right) \tag{6.23}$$

This step helps the algorithm escape from local optima.

8. Termination Criterion

The iterative process continues until one of the following conditions is satisfied, as given in equation (6.24) or equation (6.25).

$$k = k_{\max} \tag{6.24}$$

or

$$| f(G^{k+1}) - f(G^k) | < \varepsilon \tag{6.25}$$

where $k_{\max}$is the maximum number of iterations and $\varepsilon$is a predefined tolerance.

6.5 Results and Discussion

The performance of the implemented control design is analyzed through the transient response of cart position, cart velocity, pendulum angle, and angular velocity to ensure the CIP model's stability around the equilibrium state. Training and validation results are also reviewed to show the implemented neural network's learning capability. The proposed controller performance is further compared with conventional PID and existing control methodology in references [155] and [156].

6.5.1 Training Performance of Neural Network

Neural networks are universal approximators, and with sufficient neurons and layers, they can fit any complex function. Curve fitting is a process that develops a mathematical relationship between the given input and output during the training phase. The close overlap of the training, validation, and test targets and their outputs in the curve-fitting results depicted in Figure 6.4, shows that the NN has efficiently learned the nonlinear relationship between the input and output. The error plot shows that the deviations remain within a very narrow band of approximately ±0.01.

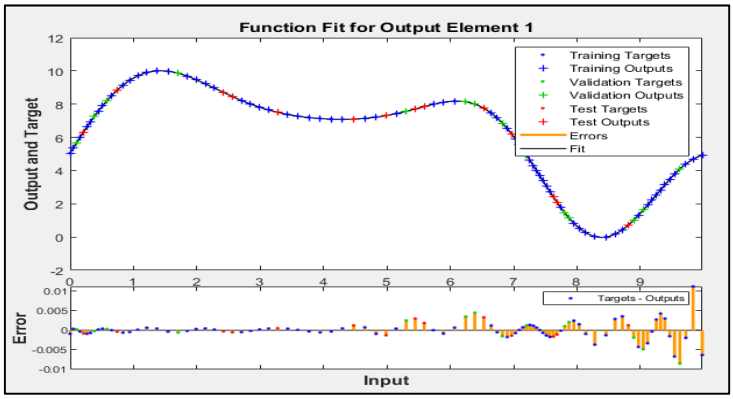

Figure 6.4 Output and the Target of the Fitness Function

The regression plot in Figure 6.5, shows that the predicted outputs efficiently track the actual target value. It confirms that the model has perfectly learned from the training data, as indicated by the correlation coefficient R = 1 in all cases. The slope of the line remains approximately 1, confirming its predictive accuracy and consistency throughout the process.

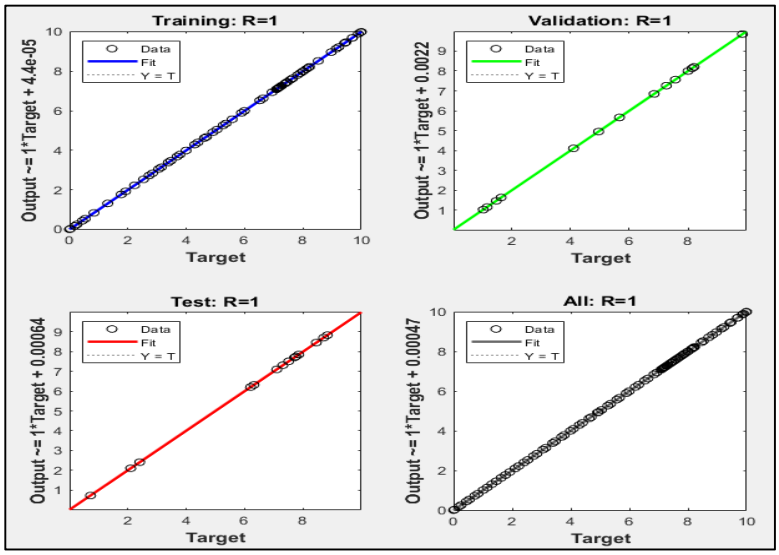

Figure 6.5 Training and Validation Results

6.5.2 Transient System Response

The transient performance parameters of CIP's two variables, cart position and pendulum angle, are given in Figure 6.6, and the controller effort is shown in Figure 6.7. The cart motion exhibits a peak of 0.4m around 0.3 seconds and is followed by an undershoot, settling down to the equilibrium state in 1.4 seconds.

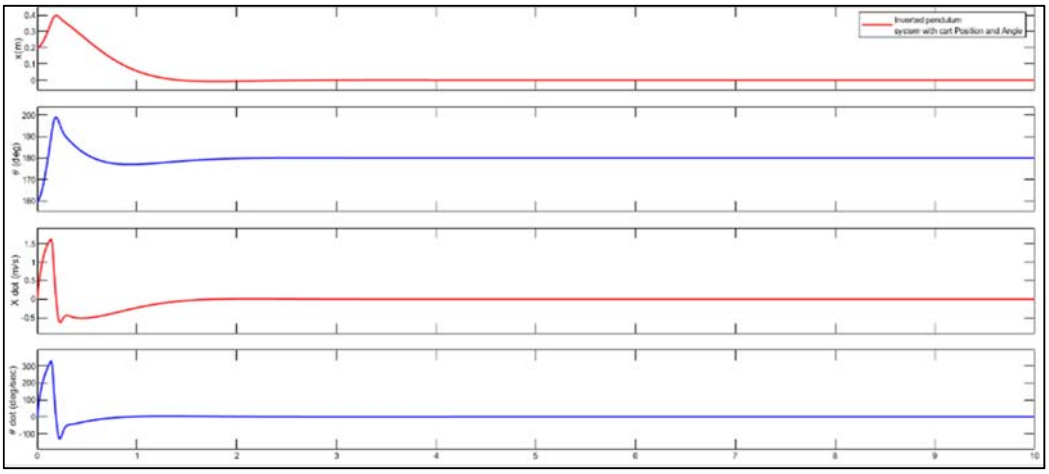

Figure 6.6 Transient Response of the Neuro-Fuzzy Controller

Similarly, a pendulum can stabilize in an upright position in 15 seconds. The controller's efforts initially reach ±12 N, reflecting a strong corrective signal in the

initial phase, and gradually converge to zero. Overall, the system demonstrates fast response, stable convergence, and effective disturbance rejection.

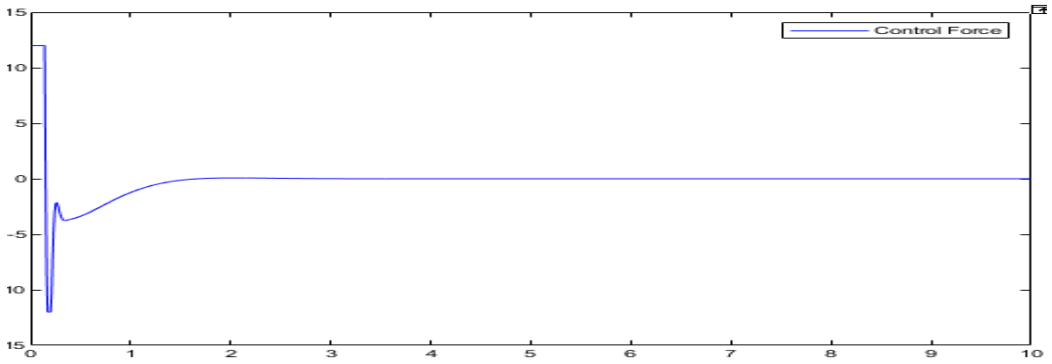

Figure 6.7 Controller Effort Signal

6.5.3 Comparative Performance Analysis

The performance comparison between the implemented control strategy and the PID controller is depicted in Figure 6.8 and Table 6.2. These results show that the proposed technique outperforms the PID controller and provides significant improvements across all transient parameters. The tuned PID controller's gain parameters are listed in Table 6.1.

Table 6.1 PID Controller's Gain Parameters

k_{P1}	k_{I1}	k_{D1}	k_{P2}	k_{I2}	k_{D2}
0.01	10	0.0023	0.01	10	0.0011

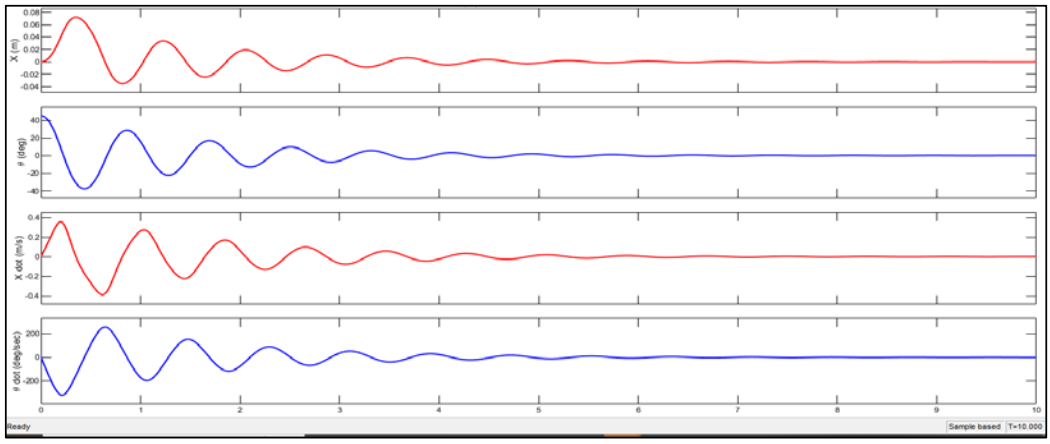

Figure 6.8 Transient Response with PID Controller

Table 6.2 Comparative Performance Analysis with PID Controller

Response	Parameter	PID	With ANFIS	% Change
Cart Position	t_r (sec)	0.6	0.35	↓ 50%
	t_p (sec)	0.8	0.4	↓ 50%
	M_p (deg)	0.075	0.40	↑ 433%
	t_s (sec)	8.0	1.42	↓ 82.5%
	e_{ss}	≈ 0	≈ 0	—
Pendulum Angle	t_r (sec)	0.7	0.25	↓ 64.3%
	t_p (sec)	1.0	0.35	↓ 65%
	M_p (deg)	45	200	↑ 344%
	t_s (sec)	9.0	1.5	↓ 83.3%
	e_{ss}	≈ 0	≈ 0	—

The performance of the proposed neuro-fuzzy controller, compared with other literature publications [155] and [156], is presented in Figure 6.9 and Table 6.3, respectively. The manuscript [155] implemented dual-mode FOPID and compared its effectiveness with that of a PID controller, tuning the controller parameters using the PSO algorithm. The controller presented in this chapter improved performance in terms of rise time, settling time, steady-state error, and ISE error index. Further, compared with paper [156], the proposed work yields a lower MSE error index.

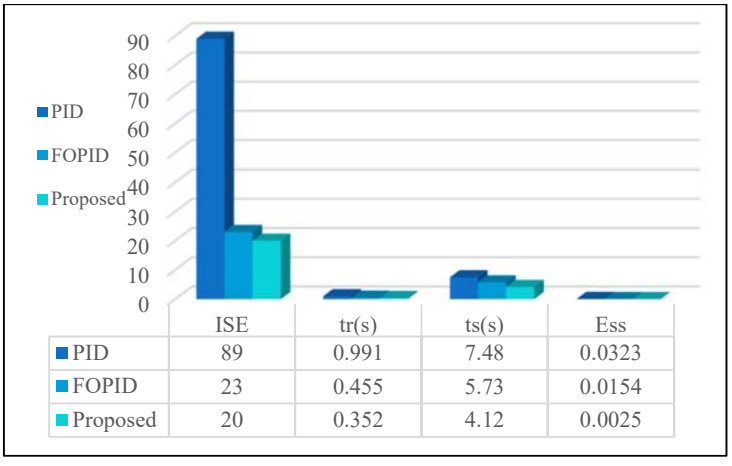

Figure 6.9 Comparative Analysis with Reference [155]

Table 6.3 Comparative Analysis with Reference [156]

Methodology	**MSE**
Existing Method	7.99E-09
Proposed Method	6.88E-09

6.6 Concluding Remarks

This chapter presented the development of an ANN-based ANFIS controller optimized using a hybrid ACO–PSO algorithm for stabilizing the cart–inverted pendulum system. The proposed approach effectively addressed the system's nonlinear and underactuated characteristics by combining neural network adaptive learning with fuzzy inference system linguistic reasoning. The hybrid metaheuristic optimization enabled efficient tuning of controller parameters, thereby enhancing the overall performance of the closed-loop system. A comparative analysis confirmed that the proposed method outperforms both the conventional PID and standalone ANFIS controllers in terms of transient response and accuracy, resulting in lower MSE values.

Chapter 7
Conclusions and Future Scope of Work

7.1 Introduction

This chapter of this thesis demonstrates the main conclusions and future scope of work for the research in the field of control for complex underactuated systems. Design of controllers for the benchmarked Cart–Inverted Pendulum (CIP) system is comprehensively investigated in detail through various conventional controllers, advanced swarm optimized control algorithms, as well as artificial intelligence-based adaptive neuro fuzzy inference system controllers. The research findings of all chapters are outlined and examined along with deliberations of future scope of work.

7.2 Main Conclusions

The research investigations presented in this thesis are targeted to contribute towards the development in the area of intelligent control theory for the control of the benchmark cart inverted pendulum system. The adopted intelligent control techniques have the ability to emulate the physical characteristics of real-time, complex, underactuated systems, which are modelled as differential equations. The primary focus of this work was to systematically demonstrate a progressive evolution from conventional control methods to advanced fractional-order, hybrid, and intelligent control techniques, with the objective of improving system stability, robustness, and dynamic performance. The investigations based on the current research work contribute to the following conclusions:

In chapter 1, motivation, a detailed introduction to the research topic is presented, along with a critical review of the existing literature, and the Cart–Inverted Pendulum model is introduced as a classical benchmark problem. Finally, the chapter outlined the key research objectives and the thesis organization, thereby laying a clear foundation for subsequent chapters focused on controller design, optimization techniques, and the performance evaluation of the proposed control strategies.

The CIP system's dynamic equations and inherent control challenges are thoroughly explained in Chapter 2 to highlight its practical significance. Subsequently, a detailed mathematical model of the system is developed, and the corresponding transfer function and state space equations are derived to facilitate controller design and analysis.

In Chapter 3, the performance of a conventional PID controller was examined under variations in key system parameters, namely cart mass, pendulum mass, and pendulum length. The analysis revealed that the CIP system is highly sensitive to parametric variations, particularly cart mass, which significantly affects transient characteristics such as overshoot, settling time, and stability. These findings identified certain limitations of conventional PID control to handle uncertainties and nonlinear dynamics.

These challenges are addressed in Chapter 4 by a Fractional-Order PID (FOPID) controller, which introduces an additional degree of freedom through fractional integral and derivative orders. The tuning of FOPID parameters using metaheuristic algorithms, such as PSO, WCA, and GOA, demonstrated notable performance improvements. Among these, the GOA-based FOPID controller exhibited superior convergence behaviour and enhanced transient response, achieving reduced overshoot, faster settling time, and improved stability.

Further advancement was achieved by developing a novel hybrid cascaded control architecture combining FOPI–FOPD with Backstepping Linear Quadratic Gaussian Control (BLQGC) in Chapter 5. The incorporation of hybrid GOA–Firefly optimization enabled effective parameter tuning, balancing exploration and exploitation capabilities. The proposed controller significantly improved both transient and frequency domain performance, ensuring robustness against disturbances and parametric uncertainties while simultaneously controlling cart position and pendulum angle.

Finally, in chapter 6, an intelligent control approach based on ANN-assisted ANFIS was proposed to address system nonlinearity and uncertainty more effectively. The integration of hybrid PSO-ACO optimization for tuning ANFIS parameters enhanced learning capability and adaptability. The AI-based controller demonstrated superior performance in minimizing error indices such as ISE, SSE, and MSE, and improved

transient performance, thereby validating its effectiveness for complex nonlinear control problems.

Overall, the main outcome of this research work demonstrates that the progression from conventional PID to fractional-order, hybrid, and intelligent control strategies results in significant improvements in system stability, robustness, and performance. The proposed methodologies provide a strong foundation for the development of efficient controllers for real-time underactuated systems.

7.3 Future Scope of Work

The further extension of this research work may be extended in the following areas:

Swarm optimization has emerged rapidly in the last few years, and tuning controllers for underactuated systems with these algorithms offers significant scope for optimizing controller parameters. Real-time implementation of such controllers can be widely used for the automation and fine control of plants and processes. Since PID controllers are the basic controllers used in almost all industries. Hence, fine-tuning them with swarm algorithms would be extremely helpful for improving the performance, robustness, and efficiency of complex underactuated systems. Extension of these proposed control strategies to other benchmarked systems, such as twin-rotor motor systems, magnetic levitation, and ball-and-plate systems, may be considered in the presence of actuator saturation, friction, backlash, and sensor noise for real-world applicability.

Further, implementation of FOPI, FOPD, FOPID with Backstepping Linear Quadratic Gaussian Control (BLQGC) for other classes of underactuated benchmark systems, such as twin-rotor motor systems, magnetic levitation, and ball and plate systems, etc.

Moreover, there is scope for hybridizing various swarm optimization algorithms, such as Particle Swarm Optimization (PSO) with the Water Cycle Algorithm (WCA) and the Grasshopper Optimization Algorithm (GOA), for PID, FOPID, and BLQGC as promising controllers for improving the performance of complex underactuated systems.

Furthermore, there is a scope to use a deep learning ANFIS system to control the CIP system, which can also be carried out.

References

[1] Krafes, Soukaina, Zakaria Chalh, and Abdelmjid Saka. "A review on the control of second order underactuated mechanical systems." *Complexity* 2018.1 (2018): 9573514.

[2] Davison, Edward J., ed. "Benchmark problems for control system design: Report of the IFAC Theory Committee." International Federation of Automatic Control, 1990.

[3] Spong, Mark W. "Underactuated mechanical systems." *Control problems in robotics and automation*. Berlin, Heidelberg: Springer Berlin Heidelberg, 2005. 135-150.

[4] Zhai, Meng, et al. "Underactuated mechanical systems with both actuator and actuated/unactuated state constraints: A predictive control-based approach." *IEEE/ASME Transactions on mechatronics* 28.3 (2022): 1359-1371.

[5] Fantoni, Isabelle, and Rogelio Lozano. *Non-linear control for underactuated mechanical systems*. Springer Science & Business Media, 2012.

[6] Olfati-Saber, Reza. *Nonlinear control of underactuated mechanical systems with application to robotics and aerospace vehicles*. Diss. Massachusetts Institute of Technology, 2001.

[7] Emran, Bara J., and Homayoun Najjaran. "A review of quadrotor: An underactuated mechanical system." *Annual Reviews in Control* 46 (2018): 165-180.

[8] Spong, Mark W. "The swing up control problem for the acrobot." *IEEE control systems magazine* 15.1 (1995): 49-55.

[9] Ge, Shuzhi Sam, Chen Wang, and Tong Heng Lee. "Adaptive backstepping control of a class of chaotic systems." *International Journal of Bifurcation and Chaos* 10.05 (2000): 1149-1156.

[10] Wang, Li-Xin. "Stable adaptive fuzzy controllers with application to inverted pendulum tracking." *IEEE Transactions on Systems, Man, and Cybernetics, Part B (Cybernetics)* 26, no. 5 (1996): 677-691.

[11] Eltohamy, Khaled Gamal, and Chen-Yuan Kuo. "Real time stabilisation of a triple link inverted pendulum using single control input." *IEE Proceedings-Control Theory and Applications* 144, no. 5 (1997): 498-504.

[12] Kajiwara, Hiroyuki, Pierre Apkarian, and Pascal Gahinet. "LPV techniques for control of an inverted pendulum." *IEEE Control Systems Magazine* 19, no. 1 (1999): 44-54.

[13] Valluru, Sudarshan K., Madhusudan Singh, and Mayank Singh. "Application of Linear Quadratic Methods to Stabilize Cart Inverted Pendulum Systems." In *2018 2nd IEEE International Conference on Power Electronics, Intelligent Control and Energy Systems (ICPEICES)*, pp. 1027-1031. IEEE, 2018.

[14] Valluru, Sudarshan K., Madhusudan Singh, S. Mayank, and V. Khattar. "Experimental validation of PID and LQR control techniques for stabilization of cart inverted pendulum system." In *3rd IEEE International Conference on Recent Trends in Electronics, Information and Communication Technology*, pp. 708-712. 2018.

[15] Sudarshan K. Valluru and Madhusudan Singh "Performance investigations of APSO tuned linear and nonlinear PID controllers for a nonlinear dynamical system" *Journal of Electrical Systems and Information Technology Vol.5, Issue 3 2018 pp.442-452*

[16] Jonathan, P. How. "Benchmarks." *IEEE Control Systems Magazine* (2015): 6-7.

[17] Wai, Rong-Jong, and Li-Jung Chang. "Adaptive stabilizing and tracking control for a nonlinear inverted-pendulum system via sliding-mode technique." *IEEE Transactions on Industrial Electronics* 53, no. 2 (2006): 674-692.

[18] Pangaribuan, Timbang, et al. "The influences of load mass changing on inverted pendulum stability based on simulation study." *IOP Conference Series: Materials Science and Engineering*. Vol. 237. No. 1. IOP Publishing, 2017.

[19] Muskinja, Nenad, and Boris Tovornik. "Swinging up and stabilization of a real inverted pendulum." *IEEE transactions on industrial electronics* 53.2 (2006): 631-639.

[20] Valluru, Sudarshan K., and Rajul Kumar. "Trajectory tracking control of TRMS using FO-PID and FOI-PD controllers: an experiment." *2019 3rd International Conference on Recent Developments in Control, Automation & Power Engineering (RDCAPE)*. IEEE, 2019.

[21] Mondal, Reetam, and Jayati Dey. "Performance analysis and implementation of fractional order 2-DOF control on cart–inverted pendulum system." *IEEE transactions on industry applications* 56.6 (2020): 7055-7066.

[22] Sambo, A. U., et al. "Optimal control of inverted pendulum on cart system." *Journal of Physics: Conference Series*. Vol. 1502. No. 1. IOP Publishing, 2020.

[23] Valluru, Sudarshan K., et al. "Design of multi-loop l-pid and nl-pid controllers: An experimental validation." *2018 2nd IEEE International Conference on Power Electronics, Intelligent Control and Energy Systems (ICPEICES)*. IEEE, 2018.

[24] Varghese, Elisa Sara, Anju K. Vincent, and Veeramani Bagyaveereswaran. "Optimal control of inverted pendulum system using PID controller, LQR and MPC." *IOP Conference Series: Materials Science and Engineering*. Vol. 263. No. 5. IOP Publishing, 2017.

[25] Astrom, Karl J. "PID controllers: theory, design, and tuning." *The international society of measurement and control* (1995).

[26] Bishop, Richard C. Dorf Robert H. *Modern control systems*. 2011.

[27] Konstantopoulos, George C., and Pablo R. Baldivieso-Monasterios. "State-limiting PID controller for a class of nonlinear systems with constant uncertainties." *International Journal of Robust and Nonlinear Control* 30.5 (2020): 1770-1787.

[28] Ezema, E. E., I. I. Eneh, and O. L. Daniya. "Improving structural limitations of PID controller for unstable processes." *International Journal of Engineering Research & Applications* 4.9 (2014): 87-90.

[29] Khalil, Hassan K., and Jessy W. Grizzle. *Nonlinear systems*. Vol. 3. Upper Saddle River, NJ: Prentice hall, 2002.

[30] Podlubny, I. "Fractional-order systems and *PI* $\lambda D\mu$-controllers." *IEEE Transactions on Automatic Control* 44.1 (1999): 208-214.

[31] Kennedy, James, and Russell Eberhart. "Particle swarm optimization." *Proceedings of ICNN'95-international conference on neural networks*. Vol. 4. ieee, 1995.

[32] Heidari, Ali Asghar, et al. "Harris hawks optimization: Algorithm and applications." *Future generation computer systems* 97 (2019): 849-872.

[33] Verma, Neelam, and Sudarshan K. Valluru. "Comparative Study of Parametric." *Modern Electronics Devices and Communication Systems: Select Proceedings of MEDCOM 2021* 948 (2023): 217.

[34] J. Huang, M. Zhang, and C. Xiong, "High-order disturbance observer-based sliding mode control for inverted pendulum systems," *IEEE Trans. Ind. Electron.*, vol. 67, no. 3, pp. 2030–2041, 2020.

[35] S. Mirjalili, "Metaheuristic optimization algorithms in engineering," *Swarm Evol. Comput.*, vol. 44, pp. 1–14, 2019.

[36] Yang, Xin-She. *Nature-inspired optimization algorithms*. Academic Press, 2020.

[37] Verma, Neelam, and Anjali Jain. "Implementation of class topper optimized fractional order proportional-integral-derivative controller for cart-inverted pendulum system." *Majlesi Journal of Electrical Engineering* 19.1 (2025): 1-10.

[38] Verma, Neelam, and Sudarshan K. Valluru. "Comparative Analysis of GOA, WCA and PSO Tuned Fractional Order-PID Controller for Cart-Inverted Pendulum." *2022 IEEE International Power and Renewable Energy Conference (IPRECON)*. IEEE, 2022.

[39] Mousa, M. E., Mohamed Ahmed Ebrahim, and M. A. Moustafa Hassan. "Optimal fractional order proportional—integral—differential controller for inverted pendulum with reduced order linear quadratic regulator." *Fractional Order Control and Synchronization of Chaotic Systems*. Cham: Springer International Publishing, 2017. 225-252.

[40] Ribeiro, Jussara MS, et al. "Comparison of PID controller tuning methods: analytical/classical techniques versus optimization algorithms." *2017 18th international Carpathian control conference (ICCC)*. IEEE, 2017.

[41] Shahnawaj, Chanana Saurabh. "Cascaded Fractional Control Approach for Frequency Regulation of Multi-Source Power System Integrating Renewable Energy Resources." *Evergreen* 11.2 (2024): 949-963.

[42] Pahadasingh, Sunita, et al. "Coati Optimization Algorithm based 3DOF-FOPIDN controller approach for improvement in frequency stability of an isolated microgrid." *2024 IEEE 4th International Conference on Applied Electromagnetics, Signal Processing, & Communication (AESPC)*. IEEE, 2024.

[43] Żegleń-Włodarczyk, Jakub. "Combination of parallel and cascade control on the example of Two Rotor Aerodynamical System with the use of FOPID and PID controllers." *Proceedings of the XXI Polish Control Conference*. Cham: Springer Nature Switzerland, 2023.

[44] Zamani, Majid, et al. "Design of a fractional order PID controller for an AVR using particle swarm optimization." *Control Engineering Practice* 17.12 (2009): 1380-1387.

[45] Mohamed, Mohamed Ahmed Ebrahim, K. Jagatheesan, and B. Anand. "Modern PID/FOPID controllers for frequency regulation of interconnected power system by considering different cost functions." *Scientific Reports* 13.1 (2023): 14084.

[46] Behera, Aurobindo, et al. "A novel cascaded PID controller for automatic generation control analysis with renewable sources." *IEEE/CAA Journal of Automatica Sinica* 6.6 (2019): 1438-1451.

[47] Tomar, Basant, Narendra Kumar, and Mini Sreejeth. "Robust control of rotary inverted pendulum using metaheuristic optimization techniques based PID and fractional order pi λ d μ controller." *Journal of Vibration Engineering & Technologies* 12.Suppl 1 (2024): 1-20.

[48] Mohanty, Prangya, et al. "Design and analysis of the 2DOF-PIDN-FOID controller for frequency regulation of the electric power systems." *International Journal of Ambient Energy* 43.1 (2022): 4463-4476.

[49] Sethy, Sushanta Kumar, et al. "Analysis and Design of IDN-FOPD Controller for Frequency Regulation of Electric Energy System." *Engineering Research Express* (2026).

[50] Rani, Monika, and Sushma S. Kamlu. "Optimal LQG controller design for inverted pendulum systems using a comprehensive approach." *Scientific Reports* 15.1 (2025): 4692.

[51] Patra, Akshaya Kumar, Sunita Swarnamayee Biswal, and Pravat Kumar Rout. "Backstepping linear quadratic gaussian controller design for balancing an inverted pendulum." *IETE Journal of Research* 68.1 (2022): 150-164.

[52] Wang, Ling, et al. "MBPOA-based LQR controller and its application to the double-parallel inverted pendulum system." *Engineering Applications of Artificial Intelligence* 36 (2014): 262-268.

[53] Hazem, Zied Ben, Mohammad Javad Fotuhi, and Zafer Bingül. "Development of a Fuzzy-LQR and Fuzzy-LQG stability control for a double link rotary inverted pendulum." *Journal of the Franklin Institute* 357.15 (2020): 10529-10556.

[54] Kemer, Emre, and Hasan Başak. "Performance analysis of fuzzy-LQR and fuzzy-LQG controllers for active vehicle suspension systems." (2024).

[55] Nguyen, Thi Van Anh, and Quy Thinh Dao. "NONLINEAR STABILITY CONTROL OF INVERTED PENDULUM ON A CART USING LQR-BASED TS FUZZY CONTROL." *Journal of Science and Technique-Vol* 18.03 (2023).

[56] Mandali, Anusree, and Lili Dong. "Modeling and cascade control of a pneumatic positioning system." *Journal of Dynamic Systems, Measurement, and Control* 144.6 (2022): 061004.

[57] Tepljakov, Aleksei, et al. "Towards industrialization of FOPID controllers: A survey on milestones of fractional-order control and pathways for future developments." *IEEE Access* 9 (2021): 21016-21042.

[58] Ghamari, Seyyed Morteza, et al. "Design of an improved robust fractional-order PID controller for buck–boost converter using snake optimization algorithm." *IET Control Theory & Applications* 19.1 (2025): e70008.

[59] Abro, Ghulam E. Mustafa, Ayman M. Abdallah, and Mohssen E. Elshaar. "Swarm coordination and trajectory tracking in quadrotor UAVs using fractional-order PID control strategy." *IEEE Transactions on Automation Science and Engineering* (2025).

[60] Choudhary, Ravi, J. N. Rai, and Yogendra Arya. "Cascade FOPI-FOPTID controller with energy storage devices for AGC performance advancement of electric power systems." *Sustainable Energy Technologies and Assessments* 53 (2022): 102671.

[61] Nagendra, K., et al. "A comprehensive approach to load frequency control in hybrid power systems incorporating renewable and conventional sources with electric vehicles and superconducting magnetic energy storage." *Energies* 17.23 (2024): 5939.

[62] Rustamova, Nodira, and Raveenthiran Vivekanantharasa. "Comprehensive Review and Hybrid Evolution of Teaching–Learning-Based Optimization." *Qubahan Techno Journal* 2.2 (2023): 1-13.

[63] Linh, Nguyen Tung. "A novel combination of genetic algorithm, particle swarm optimization, and teaching-learning-based optimization for distribution network reconfiguration in case of faults." *Engineering, Technology & Applied Science Research* 14.1 (2024): 12959-12965.

[64] Sahu, Binod Kumar, et al. "A novel hybrid LUS–TLBO optimized fuzzy-PID controller for load frequency control of multi-source power system." *International Journal of Electrical Power & Energy Systems* 74 (2016): 58-69.

[65] Gupta, Shubham. "Enhanced harmony search algorithm with non-linear control parameters for global optimization and engineering design problems." *Engineering with Computers* 38.Suppl 4 (2022): 3539-3562.

[66] Kumar, Sachan Rohit, and Kushwaha Dharmender Singh. "Nature-inspired optimization algorithms: research direction and survey." *arXiv preprint arXiv:2102.04013* (2021).

[67] Vardhini, K. Kanaka, and T. Sitamahalakshmi. "A review on nature-based swarm intelligence optimization techniques and its current research directions." *Indian Journal of Science and Technology* 9.10 (2016): 1-13.

[68] Darvishpoor, Shahin, et al. "Nature-inspired algorithms from oceans to space: A comprehensive review of heuristic and meta-heuristic optimization algorithms and their potential applications in drones." *Drones* 7.7 (2023): 427.

[69] Kalavani, Farshad, et al. "A contemporary review of the applications of nature-inspired algorithms for optimal design of automatic generation control for multi-area power systems." *Artificial Intelligence Review* 51.2 (2019): 187-218.

[70] Veerasamy, Veerapandiyan, et al. "A Hankel matrix based reduced order model for stability analysis of hybrid power system using PSO-GSA optimized cascade PI-PD controller for automatic load frequency control." *IEEE Access* 8 (2020): 71422-71446.

[71] AboRas, Kareem M., et al. "Optimized cascaded regulation strategy for robust automatic generation control in renewable-integrated power networks." *Scientific Reports* (2025).

[72] Zulkifili, Athirah Najihah, Ismayuzri Ishak, and Muhammad Aizzat Zakaria. "Adaptive Control in Mobile and Autonomous Robotics: A Unified Taxonomy and Comparative Review." *IEEE Access* (2026).

[73] Shouran, Mokhtar, et al. "A novel AVR system utilizing fuzzy PIDF enriched by FOPD controller optimized via PSO and Sand Cat Swarm Optimization algorithms." *Energies* 18.6 (2025): 1337.

[74] Jang, J-SR, and Chuen-Tsai Sun. "Neuro-fuzzy modeling and control." *Proceedings of the IEEE* 83.3 (1995): 378-406.

[75] Babuška, Robert, and Henk Verbruggen. "Neuro-fuzzy methods for nonlinear system identification." *Annual reviews in control* 27.1 (2003): 73-85.

[76] Tian, Lianfang, and Curtis Collins. "Adaptive neuro-fuzzy control of a flexible manipulator." *Mechatronics* 15.10 (2005): 1305-1320.

[77] Seng, Teo Lian, M. Bin Khalid, and Rubiyah Yusof. "Tuning of a neuro-fuzzy controller by genetic algorithm." *IEEE Transactions on Systems, Man, and Cybernetics, Part B (Cybernetics)* 29.2 (1999): 226-236.

[78] Xu, Bin, et al. "Neuro-fuzzy control of underwater vehicle-manipulator systems." *Journal of the Franklin Institute* 349.3 (2012): 1125-1138.

[79] Singh, Meetpal, Sujata Arora, and Owais Ahmad Shah. "Enhancing Hybrid Power System Performance with GWO-Tuned Fuzzy-PID Controllers: A Comparative Study." *International Journal of Robotics & Control Systems* 4.2 (2024).

[80] Yeo, Hyunho, et al. "Neuroscaler: Neural video enhancement at scale." *Proceedings of the ACM SIGCOMM 2022 Conference*. 2022.

[81] Al-Janan, Dony Hidayat, et al. "Optimizing the double inverted pendulum's performance via the uniform neuro multiobjective genetic algorithm." *International Journal of Automation and Computing* 14.6 (2017): 686-695.

[82] Sun, Zhe, Ning Wang, and Yunrui Bi. "Type-1/type-2 fuzzy logic systems optimization with RNA genetic algorithm for double inverted pendulum." *Applied Mathematical Modelling* 39.1 (2015): 70-85.

[83] Al-Araji, Ahmed S. "An adaptive swing-up sliding mode controller design for a real inverted pendulum system based on Culture-Bees algorithm." *European Journal of Control* 45 (2019): 45-56.

[84] Rafan, N. A., et al. "Nonlinear Friction Analysis of a Modified Switching Function Controller in Pre-sliding Regime." *Advances in Material Sciences and Engineering*. Singapore: Springer Singapore, 2019. 309-318.

[85] Yazdani, Danial, et al. "Robust optimization over time: A critical review." *IEEE Transactions on Evolutionary Computation* 28.5 (2023): 1265-1285.

[86] Vargas, Oscar Sánchez, et al. "Adaptive network-based fuzzy inference system (ANFIS) applied to inverters: a survey." *IEEE transactions on power electronics* 39.1 (2023): 869-884.

[87] Kusagur, Ashok, S. F. Kodad, and BV Sankar Ram. "Modeling, design & simulation of an adaptive neuro-fuzzy inference system (ANFIS) for speed control of induction motor." *International Journal of Computer Applications* 6.12 (2010): 29-44.

[88] Kapnopoulos, Aristotelis, Charalampos Kazakidis, and Alex Alexandridis. "Quadrotor trajectory tracking based on backstepping control and radial basis function neural networks." *Results in Control and Optimization* 14 (2024): 100335.

[89] Talpur, Noureen, et al. "A comprehensive review of deep neuro-fuzzy system architectures and their optimization methods." *Neural Computing and Applications* 34.3 (2022): 1837-1875.

[90] Sajid, M., M. Tanveer, and Ponnuthurai N. Suganthan. "Ensemble deep random vector functional link neural network based on fuzzy inference system." *IEEE Transactions on Fuzzy Systems* 33.1 (2024): 479-490.

[91] Senthilselvi, A., et al. "Performance evaluation of adaptive neuro fuzzy system (ANFIS) over fuzzy inference system (FIS) with optimization algorithm in de-noising of images from salt and pepper noise." *Journal of Ambient Intelligence and Humanized Computing* (2021): 1-6.

[92] Das, Rangan, Sagnik Sen, and Ujjwal Maulik. "A survey on fuzzy deep neural networks." *ACM Computing Surveys (CSUR)* 53.3 (2020): 1-25.

[93] Shi, Qian, et al. "Adaptive neuro-fuzzy PID controller based on twin delayed deep deterministic policy gradient algorithm." *neurocomputing* 402 (2020): 183-194.

[94] Bejarbaneh, Elham Yazdani, et al. "Optimization of model reference adaptive controller for the inverted pendulum system using CCPSO and DE algorithms." *Automatic Control and Computer Sciences* 52.4 (2018): 256-267.

[95] Wang, Shirui, et al. "Metaheuristic Optimization of PID Controllers: Methods, Applications, and Trends." *Archives of Computational Methods in Engineering* (2026): 1-47.

[96] Mai-Phuong, Dao-Thi, et al. "Balancing a practical inverted pendulum model employing novel meta-heuristic optimization-based fuzzy logic controllers." *Int. J. Adv. Comput. Sci. Appl* 13.4 (2022).

[97] Siddique, Nazmul. *Intelligent control: a hybrid approach based on fuzzy logic, neural networks and genetic algorithms*. Vol. 517. Springer, 2013.

[98] Blondin, Maude Josée. *Controller Tuning Optimization Methods for Multi-Constraints and Nonlinear Systems: A Metaheuristic Approach*. Berlin/ Heidelberg, Germany: Springer, 2021.

[99] Mourad, Achouri, Youce Zennir, and Cherif Tolba. "Intelligent and Robust Controller Tuned with WOA: Applied for the Inverted Pendulum." *Journal Européen des Systèmes Automatisés* 55.3 (2022).

[100] Homaifar, Abdollah, and Ed McCormick. "Simultaneous design of membership functions and rule sets for fuzzy controllers using genetic algorithms." *IEEE transactions on fuzzy systems* 3.2 (2002): 129-139.

[101] [100] Abdo, Mohamed I., and Emad A. Elsheikh. "Optimization of a fractional-order interval type-2 fuzzy PID controller based on BBO for real-time applications." *Franklin Open* 8 (2024): 100121.

[102] Mahmood abadi, Mohammad Javad, and Mohammad Mehdi Shahangian. "A new multi-objective artificial bee colony algorithm for optimal adaptive robust controller design." *IETE Journal of Research* 68.2 (2022): 1251-1264.

[103] Liu, Lunhaojie, Juntao Fei, and Cuniculi An. "Adaptive sliding mode long short-term memory fuzzy neural control for harmonic suppression." *IEEE Access* 9 (2021): 69724-69734.

[104] Tomar, Basant, Narendra Kumar, and Mini Sreejith. "Robust control of rotary inverted pendulum using metaheuristic optimization techniques based PID and fractional order pi λ d μ controller." *Journal of Vibration Engineering & Technologies* 12.Suppl 1 (2024): 1-20.

[105] Chiou, Juing-Shian, Shun-Hung Tsai, and Ming-Tang Liu. "A PSO-based adaptive fuzzy PID-controllers." *Simulation Modelling Practice and Theory* 26 (2012): 49-59.

[106] SAIHI, Lakhdar, et al. "Grey Wolf-Optimized Super-Twisting Sliding Mode Control for DFIG Wind Turbines under Variable Speeds." *Electrotehnica, Electronica, Automatica* 73.4 (2025).

[107] Charkoutsis, Stefanos, and Mohamed Kara-Mohamed. "A Particle Swarm Optimization tuned nonlinear PID controller with improved performance and robustness for First Order Plus Time Delay systems." *Results in Control and Optimization* 12 (2023): 100289.

[108] Amiri Ebrahim abadi, Mohammad, and Najme Mansouri. "A comprehensive survey of feature selection techniques based on whale optimization algorithm." *Multimedia Tools and Applications* 83.16 (2024): 47775-47846.

[109] Abualigah, Laith, et al. "Ant Lion Optimizer: A Comprehensive Survey of Its Variants and Applications: L. Abualigah et al." *Archives of computational methods in engineering* 28.3 (2021): 1397-1416.

[110] Durgut, Pinar G., Mirac Bugse Tozak, and M. Tamer Ayvaz. "Shuffled Ant Lion Optimization approach with an exponentially weighted random walk strategy." *Neural Computing and Applications* 36.18 (2024): 10475-10499.

[111] Yahia, Selma, et al. "A comprehensive survey of manta ray foraging optimization: theory, variants, hybridization, and applications." *Archives of Computational Methods in Engineering* (2025): 1-66.

[112] Nguyen, Ngoc-Khoat, et al. "A Novel Integration of Metaheuristic–Based Optimization Methods for Enhancing Fuzzy Logic Control Performance on Inverted Pendulum-Cart Systems." *Journal Européen des Systèmes Automatisés* 58.4 (2025): 773.

[113] Zhang, Jing, Lixiang Zhang, and Jing Xie. "Application of memetic algorithm in control of linear inverted pendulum." *2011 IEEE International Conference on Cloud Computing and Intelligence Systems*. IEEE, 2011.

[114] Ribeiro, Victor Henrique Alves, and Gilberto Reynoso-Meza. "Ensemble learning by means of a multi-objective optimization design approach for dealing with imbalanced data sets." *Expert Systems with Applications* 147 (2020): 113232.

[115] Santana, Laura Emmanuella A. dos S., and Anne M. de Paula Canuto. "Filter-based optimization techniques for selection of feature subsets in ensemble systems." *Expert Systems with Applications* 41.4 (2014): 1622-1631.

[116] Amer, T. S., et al. "Vibrational and stability analysis of planar double pendulum dynamics near resonance." *Nonlinear Dynamics* 112.24 (2024): 21667-21699.

[117] Chatterjee, Debasish, Amit Patra, and Harish K. Joglekar. "Swing-up and stabilization of a cart–pendulum system under restricted cart track length." *Systems & control letters* 47.4 (2002): 355-364.

[118] Yang, Ji-Hyuk, et al. "Swing-up control for an inverted pendulum with restricted cart rail length." *International Journal of Control, Automation and Systems* 7.4 (2009): 674-680.

[119] Jayaram, Sabavath, Cristiano Maria Verrelli, and Nithya Venkatesan. "Real-time implementation of a fractional PID controller for a nonlinear system with fractional-order modeling." *Computers and Electrical Engineering* 135 (2026): 111205.

[120] Nassef, Ahmed M. "Optimal tuning of FOPID-like fuzzy controller for high-performance fractional-order systems." *Computers, Materials & Continua* (2022).

[121] Zhang, Qing-Hao, Jun-Guo Lu, and Zhen Zhu. "A review on robust control of continuous time fractional-order systems: QH Zhang et al." *Nonlinear Dynamics* 113.19 (2025): 25405-25428.

[122] Moreira, Walter Ernest Müller, and Claudio Garcia. "Performance comparison between IOPID and FOPID controllers in an industrial flow pilot plant." *IFAC-PapersOnLine* 54.4 (2021): 232-237.

[123] Hussain, K. Mohamed, R. Allwyn Rajendran Zepherin, and M. Shantha. "Comparison of PID controller tuning methods with genetic algorithm for FOPTD system." *criterion* 16 (2014): 17.

[124] Essa, Mohamed El-Sayed M., Magdy AS Aboelela, and Mohammed AM Hassan. "A comparative study between ordinary and fractional order pid controllers for modelling and control of an industrial system based on Genetic Algorithm." *2017 6th international conference on modern circuits and systems technologies (MOCAST)*. IEEE, 2017.

[125] Pan, Indranil, and Saptarshi Das. "Frequency domain design of fractional order PID controller for AVR system using chaotic multi-objective optimization." *International Journal of Electrical Power & Energy Systems* 51 (2013): 106-118.

[126] Nasir, Mohannad, Majd Saloumi, and Ali Bou Nassif. "Review of various metaheuristics techniques for tuning parameters of PID/FOPID controllers." *ITM web of conferences*. Vol. 43. EDP Sciences, 2022.

[127] Nassef, Ahmed M., et al. "Metaheuristic-based algorithms for optimizing fractional-order controllers—a recent, systematic, and comprehensive review." *Fractal and Fractional* 7.7 (2023): 553.

[128] Oladipo, Stephen, Yanxia Sun, and Zenghui Wang. "Optimization of PID and FOPID controllers with new generation metaheuristic algorithms for controlling AVR system: Concise Survey." *2020 12th International Conference on Computational Intelligence and Communication Networks (CICN)*. IEEE, 2020.

[129] Dey, Bishal, Sumit Kr Pandey, and Anindita Sengupta. "Design of modified fractional order PID controller for cart inverted pendulum system." *International Journal of Dynamics and Control* 13.4 (2025): 148.

[130] Mondal, Reetam, and Jayati Dey. "A novel design methodology on cascaded fractional order (FO) PI-PD control and its real time implementation to Cart-Inverted Pendulum System." *ISA transactions* 130 (2022): 565-581.

[131] Mondal, Reetam, and Jayati Dey. "An extended experimental study on control of unstable and non-minimum phase plants with the cascaded form of a fractional order compensator." IEEE Transactions on Industry Applications 59.3 (2023): 3086-3097.

[132] Yeh, Po-Chiang, and Petar V. Kokotovic. "Adaptive tracking designs for input-constrained linear systems using backstepping." *Proceedings of 1995 American Control Conference-ACC'95*. Vol. 3. IEEE, 1995.

[133] Meraihi, Yassine, et al. "Grasshopper optimization algorithm: theory, variants, and applications." *Ieee Access* 9 (2021): 50001-50024.

[134] Fister, Iztok, et al. "A comprehensive review of firefly algorithms." *Swarm and evolutionary computation* 13 (2013): 34-46.

[135] Alirezapour, Hanie, Najme Mansouri, and Behnam Mohammad Hasani Zade. "A comprehensive survey on feature selection with grasshopper optimization algorithm." *Neural Processing Letters* 56.1 (2024): 28.

[136] Saleh, Amjed H., and Shuruq A. Al-khafaji. "Anti-Swing Rejection Based on PID Controller Optimized by Firefly Algorithm." *Mathematical Modelling of Engineering Problems* 10.1 (2023).

[137] Okwu, Modestus O., and Lagouge K. Tartibu. "Firefly algorithm." *Metaheuristic Optimization: Nature-Inspired Algorithms Swarm and Computational Intelligence, Theory and Applications*. Cham: Springer International Publishing, 2020. 61-69.

[138] Kumar, V. R., and N. Mani. "The application of artificial intelligence techniques for intelligent control of dynamical physical systems." *International Journal of adaptive control and signal processing* 8.4 (1994): 379-392.

[139] Benderskaya, Elena N. "Nonlinear trends in modern artificial intelligence: a new perspective." *Beyond Artificial Intelligence: Contemplations, Expectations, Applications*. Berlin, Heidelberg: Springer Berlin Heidelberg, 2013. 113-124.

[140] Talpur, Noureen, et al. "Deep Neuro-Fuzzy System application trends, challenges, and future perspectives: A systematic survey." *Artificial intelligence review* 56.2 (2023): 865-913.

[141] Sathya, D., G. Saravanan, and R. Thangamani. "Fuzzy logic and its applications in mechatronic control systems." *Computational Intelligent Techniques in Mechatronics* (2024): 211-241.

[142] Fahmy, A. A. *Neuro-fuzzy modelling and control of robotic manipulators*. Cardiff University (United Kingdom), 2005.

[143] Kaul, Supriya, et al. "Deep Learning-based Advancement in Fuzzy Logic Controller." *2023 International Conference on Artificial Intelligence and Smart Communication (AISC)*. IEEE, 2023.

[144] Daksh, ManMahendra Singh, and Puneet Mishra. "A Feedback-Assisted Inverse Neural Network Controller for Cart-Mounted Inverted Pendulum." *Applied Computational Intelligence and Soft Computing* 2025.1 (2025): 4873425.

[145] Tehrani, Kambiz, et al. "A Survey of AI in System of Systems With a Focus on Power Electronic Systems—Part I: Design and Control." *IEEE Systems Journal* 19.4 (2026): 1011-1024.

[146] Raol, Jitendra R., and Ramakalyan Ayyagari. *Control systems: classical, modern, and AI-based approaches*. CRC Press, 2019.

[147] Mohan, Vijay, Asha Rani, and Vijander Singh. "Robust adaptive fuzzy controller applied to double inverted pendulum." *Journal of Intelligent & Fuzzy Systems* 32.5 (2017): 3669-3687.

[148] Veeramani, T., et al. "Neuro-Fuzzy Systems: A Study of Architectures, Applications, and Future Directions." *2025 5th International Conference on Soft Computing for Security Applications (ICSCSA)*. IEEE, 2025.

[149] Goher, Khaled M., and Sulaiman O. Fadlallah. "Control of a two-wheeled machine with two-directions handling mechanism using PID and PD-FLC algorithms." *International Journal of Automation and Computing* 16.4 (2019): 511-533.

[150] Bounemeur, Abdelhamid, and Mohamed Chemachema. "Adaptive fuzzy fault-tolerant control for a class of nonlinear systems under actuator faults: application to an inverted pendulum." *International Journal of Robotics and Control Systems* 1.2 (2021): 102-115.

[151] Elhabib, Mohamed O., Herman Wahid, and Zaharuddin Mohamed. "An Optimal Fuzzy Logic Controller Design for a Single-Linked Inverted Pendulum System." *Control, Instrumentation and Mechatronics: Theory and Practice*. Singapore: Springer Nature Singapore, 2022. 285-298.

[152] Abougarair, Ahmed J., and MOHAMED M. Edardar. "Adaptive Neural Networks Based Robust Output Feedback Control for Nonlinear System." *Wseas Trans. Comput. Res* 9.1 (2021): 125-136.

[153] Can, Erol. "UAV DC Motor behaviors control using new hybrid PSO-fuzzy logic with a dynamic error based optimization." *Aerospace Science and Technology* (2025): 111156.

[154] Rubaai, Ahmed, and Paul Young. "Hardware/software implementation of fuzzy-neural-network self-learning control methods for brushless DC motor drives." *IEEE Transactions on Industry Applications* 52.1 (2015): 414-424.

[155] R. Ramakrishnan and D. Subramaniam Nachimuthu, "Design of State Feedback LQR Based Dual Mode Fractional-Order PID Controller using Inertia Weighted PSO Algorithm: For Control of an Underactuated System," *Journal of The Institution of Engineers (India): Series C,* vol. 102, no. 6, pp. 1403-1417, 2021.

[156] I. Chawla and A. Singla, "System identification of an inverted pendulum using adaptive neural fuzzy inference system," in *Harmony Search and Nature-Inspired Optimization Algorithms*: Springer, 2019, pp. 809-817

List of Publications

Papers in Referred Journals

[1] **Neelam Verma**, and Sudarshan K. Valluru. "ANN based ANFIS controller design using hybrid meta-heuristic tuning approach for cart inverted pendulum system." *Multimedia Tools and Applications* 83.18 (2024): 54839-54861, https://doi.org/10.1007/s11042-023-17699-3 (SCIE Indexed)

[2] **Neelam Verma**, and Sudarshan K. Valluru. " Design of Cascaded FOPI-FOPD-BLQG Controller tuned with Hybrid 1 Grasshopper and Firefly algorithms for Stabilizing Cart Inverted Pendulum System." *Mechanics & Industry* 27,14(2026), https://doi.org/10.1051/ meca/2026009. (SCIE Indexed)

[3] **Neelam Verma**, and Sudarshan K. Valluru. "Design of Neural Network Tuned Cascaded FOPI-FOPD Controller for Stabilizing Cart Inverted Pendulum System" *Springer* (Communicated)

International Conference Proceedings

[1] **Neelam Verma**, and Sudarshan K. Valluru. "Comparative Study of Parametric Disturbances Effect on Cart-Inverted Pendulum System Stabilization." *Modern Electronics Devices and Communication Systems: Select Proceedings of MEDCOM 2021* Lecture Notes in Electrical Engineering, vol 948, pp.217-230 Springer, Singapore. https://doi.org/10.1007/978-981-19-6383-4_17

[2] **Neelam Verma**, and Sudarshan K. Valluru. "Comparative Analysis of GOA, WCA and PSO Tuned Fractional Order-PID Controller for Cart-Inverted Pendulum." 2022 IEEE International Power and Renewable Energy Conference (IPRECON), Kollam, India, 2022, pp. 1-7, doi: 10.1109/IPRECON55716.2022. 10059474.

Brief Biodata

Neelam Verma is graduate from I.E.R.T., Allahabad, India in 2006 B.Tech in Electronics Engineering. She received M.Tech Degree in Electrical Engineering from Indian Institute of Technology, Roorkee in 2009. She is currently working as an Assistant Professor in the Department of Electrical Engineering at Amity University, Noida. Prior to this, she worked as an Assistant Professor at Lingaya's University, Faridabad. Her research areas are Sensor Networking Technologies, Linear and Nonlinear Control, and Automation & Control.